VANADIUM AND MOLYBDENUM INCORPORATED MCM-41
CATALYSTS FOR SELECTIVE OXIDATION OF ETHANOL

A THESIS SUBMITTED TO
THE GRADUATE SCHOOL OF NATURAL AND APPLIED SCIENCES
OF
MIDDLE EAST TECHNICAL UNIVERSITY

BY

YEŞİM GÜÇBİLMEZ

IN PARTIAL FULFILLMENT OF THE REQUIREMENTS
FOR
DOCTOR OF PHILOSOPHY
IN
CHEMICAL ENGINEERING

JUNE 2005

Approval of the Graduate School of Natural and Applied Sciences

_____

Prof. Dr. Canan Özgen
Director

I certify that this thesis satisfies all the requirements as a thesis for the degree of Doctor of Philosophy.

_____

Prof. Dr. Nurcan Baç
Head of Department

This is to certify that we have read this thesis and that in our opinion it is fully adequate, in scope and quality, as a thesis for the degree of Doctor of Philosophy.

_____   _____
Prof. Dr. Suna Balcı   Prof. Dr. Timur Doğu
   (Co-supervisor)   (Supervisor)

Examining Committee Members

Prof. Dr. İnci Eroğlu   (METU, CHE)   _____

Prof. Dr. Timur Doğu   (METU, CHE)   _____

Prof. Dr. Serpil Takaç   (AU, CHE)   _____

Assoc. Prof. Dr. Gürkan Karakaş   (METU, CHE)   _____

Assoc. Prof. Dr. N. Aslı Sezgi   (METU, CHE)   _____

I hereby declare that all information in this document has been obtained and presented in accordance with academic rules and ethical conduct. I also declare that, as required by these rules and conduct, I have fully cited and referenced all material and results that are not original to this work.

Name, Last name : Yeşim Güçbilmez

Signature   :

ABSTRACT

VANADIUM AND MOLYBDENUM INCORPORATED MCM-41 CATALYSTS FOR SELECTIVE OXIDATION OF ETHANOL

Güçbilmez, Yeşim

Ph.D., Department of Chemical Engineering

Supervisor   : Prof. Dr. Timur Doğu

Co-Supervisor: Prof. Dr. Suna Balcı

June 2005, 144 pages

In this study, V-MCM-41, MCM-41 and Mo-MCM-41 catalysts were synthesized by the one-pot alkaline and acidic synthesis methods.

The as-synthesized catalysts were found to have high BET surface areas (430-1450 m^2/g), homogeneous pore size distributions (2-4 nm), good crystalline patterns and high metal loading levels (Metal/Si atomic ratio in the solid = 0.01-0.16) as determined by the characterization studies.

MCM-41 and Mo-MCM-41 catalysts were highly active in the selective oxidation of ethanol with conversion levels of 56% and 71%, respectively, at 400°C for an O$_2$/EtOH feed ratio of 0.5. Both catalysts had very high selectivities to acetaldehyde at temperatures below 300°C.

Conversions exceeded 95% with the V-MCM-41 catalyst having a V/Si molar ratio (in the solid) of 0.04 in the temperature range of 300°C-375°C for

the O_2/EtOH feed ratios of 0.5-2.0. Acetaldehyde selectivities changed between 0.82-1.00 at the temperature range of $150^{o}C$-$250^{o}C$.

Ethylene, which is listed as a minor side product of the selective oxidation of ethanol in literature, was produced with a maximum yield of 0.66 at $400^{o}C$ at the O_2/EtOH feed ratio of 0.5. This yield is higher than the yields obtained in the industrial ethylene production methods such as thermal cracking and oxidative dehydrogenation of ethane. Besides, the feedstock used in this work is a non-petroleum chemical, namely ethanol, which can be produced from sugar and crop wastes by fermentation. Thus, the findings of this study are also proposed as an alternative ethylene production method from a non-petroleum reactant at lower temperatures with higher yields.

ÖZ

ETANOLÜN SEÇİCİ OKSİDASYONUNDA KULLANILMAK ÜZERE VANADYUM VE MOLİBDEN İÇEREN MCM-41 KATALİZÖRLERİNİN ÜRETİMİ

Güçbilmez, Yeşim

Doktora, Kimya Mühendisliği Bölümü

Tez Yöneticisi   : Prof. Dr. Timur Doğu

Ortak Tez Yöneticisi: Prof. Dr. Suna Balcı

Haziran 2005, 144 sayfa

Bu çalışma kapsamında, doğrudan sentez metoduyla, alkali ve asit ortamlarında, V-MCM-41, MCM-41 ve Mo-MCM-41 katalizörleri sentezlenmiştir.

Bu şekilde sentezlenen katalizörlerin yüksek BET yüzey alanlarına (430-1450 m^2/g), homojen gözenek boyutu dağılımlarına (2-4 nm), iyi kristal yapılarına ve yüksek metal yükleme oranlarına (Metal/Si katıdaki molar oranı =0.01-0.16) sahip oldukları karakterizasyon çalışmaları sonucunda görülmüştür.

MCM-41 ve Mo-MCM-41 katalizörleri etanolün seçici oksidasyonunda, 400°C'de ve reaktör girişinde 0.5'lik O$_2$/EtOH oranında, sırasıyla, 56% ve 71% dönüşüm seviyeleriyle, yüksek aktivite göstermişlerdir.

Her iki katalizör de 300°C'nin altında çok yüksek asetaldehit seçiciliği göstermiştir.

Dönüşüm değerleri, V/Si katıdaki molar oranı 0.04 olan V-MCM-41 katalizörü için; 300°C-375°C aralığında ve 0.5-0.2 O$_2$/EtOH reaktör girişi oranlarında, 95%'i geçmiştir. Asetaldehit seçicilikleri, 150°C-250°C aralığında, 0.82-1.00 arasında değişmiştir.

Literatürde, etil alkolün seçici oksidasyonunda önemsiz bir yan ürün olarak sözü geçen etilen, 400°C'de ve 0.5'lik O$_2$/EtOH reaktör giriş oranında 0.66 maksimum verimle üretilmiştir. Bu verim değeri ısıl parçalanma ve etanın kısmi oksidasyonu gibi endüstriyel etilen üretim yollarıyla elde edilen verimlerden daha yüksektir. Ayrıca, bu çalışmada kullanılan etanol petrol-bazlı olmayan bir hammaddedir ve şeker pancarı atıklarından fermentasyonla üretilebilmektedir. Bu sebeple, bu çalışmadaki bulgular, petrol-bazlı olmayan bir hammaddeden, daha düşük sıcaklıkta, daha yüksek verimle etilen elde etmek için alternatif bir üretim metodu olarak da önerilmiştir.

Anahtar Kelimeler: Etilen, Etil alkol, Seçici Oksidasyon, MCM-41, V-MCM-41, Mo-MCM-41, Oksidatif Dihidrojenasyon, Kısmi Oksidasyon

To My Family

ACKNOWLEDGEMENTS

TABLE OF CONTENTS

LIST OF FIGURES

LIST OF TABLES

CHAPTER 1

INTRODUCTION

According to the IUPAC definition, porous materials can be classified into three groups: Microporous materials have pore diameters less than 2 nm, mesoporous materials have pore diameters between 2 to 50 nm and macroporous materials have pore diameters larger than 50 nm [1].

Microporous materials involve amorphous silica, inorganic gels, pillared clays, molecular sieving carbons, crystalline materials such as zeolites, aluminophosphates, gallophosphates and related materials [2-4]. Among these materials, zeolites are the most widely studied ones due to their advantageous properties such as high adsorption capacities, large surface areas and shape selective properties. However, they have one important drawback that limits their application; reactions with bulky molecules can not be handled due to pore size limitations (their pore size changes in the range of 0.5 to 1.2 nm). Hence, it has been an important field of research to synthesize materials that would both resemble zeolites structurally and have larger pore systems [4].

The natural way to follow in order to synthesize materials with larger pores would be to increase the size of the structure-directing agents used in the synthesis. As a result of this strategy, materials called aluminophosphates (AlPO$_4$) were successfully synthesized in the 1980's, [5]. Aluminophosphates such as cloverite [6], VPI-5 [7] and AlPO$_4$-8 [8] were found to have pore sizes in the range of 1.3-1.5 nm; however they suffered from low thermal or hydrothermal stability [4].
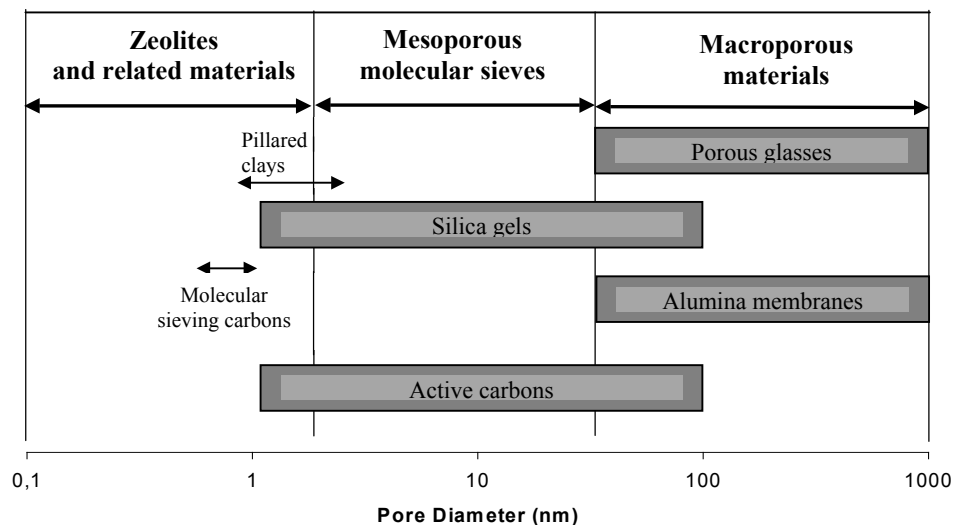
Fig. 1.1 Porous materials as classified by their pore sizes (adapted from [3])

In the year 1996, Balkus and co-workers reported the synthesis of a large pore zeolite they named as UTD-1 [9]. UTD-1 was made up of pure silica and had a one-dimensional pore system consisting of elliptical pores [4,10]. It was much more stable than VPI-5, $AlPO_4$-8 and cloverite; however, the large Co-complex (the structure-directing agent) remaining in the pores was hard to remove and this would limit the practical applications of UTD-1 [4].

In 1988, Yanagisawa et al. reported the syntheses of ordered mesoporous materials with narrow pore size distributions and large surface areas which were prepared from a layered polysilicate called kanemite [11-13]. Later, Inagaki et al. proposed a two-step formation mechanism for the synthesis of kanemite-derived materials [14,15]. They suggested that as the first step, the Na^+ ions in the kanemite interlayers exchanged ions with the surfactant cations and as the second step the silicate sheets warped and transformed into a hexagonally packed phase [4,16].

In 1992, researchers at the Mobil (now ExxonMobil) Corporation published the syntheses of a family of mesoporous materials, designated **M41S**

[17,18]. These materials were characterized by narrow pore size distributions, and large surface areas. The three members of this family were MCM-41, which had a hexagonal array of unidirectional pores, MCM-48, which had a cubic pore system indexed in the space group Ia3d and MCM-50 which had an unstable lamellar structure [4,19]. These materials were fundamentally different from zeolites by the fact that their pore walls were amorphous; the ordering lied in their pore arrangements [4].

M41S family of materials are mainly made up of silica, SiO_2. Silica has specific advantages as a support such as: Excellent thermal and chemical stability, ease of handling and profusion of exposed silanol (Si-OH) groups. Also, it has a rather rigid structure and does not swell in solvents, so it may be used both at high and low temperatures and at high pressures. Its very inflexibility and non-compresibility makes silica-anchored catalysts suitable for use in continuous reactors [20].

M41S family of materials have attracted far more attention than kanemite-derived materials although they had similar structures. MCM-41 became the most popular member of the family due to its flexible synthesis conditions (the three dimensional structure of MCM-48 was harder to obtain) and advantageous properties such as exceptionally high surface areas (see Table 1.1) and narrow pore size distributions.

MCM-41 is frequently used as a support on which acids, bases, heteropolyacids, metals, metal oxides, amines or complexes are supported. Besides its favourite uses as a support, it is also possible to generate Bronsted acid sites on the surface of MCM-41 so that monofunctional acid and acid/metal oxide bifunctional catalysts can be produced. It is also possible to produce mildly-basic MCM-41 materials through increasing the basicity of the conjugated base by exchanging the protons with alkaline ions. Finally, there is also the possibility of introducing transition metals into the MCM-41 structure to obtain various redox catalysts [21].

Table 1.1 Literature Values of the BET Surface Areas and Average Pore Diameters of
MCM-41 Molecular Sieves

Authors	BET Surface Area (m²/g)	Average Pore Diameter (nm)
Araujo and Jaroniec [22]	639, 694	3.6, 3.7
Gucbilmez et al. [23]	1400, 1452	2.7
Lang et al. [24]	1184	2.7
Laha and Kumar [25]	1167-1480	2.7-2.8

The following list illustrates some different applications where the mesoporous MCM-41 molecular sieve is successfully used:

1. Acid catalysis: Cracking [26,27], mild hyrdocracking [21], upgrading olefins [28], oligomerization of olefins [29], Friedel-Crafts alkylations and acylations [30,31].

2. Base-catalysis: Knoevenagel reactions [32] and transesterification reactions [33].

3. Catalytic preparation of acetals for use in pharmaceuticals [34] and as fragrances in perfumes and detergents [35].

4. Polymerization catalysis [36].

5. Wastewater treatment [37].

6. Enzyme catalysis [38, 39].

7. Film and membrane applications [40].

8. Applications with electron-transfer materials [41].

In this study, the MCM-41 molecular sieve was investigated in detail. First, the purely-siliceous MCM-41 catalysts were synthesized and characterized with X-Ray Diffraction (XRD), Nitrogen Adsorption, Helium Pycnometry, Scanning Electron Microscopy (SEM) and Atomic Force Microscopy (AFM) techniques. As the second step, vanadium and molybdenum incorporated MCM-41 catalysts (V-MCM-41 and Mo-MCM-41 catalysts) were synthesized and characterized with XRD, Nitrogen Adsorption, Helium Pycnometry, Energy-Dispersive X-Ray Spectroscopy (EDS), Atomic Absorption Spectroscopy (AAS), Scanning Electron Microscopy (SEM) and Atomic Force Microscopy (AFM) techniques. Finally, the catalytic properties of the synthesized V-MCM-41, MCM-41 and Mo-MCM-41 catalysts were tested in the selective oxidation of ethanol at different temperatures with different O_2/EtOH feed ratios.

The main product of the selective oxidation of ethanol is acetaldehyde with the following stoichiometry:

$$C_2H_5OH + 1/2O_2 \rightarrow CH_3CHO + H_2O \dots\dots\dots\dots\dots\dots\dots (1.1)$$
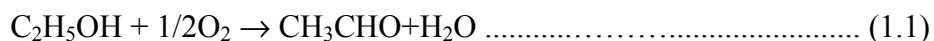
However, this process has several side reactions which results in production of several by-products as discussed in Section 4.5.4.

It was shown in this work that for a certain range of O_2/Ethanol feed ratios and in a certain range of temperatures, the main product of the selective oxidation of ethanol became ethylene. Indeed, ethylene was obtained with yield values **above 0.65** for certain reaction conditions as discussed in Section 4.5.1.

CHAPTER 2

LITERATURE SURVEY

In the mid-1980's, Mobil (now ExxonMobil) Research Group had a significant effort of synthesizing new porous materials that could selectively convert high molecular weight, bulky products into more valuable fuel and lubricant products. Kresge et al. [42] tried to synthesize large pore materials by combining the synthesis concepts of pillared layered materials and zeolites. The aim was to isolate the layered intermediates formed during zeolite synthesis and use them to obtain pillared porous materials with large pores. This idea had credibility because a newly-discovered material, MCM-22, was found to transform from a layered precursor into a zeolitic structure [43].

Hence, as the next step, the Mobil researchers attempted to separate the crystalline layers of MCM-22 prior to any thermal procedure, intercalate these layers using an alkyltrimethylammonium compound and insert stable inorganic oxide pillars between the layers. A pillared layered material named MCM-36 was formed as a result of this separation and subsequent pillaring process [44, 45].

This general approach of interrupting the zeolite synthesis, isolating the layered zeolite precursors and using them as reagents to form large pore materials was investigated further. The traditional zeolite synthesis was interrupted prior to any X-ray diffraction evidence of crystallinity (at a point in the 25% to 75% of the total synthesis time) . A high concentration of the intercalate and an alkyltrimethylammonium salt were added to the synthesis media at high pH values. These reaction mixtures were then subjected to hydrothermal treatment at temperatures around $100^{o}C$ to

obtain zeolite-layered hybrid materials. Many of the obtained products had very unusual properties: Their XRD patterns were essentially featureless except for one low-angle broad peak at around $2\theta \cong 2^o$, they had extremely high BET surface areas and high hydrocarbon sorption capacities (BET areas greater than 1000 m^2/g and sorption capacities in excess of 50 wt%), [42].

In a parallel synthesis effort, cetyltrimethylammonium hydroxide was used directly as a structure-directing agent in a zeolite-like hydrothermal synthesis procedure. The properties of the obtained products were similar to those obtained in the interrupted zeolite synthesis method. That is, the products had low angle peaks in XRD patterns, exceptionally high BET surface areas and high hydrocarbon sorption capacities. Thus, both the interrupted zeolite synthesis method and the direct introduction of cetyltrimethylammonium hydroxide as the structure-directing agent brought about the formation of a new family of mesoporous molecular sieves. Mobil researchers also made use of Transmission Electron Microscopy (TEM) analysis in order to understand the nature of the newly-discovered materials. In one of the TEM photographs, a trace amount of a material with uniform hexagonal pore structure was detected [42]. This material was designated MCM-41 (Mobil Composition of Matter 41 or Mobil Crystalline Material 41 where the number 41 is merely a batch number) and in time it became one of the most popular mesoporous members of the materials' synthesis literature.

2.1 Synthesis Outlines of MCM-41 Catalysts

MCM-41 can be synthesized through a wide range of synthesis conditions in a wide range of methods. However, in all of these methods, there are four main components: A silica source, a templating agent (i.e., a surfactant), a solvent and a mineralizing agent (an acid or a base).

2.1.1 Silica sources

The synthesis of mesoporous materials predominantly takes place in a basic medium, however, sometimes an acidic medium can also be used. When the synthesis takes place in a basic medium, any silica source can be used including sodium silicate (Na_4O_4Si), sodium meta-silicate (Na_2SiO_3), fumed silica, silica gel and tetraethyl orthosilicate (TEOS). In the case of an acidic synthesis route, however, TEOS is usually the preffered silica source [46, 47].

2.1.2 Surfactants

The term surfactant is the short form of "surface active agent" and refers to a class of chemical compounds known technically as amphiphiles (from two Greek words meaning they are not certain what they like). The molecules of surfactants contain two regions of different characteristics: One part is polar (dipole or charged group), and the other part is non-polar (usually a hydrocarbon or halocarbon chain), [48]. The polar part is hydrophilic in nature and the non-polar part is hydrophobic in nature, hence the molecule self-organizes itself in water in such a way as to minimize contact between incompatible ends [49].

Ionic surfactants such as cetyltrimethylammonium bromide (CTMABr), cetyltrimethylammonium chloride (CTMACl) are the most commonly used templating agents for the synthesis of MCM-41. In general, the use of low-molecular-weight amphiphiles with the formulae $C_nH_{2n+1}(CH_3)_3N^+$ (n = 8-22) or $C_nH_{2n+1}C_5H_5N^+$ (n = 12 or 16) result in the formation of MCM-41 [50,51]. The formation mechanism of MCM-41, by using these surfactants, is based on the electrostatic interactions between the positively charged surfactants and negatively charged silicate species in solution [16].

The pore sizes of MCM-41 materials can be modified in the range of 2-5 nm by varying the alkyl chain length of the surfactant molecules [16, 50-53]. Table 2.1 lists some pore diameter values reported by Grün et al. [54]

Table 2.1 Pore Sizes of MCM-41 Materials Synthesized Using
Different Surfactants (adapted from [54])

Surfactant	Pore diameter (nm) $(4V_p/a_s)$	Pore diameter (nm) ([a])
$C_{12}TMABr$	1.8	2.5
$C_{14}TMABr$	2.6	2.9
$C_{16}TMABr$	3.2	3.3
$C_{18}TMABr$	4.1	3.8
$C_{20}TMABr$	5.0	-[b]

[a] found using d_{100} values and assuming a pore wall thickness of 1.0 nm for the sample
   synthesized with $C_{16}TMABr$.

[b] very broad X-ray diffraction peak.

V_p: specific pore volume, a_s: specific surface area.

obtained for MCM-41 materials using different surfactants with different
alkyl chain lengths. It is seen that the values of the pore diameters increase as
the lengths of the surfactant alkyl chains increase.

2.1.3 Solvent

During the synthesis of MCM-41, water is used as the solvent. The
amount of water added to the synthesis mixture is crucial since it
determines the properties of the silicate and the surfactant mixture formed
during the synthesis. If less than sufficient water is added, a compact
synthesis medium is formed where the precipitation of the MCM-41
crystals becomes difficult since they can not move easily. On the other hand, if
too much water is used as the solvent, the interaction between the
surfactant and silicate molecules becomes weaker and it is not possible to
produce a gel during the synthesis.

2.1.4 Mineralizing agents

The mineralizing agent used can be an acid or a base. Mineralizing agents mineralize the silica sources into soluble species with suitable morphologies capable of associating with surfactant molecules to form various periodic mesophases [55]. For this purpose, sodium hydroxide [56,57], tetramethylammonium hydroxide [17,18] or tetraethylammonium hydroxide [21] can be used as basic additives and HCl, HF or HNO_3 can be used as acidic additives [21, 58].

2.2 Formation Mechanisms of MCM-41 Catalysts

The discovery of the mesoporous M41S family caused several discussions within the Mobil Group for the understanding of the formation mechanisms. Initially, a mechanism similar to zeolite formation was proposed. It was stated that the materials might have been formed by a templating structure or a pore filling agent. For zeolites, the templating structures were discrete molecules and for the M41S family the templating structures were aggregates of molecules [42]. It was proposed by some Mobil researchers that a liquid crystal structure existed prior to the formation of the mesoporous structure. In the case of MCM-41, this would be a hexagonal liquid phase. This simple pathway was not universally accepted within the Mobil Group. Alternatively, another proposal was made which stated that it was the silicate species that caused the formation of the mesoporous structures by organizing the surfactants into various geometries. A group of experiments was designed to see if it was indeed the silicate species that caused the formation of the ordered mesophases. In these experiments, all the experiment conditions were kept the same except for the silicate amount added. By changing only the Surfactant/Si molar ratio, it was possible to obtain all three different mesoporous structures; MCM-41, MCM-48 and MCM–50 [59]. The possibility of any preformed crystalline phase prior to the formation of the silicon phase was excluded since the same surfactant concentration was used in all

experiments (only the amount of silica added to each solution was changed). These data supported the idea that it was the silicate species that caused the assembly of the surfactant molecules to form the mesophases [42].

It was recognized by Mobil researchers and other study groups that there were many similarities between mechanisms of formation of liquid crystals in surfactant-water systems and mechanisms of formation of the members of the M41S family. Hence, in order to understand the mechanisms of formation of the members of the M41S family, it is a priori to understand the chemistry of the surfactant-water systems.

In a surfactant-water system, surfactant molecules are found in various structures depending on their concentrations: At low concentrations, surfactants exist as monomolecules. As concentration increases, they aggregate to form micelles in order to decrease the systems' entropy. The minimum concentration at which molecules aggregate to form micelles is the critical micelle concentration, cmc, [60]. As concentration increases further, hexagonal arrays appear [61]. Then, the next step is the coalescent of adjacent cylinders to produce a lamellar phase. In some cases, a cubic phase which is thought to be made up of networks of rod shaped aggregates [62], appears before the lamellar phase.

Myers et al. [63], suggests that the particular phase present in a surfactant- water system depends not only on the concentration but also on the nature of the surfactant and the environmental parameters. The environmental parameters include temperature, pH, ionic strength of the solution and the valency of the counter ion.

The nature of the surfactant can be described by a dimensionless group called the molecular packing ratio, g, as given in Equation 2.1:

$$g = V_o /al \text{ ....(2.1)}$$

In Equation 2.1, V_o is the topographical volume of the hydrocarbon chain, a is the effective area of the surfactant head group and l is the effective

length of the surfactant chain [64]. The molecular packing parameter, g, is a useful structure-directing index that can be used to predict the geometry of the micellar aggregates to some extent before the synthesis [4].

The aforementioned similarities between surfactant-water systems and mesoporous crystals were recognized by several researchers and several models were developed to explain the formation mechanisms of the mesoporous molecular sieves. In common, all of these models state that the templates formed by the surfactants direct the soluble silicate sources to form the mesoporous structures. How the silicate source interacts with the surfactant is the point where the models diverge from each other [49].

According to Alfredsson et al. [65], who used the results of ^{14}N-NMR spectroscopy to study the synthesis of MCM-41, the addition of the silicate species to the surfactant solution immediately leads to the formation of a hexagonal liquid crystalline assembly. Next, the cylindrical rods are intercalated between the ordered silicate sheets, and finally a transformation into the as-synthesized MCM-41 structure occurs during the aging of the solution [4].

Davis and co-workers [66] suggested that a hexagonal liquid crystal phase is not formed during the synthesis of MCM-41. Instead, MCM-41 formation begins with deposition of two to three monolayers of silicate precursor onto isolated surfactant micellar rods. These silicate-encapsulated rods are randomly ordered and they eventually pack into a hexagonal meso-structure.

Instead of the formation of silicate-covered micellar rods, Steel et al. [67] postulated that the surfactant molecules assemble directly into the hexagonal liquid crystal phase upon addition of the silicate species. The silicates are organized into layers, with rows of cylindrical rods intercalated between layers. Aging the mixture causes the layers to pucker and collapse around the rods, which then transform into a surfactant-containing MCM-41 hexagonal-phase.

A charge density matching model was proposed by Monnier et al.[68] and Stucky et al.[69] suggested that MCM-41 can be derived from a lamellar phase. The initial phase of the synthesis mixture is layered and formed from the electrostatic attraction between the anionic silicates and the cationic surfactant head groups. As the silicate species begins to condense, the charge density is reduced. Accompanying this process, curvature is introduced into the layers to maintain the charge density balance, which transforms the lamellar phase into the hexagonal phase.

The lamellar-to-hexagonal phase conversion also appears in materials called FSM (folded sheet materials) prepared from intercalation of ammonium surfactants in kanemite [70-72]. It is proposed for kanemite-derived materials that after the surfactants are ion-exchanged into the layered structure, the silicate sheets fold around them and condense into a hexagonal mesophase. The final product is claimed to be very similar to MCM-41, with no resemblance to the original kanemite structure. However, Vartuli et al.[73] found that the layered structures are still retained in the kanemite-derived products.

The previous theories have regarded the formation of MCM-41 as a series of events that occur homogeneously in an aqueous solution. Recent work has also shown that MCM-41 may be formed heterogeneously. Regev [74] found, through low temperature transmission electron microscopy (TEM) and small-angle X-ray scattering, that MCM-41 intermediate structures existed in the form of clusters of rodlike micelles wrapped by a coating of silicate. The clusters of elongated micelles were present before precipitation occurred. As the reaction continued, the silicate species diffused to and deposited onto the individual surfaces of the micelles within the cluster and the clusters of elongated micelles eventually became clusters of silicate-covered micelles. In other words, the clusters of micelles served as nucleation sites for the formation of MCM-41 materials.

2.3 Synthesis Methods of MCM-41 Catalysts

After the initial discovery of the M41S family, synthesis and characterization studies of mesoporous materials have continued with increasing number of publications. Several synthesis methods have been developed which have the same basic idea; i.e., the formation of a mesoporous structure as a result of the interaction between a surfactant and a silicate species in the presence of a catalyst (an acid or base) in an aqueous medium. In this section, some of the different synthesis methods found in literature are summarized.

Grün et al. [54] used tetra-n-alkoxysilanes such as TEOS and tetra-n-propoxysilane (TPS) as a silica source, n-alkyltrimethylammoniumbromides and n-alkylpyridinium chlorides as templates in the presence of ammonia as the mineralizing agent. The addition of an alcohol (ethanol or isopropanol) to this synthesis mixture led to the formation of spherical MCM-41 particles which were produced with good reproducibility and in short reaction times.

High quality MCM-41 samples were obtained by Ryoo et al. [75] using the salt effect and these samples had negligible structural losses as judged by X-ray diffraction during heating for 12 h in boiling water.

Lee et al., [76] synthesized MCM-41 materials with high structural stabilities and long range order using ethylamine (EA) as an additive instead of conventional mineralizers such as NaOH and TPAOH. The samples had walls approximately 2 nm thick and they did not loose their structure entirely even after heat treatment at 1000^0C.

A new procedure was developed by Ekloff et al. [77] to synthesize mesoporous materials with controlled porous structure and regular morphology. It was based on the precipitation of the solid product from a homogeneous medium by using cetyltrimethylammonium bromide as the surfactant. The hydrolysis of ethyl acetate decreased the pH which caused the formation of solid particles. This procedure enabled to obtain bimodal silicas which could be used in separation processes or as supports.

2.4 Modified MCM-41 Catalysts

Ordered mesoporous silicas are not often used as catalysts in the purely siliceous form. Instead, additional catalytic functions are introduced by the incorporation of active sites into the silica walls or by the deposition of active species on the inner surfaces of the materials. The advantage of using ordered mesoporous solids such as MCM-41 in catalysis are the relatively large pores which decreases the mass transfer limitations and the exceptionally high surface areas which allows a high concentration of active sites per mass of the material. There are several methods to modify the mesoporous materials in order to give them a new catalytic function [16].

The first method of the modification of the MCM-41 structure is the direct hydrothermal synthesis method in which the metal to be incorporated is directly added to the synthesis mixture. In this method, the silica source, the surfactant and the metal precursor are allowed to react all together in a certain sequence to form a gel and the resulting gel is autoclaved in an etuve for the hydrothermal synthesis stage. During the hydrothermal synthesis stage, the MCM-41 crystals form and precipitate and the mixture obtained from the autoclave yields the uncalcined solid product upon filtration and washing. As a result of the direct hydrothermal synthesis, a relatively homogeneous incorporation of the desired metal into the wall surface of the MCM-41 is achieved [16] and a catalyst with successful redox properties is obtained [78-80].

Another method for the modification of the MCM-41 structure is the substitution of the silicon atoms in the framework with the desired metal ions. In this case, the incorporated metal atoms will be added to the inner surface of the mesopores [20] to form acid or redox active sides which can be used in many different classes of chemical reactions. However, since MCM-41 has amorphous walls, the catalysts thus prepared will not have uniform properties throughout the structure. Instead, the local environments for the incorporated metals will vary throughout the structure and the properties of the resulting

catalyst will resemble the properties of the metal substituted-amorphous silica systems [16].

Another common modification method is impregnation. During impregnation, a support material is contacted with a solution of the precursor of the active phase. Upon drying, the solvent (usually water) evaporates and the precursor of the active phase adheres to the support surface. This method, theoretically, offers the deposition of the active components completely inside the mesopores however some problems (such as the inhomogeneous distribution of the active phase) occur during practical applications [58].

The ion-exchange method is also a common method for the modification of the MCM-41 structure. In order to use this method, the support material has to have an excess negative charge in the framework so that it may adsorb the metal cations. However, in order to generate sufficient negative charge in the framework of MCM-41, it is necessary to incorporate aluminium ions inside the pore walls during the synthesis and this results in a decrease in the stability of the support. Ion exchange procedure has other disadvantages such as long reaction times (since it is a diffusion-limited process with long equilibration times) and limited metal loadings [58].

Chemical Vapor Deposition (CVD), which is another modification method relies on the adsorption of a volatile metal precursor onto the surface of the support material. Upon interaction, the precursor usually decomposes and the desired element deposits onto the support surface [58].

The pore system of MCM-41 with large pore openings also enables the fixation/trapping of various regio- and enantio-selective complexes and this can be advantegous compared to microporous and macroporous supports since the size of the pores can exactly be adapted to the requirements of the anchored species [16].

Finally, (organo)metallic precursors can be applied for the preparation of supported heterogeneous catalysts, via grafting or tethering. During grafting, a precursor complex reacts chemically with a hydroxyl group at the surface of

the support material. As a result, a covalent bond is formed between the metal atom and the support material. Tethering involves the use of both a metal complex and a "spacer". The spacer, is generally a small organic linking agent and reacts with a hydroxyl group of the support surface so that the metal atom becomes complexed to the other end of the spacer. Using grafting or tethering, it is possible to produce truly heterogeneous catalysts. However, these methods are generally very laborious and expensive [58].

2.4.1 V-MCM-41 catalysts

A key advantage possessed by silica is that it has a high surface concentration of pendant silanol groups (in the range of 1 to 2 Si-OH groups per nm^2). This means it is possible to introduce almost a limitless range of elements and compounds into the inner walls of the high surface area MCM-41 materials by anchoring them to the pendant Si-OH groups [20].

From the view-point of catalysis, it is known that the vanadium metal is active in oxidation reactions. Hence, vanadium incorporated MCM-41 materials could be used as active and selective oxidation catalysts.

It has been observed that SiO_2-supported vanadia catalysts show high selectivity to olefins for the oxidative dehydrogenation of short chain alkanes such as ethane [81-85], propane [86] and n-butane [85,87]. Unfortunately, these catalysts usually have a very low concentration of active species due to the low surface area of the support used. Hence, high amounts of catalysts are required to achieve high yields to desired products [88]. As a remedy, high surface area supports must be used to obtain high conversions while keeping the selectivities at the desired level [88]. MCM-41 with its high specific surface area, therefore, is a good candidate for the preparation of vanadium incorporated oxidation catalysts with beneficial oxidation properties.

In the following paragraphs, a summary of the literature related to the syntheses and the uses of vanadium incorporated MCM-41 materials are presented:

Zhang et al [89] the Direct Hydrothermal Synthesis Method (DHT) and Template Ion Exchange Method (TIE) in order to synthesize V-MCM-41 catalysts. They found that the DHT method provided tetrahedrally coordinated vanadium species mainly dispersed on the wall surface and the TIE method provided vanadium sites mainly incorporated into the MCM-41 framework. They also found, using H_2-TPR measurements, that the samples synthesized using the DHT method can be reduced at lower temperatures than those synthesized with the TIE method. Moreover, the introduction of vanadium with the TIE method increased the amount of the weak acid sites while both weak and medium acid sites were decreased up to a certain content with the DHT method. The ethane and propane conversions increased remarkably with the increasing content of vanadium and moderate selectivities to ethylene and propylene were obtained on the catalysts prepared with the TIE method. The same catalysts, however, were not selective for the oxidative dehydrogenation of isobutane. On the other hand, propylene and isobutene were obtained with high selectivities over the DHT catalysts with vanadium contents exceeding 1% by mass. Moreover, acrolein and methacrolein were also formed with considerable selectivity on DHT catalysts with low vanadium contents. It is thought that the medium acid sites which remained in the DHT catalysts played role in the formation of oxygenates through adsorption of alkenes or allyic intermediates.

Pena et al. [88] synthesized vanadium containing (0.3-1% by mass of V) MCM-41 materials with one-pot synthesis and grafting methods using $VOSO_4$ and $VOCl_3$ as vanadium sources, respectively. They characterized the synthesized catalysts with Ar and N_2 Adsorption, XRD, Diffuse Reflectance-UV-VIS (DR-UV-VIS) Spectroscopy and Temperature Programmed Reduction (TPR). They found that vanadium species were in the form of vanadyl ions (VO^{+2}) in the as-prepared samples, while highly dispersed V^{+5} species with tetrahedral coordination were found in calcined materials. Catalytic properties of synthesized samples were tested in the gas phase oxidation of propane to

propene using low propane/oxygen ratios at the temperature range of 500°C - 550°C. It was seen that, in all cases, propylene, CO and CO_2 were the main reaction products although partial oxygenated products (with selectivities lower than 10%) were also obtained. The comparison of the synthesized catalysts with the vanadium-silica systems of similar vanadium contents showed that the vanadium incorporated MCM-41 materials showed higher selectivities to propylene.

Solsona et al. [90] used both a one-pot synthesis method and a wet-impregnation method to synthesize V-MCM-41 catalysts. They found, through NMR studies, that the V-MCM-41 samples showed one type of VO_4 in the as-synthesized samples and two types of mono-dipersed and distorted to various extents VO_4 tetrahedra, chemically bound to the walls of MCM-41, in the calcined and rehydrated samples.

Laha et al. [91] synthesized V-MCM-41 materials with a direct hydrothermal synthesis method using promoters such as phosphate salts. They found that introduction of the promoters reduced the synthesis time considerably and the properties of the MCM-41 materials synthesized using promoters were comparable to those synthesized without using promoters.

Lang et al. [92] synthesized V-MCM-41 materials by the post-synthesis modification of the purely siliceous MCM-41 material in the liquid phase. They found that; using this method, relatively high concentrations of vanadium could be introduced into the structure without affecting the long-range order of MCM-41.

Grubert et al. [93] synthesized V-MCM-41 materials by the one-pot synthesis, chemical vapor decomposition and impregnation techniques. Using XRD patterns, they found that all the samples had well resolved reflections however the impregnated samples had the minimum amount of the amorphous, non-porous by-product. They also found that for all the synthesized samples the vanadium species were dominantly in the form of mononuclear V^v oxide in fourfold tetrahedral coordination and the highest amount of polynuclear V^v

oxide species were found in the samples synthesized with the chemical vapor decomposition method. Finally, they found that the largest amount of reducible V^v species were present in the impregnated samples.

Centi et al. [94] observed low selectivities to benzaldehyde during the oxidation of toluene on the V-MCM-41 catalysts (2 % by mass) although phenol was formed at high reaction temperatures with high vanadium contents.

2.4.2 Mo-MCM-41 catalysts

In the recent years, due to the increasingly severe legislation rules about the specifications of sulphur in the transportation fuels, the development of new molybdenum based catalysts has become greatly important. Hence, several researchers have tried to take advantage of the unique textural properties of the ordered mesoporous materials (high surface area and accessibility) to prepare cobalt- or nickel-promoted catalysts which will disperse the MoS_2 phase. For this and other reasons, many efforts have been undertaken so far to introduce molybdenum into MCM-41 and related materials [58].

In general, the methods used to prepare molybdenum incorporated MCM-41 catalysts can be divided into four main groups: Incorporation during synthesis (direct or one-pot synthesis), thermal spreading, impregnation with a suitable precursor solution and more exotic preparation techniques such as use of electrochemical cells [58].

In literature, the direct synthesis of molybdenum incorporated MCM-41 materials have been frequently studied [95-104]. The method mostly employed involved the incorporation of the molybdate anions into the framework under alkaline conditions with ambient or hydrothermal synthesis conditions [95-99]. Usually very low loadings of molybdenum (below 0.2% by mass) was achieved this way [95-98] except for the study performed by Cho et al [99] who managed to prepare stable Mo catalysts up to Mo/Si ratios (in the solid) of 0.06.

Cho et al. [99] used an alkaline synthesis method where the molybdenum source was $Na_2MoO_4.2H_2O$, the surfactant was CTACl, the silica source was Ludox AS and the mineralizing agents were NaOH and acetic acid. $EDTANa_4$ was also added to the synthesis mixture in order to increase the stability of the produced samples. The reaction gel thus formed was heated at 373^oK for 24 hours for the hydrothermal synthesis stage. The Si/Mo ratios of the obtained products were determined by Atomic Absotion Spectroscopy (AAS). It was seen by XRD patterns that up to Mo/Si ratios (in the solid) 0.06, the MCM-41 structure was not destroyed. However, the nitrogen isotherms obtained indicated that a second pore system, containing slit-shaped pores, might be present in the support and catalysts [58].

Li et al. [105] made use of the thermal spreading technique to synthesize Mo-MCM-41 catalysts as follows: First the MCM-41 molecular sieves were synthesized through an alkaline route and then it was mixed the molybdenum source in an agate mortar for 30 min by hand-grinding. Then, this mixture was treated thermally at 773 K for 24 hours in a temperature programmed furnace. It was found that the nitrogen isotherms of the as-synthesized samples followed the type IV adsorption isotherm of mesoporous materials. Also, the XRD patterns in the range of $10-70^o$ showed that the peaks related to MoO_3 crystals had dissappeared completely for low loadings of molybdenum after the thermal treatment. However, the XRD patterns at low angles ($2\theta = 2-10^o$) showed that the MCM-41 structure was destroyed when molybdenum loadings were higher than 0.25 g/g MCM-41. Hence, with this method it was not possible to incorporate sufficient amounts of molybdenum into the structure.

Wong et al. [106] synthesized MCM-41 materials both with tubular and particulate morphologies and used them as supports for molybdenum catalysts in the ethylbenzene dehydrogenation reaction. The catalysts are prepared by two different methods, namely, solution impregnation and physical mixing followed by calcination. The analysis results showed that the physically mixed

samples showed more structural collapse than the impregnated ones. The reaction results showed that the physically mixed samples had lower rates of deactivation and higher catalytic activities than solution impregnated ones.

Ramirez et al. [107] used the wet-impregnation technique to prepare Co-Mo-Al-MCM-41 catalysts. The synthesized catalysts are found to have surface area values in the range of 167-385 m^2/g and pore volumes in the range of 0.38-0.47 cm^3/g. The dibenzothiophene hydrodesulfurization reaction is carried on these catalysts and it is seen that the catalysts gave higher activities than the catalysts supported on pure alumina.

Rana and Viswanathan [108] prepared Mo-MCM-41 materials both by the direct synthesis and the impregnation methods by using ammonium molybdate as the molybdenum source. XRD patterns and nitrogen isotherms of the as-synthesized catalysts showed that the samples were crystalline with MCM-41 structure and high surface areas. (<900 m^2/g). The catalysts are tested in the oxidation reactions of cyclohexanol and cyclohexane and the samples synthesized by the direct route are found to be more active than those synthesized by the impregnation route.

Co-Mo-MCM-41 catalysts were synthesized by the co-impregnation of $Co(NO_3)_2.6H_2O$ and $(NH_4)_6Mo_7O_{24}$ followed by calcination and sulfidation by Song et al. [109]. For comparison, conventional Al_2O_3-supported sulfided Co-Mo catalysts were also prepared using the same procedure. These catalysts were examined at two different metal loadings in the hydrodesulfurization of a model fuel. It was seen that at 350-375°C under high H_2 pressure (6.9 MPa), sulfided Co-Mo/MCM-41 catalysts showed higher hydrogenation and hydrocracking activities at both normal and high metal loadings whereas Co-Al_2O_3 catalysts showed higher selectivities to desulfurization.

Piquemal et al. [100-101], synthesized Mo-MCM-41 catalysts with variable amounts of molybdenum (VI) in acidic media from MoO_3, aqueous hydrogen peroxide and tetraethyl orthosilicate. The hydrogen peroxide solution was added to dissolve the molybdenum species and eliminate the need

to carefully control the rate of hydrolysis. The synthesized materials were found to have Mo/Si ratios of 0.04 and greater dispersions.

In summary, literature studies on Mo-MCM-41 catalysts show that all synthesis methods have some disadvantages. The application of ion-exchange and impregnation methods are not straightforward. The thermal spreading method is easy however it may result in the collapse of the structures above certain loadings. The direct synthesis method in alkaline medium results in low loadings of molybdenum. Hence, with all these considerations, the direct synthesis method in acidic medium suggested by Piquemal et al. [100-101] seems to be the most successful one among others.

2.5 Non-Oxidative and Oxidative Dehydrogenation Reactions of Ethanol and Methanol

Oxidative dehydrogenation (selective oxidation or partial oxidation) and non-oxidative dehydrogenation reactions of methanol and ethanol have been frequently studied in literature for the production of materials such as formaldehyde, acetaldehyde and acetic acid. In the recent years, these reactions (especially the oxidative dehydrogenation of methanol) have become more important due to the increased demand for the production of hydrogen (these reactions may also produce hydrogen when suitable catalysts and reaction conditions are employed), the clean fuel. In this section, a summary of the literature about oxidative and non-oxidative dehydrogenation of methanol and ethanol are given with emphasis on oxidative dehydrogenation of ethanol.

2.5.1 Non-oxidative dehydrogenation

Non-oxidative dehydrogenation of methanol and ethanol are studied in literature for two important reasons: 1. To simulate and improve the conditions of industrial-scale dehydrogenation reactions. 2. To test new catalysts in terms of their acidic/ basic properties and adsorption characteristics (i.e., as model reactions), [110].

Non-oxidative dehydrogenation reactions (depending on the reaction temperature and the catalyst used) produce one of the following compounds as the main product: Formaldehyde (for methanol dehydrogenation), acetaldehyde or acetic acid (for ethanol dehydrogenation). In these dehydrogenation reactions, hydrogen is also produced however until recent years its production has not been given emphasis. There are also some side products such as methyl formate for methanol dehydrogenation and ethene and diethyl ether for ethanol dehydrogenation. CO and CO_2 can also be formed in both reactions.

If we consider the main products, formaldehyde is one of the world's most important chemicals with an ever increasing production of (2.5-2.7)$*10^7$ tons per year worldwide in the year 2000. It is used for the production of urea-phenolic, melamine and acetal resins [111]. Acetaldehyde is used as a chemical intermediate, principally for the production of acetic acid, pyridine and pyridine bases, peracetic acid, pentaeythritol, butylene glycol and chloral [112]. Acetic acid is used to produce vinyl acetate, cellulose acetate, acetic anhydried, acetate esters, terephtalic acid, chloroacetic acid and textiles [113].

The stiochiometries of the reactions involved in the non-oxidative dehydrogenations of methanol and ethanol are given in Equations 2.1 and 2.2, respectively [111, 114]. Many of these dehydrogenation reactions are reversible and in many cases equilibrium limitations are significant which means that high temperatures are required for high conversions.

Methanol reactions:

$CH_3OH \Leftrightarrow CH_2O + H_2$ ....(2.1.1)

$CH_3O \Leftrightarrow CO + 3/2H_2$ ....(2.1.2)

$2CH_3OH \Leftrightarrow CH_3OOCH + 2H_2$ ....(2.1.3)

Ethanol reactions:

$$CH_3CH_2OH \Leftrightarrow CH_3CHO + H_2 \quad ....(2.2.1)$$

$$CH_3CH_2OH \Rightarrow C_2H_4 + H_2O \quad ....(2.2.2)$$

$$2C_2H_5OH \Leftrightarrow C_2H_5OC_2H_5 + H_2 \quad ....(2.2.3)$$

$$CH_3CH_2OH + H_2O \Leftrightarrow CH_3COOH + 2H_2 \quad ....(2.2.4)$$
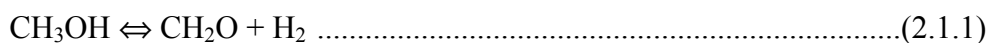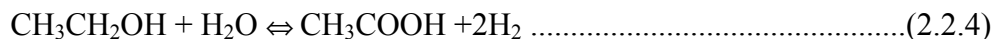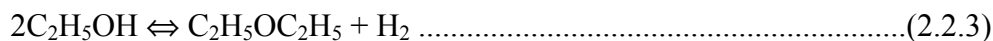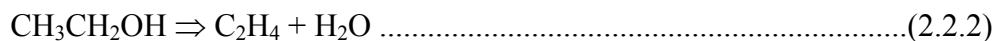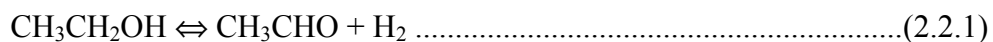
2.5.2 Oxidative dehydrogenation

Similar to non-oxidative dehydrogenation reactions, oxidative dehydrogenation (selective oxidation or partial oxidation) reactions of alcohols are also mainly carried out to produce the corresponding aldehydes. This time, however, oxygen is also supplied to the mixture in the desired ratios and the use of oxygen as an oxidant offers an exothermic reaction and a higher reaction rate, which can lessen the time needed for the apparatus to reach steady state from cold start-up and work under thermo-balanced conditions [111]. In the oxidative dehydrogenation reactions, the equilibrium limitations are less significant than in the non-oxidative dehydrogenation reactions. Hence, these reactions may be carried out at lower temperatures.

The oxidative dehydrogenation reactions of methanol and ethanol to produce the corresponding aldehydes are given in equations 2.3 and 2.4, [114, 115].

$$CH_3OH + \tfrac{1}{2} O_2 \Rightarrow CH_2O + H_2O \quad ....(2.3)$$

$$C_2H_5OH + \tfrac{1}{2} O_2 \Rightarrow C_2H_4O + H_2O \quad ....(2.4)$$

Reactions 2.3 and 2.4 are the main reactions of the oxidative dehydrogenation of ethanol and methanol. The determination of the side reactions and reaction mechanisms require a detailed experimental work.

Tesser et al. [116] tested V_2O_5/TiO_2-SiO_2 catalysts in the oxidative dehydrogenation of ethanol and they proposed the following set of reactions to take place:

$CH_3CH_2OH + \frac{1}{2} O_2 \Rightarrow CH_3CHO + H_2O$ ..(acetaldehyde formation)............(2.5.1)

$CH_3CHO + \frac{1}{2} O_2 \Rightarrow CH_3COOH$ ....(acetic acid formation)...............(2.5.2)

$CH_3COOH + 2O_2 \Rightarrow 2CO_2 + 2H_2O$ ....(total combustion).....................(2.5.3)

$2CH_3CH_2OH + CH_3CHO \Leftrightarrow CH_3CH(OCH_2CH_3)_2 + H_2O$ ....(2.5.4)

(diethylacetal formation)

$2CH_3CH_2OH \Rightarrow C_2H_5OC_2H_5 + H_2O$ ....(diethyl ether formation)..........(2.5.5)
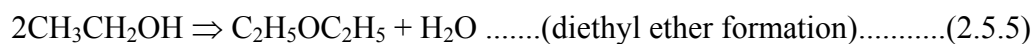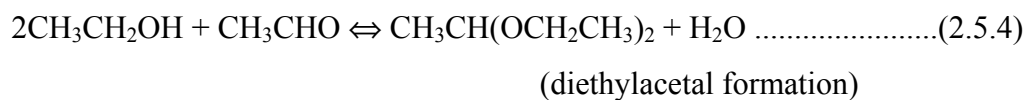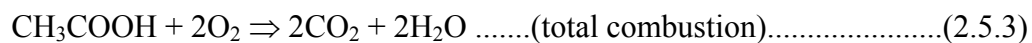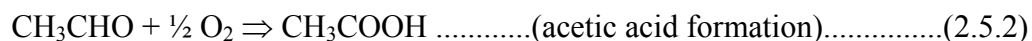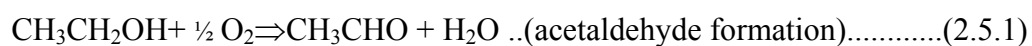
Reactions 2.5.1-2.5.5 represent the selective oxidation of ethanol to acetaldehyde, oxidation of the produced acetaldehyde to acetic acid, oxidation of the produced acetic acid to carbon dioxide and water (total combustion), reaction of ethanol with the produced acetaldehyde to give diethyl acetal and the decomposition of ethanol to diethyl ether and water, respectively.

CHAPTER 3

EXPERIMENTAL METHODS, CHARACTERIZATION TECHNIQUES AND EXPERIMENTAL SYSTEM

In this study, it was aimed to synthesize large surface area vanadium and molybdenum incorporated MCM-41 molecular sieves to be used in a selective oxidation reaction. Hence, literature was revised to find recipes where vanadium or molybdenum incorporated MCM-41 materials were synthesized to be used in selective oxidation reactions. The one-pot alkaline synthesis procedure given by Zhang et al. [89] was found to be useful since it involved the synthesis of vanadium incorporated MCM-41 materials with desirable properties (such as high surface areas and good XRD patterns) that were later used in the selective oxidation reactions of ethane, propane and isobutane.

3.1 Synthesis of the MCM-41 Catalysts

The original one-pot alkaline synthesis recipe given by Zhang et al. [89] had some missing points like the total amount of water to be used, the dissolution temperature of the surfactant, the details of the washing procedure (such as the final value of the pH of the filtrate) and the details of the calcination step. These important details were determined experimentally. Then, the reagents given in Section 3.1.1 and the recipe given in Section 3.1.2 were used to synthesize the purely siliceous MCM-41 materials.

The recipe given in Section 3.1.2 illustrates that the procedure for the synthesis of MCM-41 consists of nine different steps. In the first step, the surfactant is solubilized in water to form a solution. The amount of surfactant given in the recipe (i.e., 26.4 gram) is not soluble in the amount of water given

(i.e., 150 gram) at room temperature. Hence, the surfactant-water system should be heated on a hot plate to dissolve the surfactant. Heating up to 28°C is sufficient since at this temperature the surfactant-water system forms a true solution.

The second step of the synthesis procedure is the addition of the surfactant solution to the silica source. It is important, at this stage, to add the surfactant solution slowly to the silica source so that a homogeneous gel can form with no undissolved species.

The third step after the formation of the gel is the addition of HCl to the synthesis mixture for the adjustment of the pH to 11. The pH of the gel formed in step 2 is usually around 11.4 and some amount of HCl must be added to the synthesis mixture in order to reduce the pH to 11.0 which is the optimum value for the precipitation of the MCM-41 crystals.

The fourth step in the procedure is the stirring of the formed gel for an additional hour in order to get rid of any remaining undissolved species.

The fifth step is the transfer of the formed gel into an autoclave. It is very important to keep the gel composition the same throughout the synthesis procedure by preventing the loss of water vapor and so an autoclave is used to prevent the loss of water vapor from the system.

The sixth step in the procedure is the hydrothermal synthesis stage which takes place in an etuve at 120°C for 96 hours. This is the step where the MCM-41 crystals form and precipitate.

The seventh step is the filtration and the washing stage. In this stage, deionized water must be preferrably used since the aim is to obtain an alkaline-free solid product. It is desired (ideally) to decrease the pH to the neutral value of 7.0; in order to get rid of any excess surfactant molecules or OH⁻ ions that may be present.

Eight step is the drying of the washed product. The solid product may be dried preferrably in a vacuum etuve for 24 hours at 40°C or a longer time at room temperature.

Ninth step is the calcination stage where dry air is passed over the product at a flow rate ≥ 1 l/min. The flow rate of the dry air is important since it affects the final product properties.

3.1.1 Reagents used

1. Aqueous sodium silicate solution (27 wt% SiO_2 and 14wt% NaOH, Aldrich) as the silica source.
2. CTMABr (cetyltrimethylammonium bromide), (powder, 99% pure, Sigma) as the surfactant.
3. HCl (4 N solution prepared in the lab) to adjust the pH of the synthesis mixture.
4. Deionized water (due to pH considerations, deionized water with neutral pH were used for the syntheses of MCM-41 materials).

3.1.2 Recipe used

1. A surfactant solution was prepared by dissolving 26.4 grams of surfactant in 150 gram of water at 28^oC.
2. After the surfactant solution was formed, it was added to 22.6 ml of sodium silicate solution slowly with continuous stirring.
3. The pH of the gel formed at step 2 was around 11.4 and it was lowered to 11.0 by adding sufficient amount of 4 N HCl.
4. The gel was mixed for an additional hour in order to get rid of any remaining undissolved species.
5. After the mixing step, the gel was transferred into a teflon lined stainless steel autoclave.
6. The autoclave was placed in an etuve for 96 hours at 120^oC for the hydrothermal synthesis stage.
7. The autoclave was removed from the etuve and discharged. The discharged mixture of mother liquor and precipitated solid product was filtered and washed with deionized water until the pH of the filtrate (ideally) fell to 7.

8. The washed product was dried in a vacuum etuve at 40$^{\text{o}}$C for 24 hours.

9. The dried product was calcined in a flow of dry air by heating from ambient temperature to 550$^{\text{o}}$C at a heating rate of 1$^{\text{o}}$C/min and keeping at 550$^{\text{o}}$C for 6 hours.

3.2 Synthesis of the V-MCM-41 Catalysts

V-MCM-41 catalysts were also synthesized by using a modified version of the one-pot alkaline synthesis recipe given by Zhang et al [89].

The recipe used was similar to the recipe used for the synthesis of the purely siliceous MCM-41 catalysts. The only modifications were in the amount of water added and the dissolution temperature of the surfactant-metal-precursor solution. More water (165 gram) was added to the synthesis mixture and a higher dissolution temperature (in the range of 28-40$^{\text{o}}$C) was preferred since the presence of the metal precursor decreased the solubility of the surfactant.

3.2.1 Reagents used

1. Aqueous sodium silicate solution (27 wt% SiO_2 and 14wt% NaOH, Aldrich) as the silica source.

2. CTMABr (cetyltrimethylammonium bromide), (powder, 99% pure, Sigma) as the surfactant.

3. Vanadyl sulfate hydrate ($VOSO_4.xH_2O$, Aldrich) and ammonium vanadate (NH_4VO_3, Merck) as the vanadium sources.

4. HCl (4 N solution prepared in the lab) to adjust the pH of the synthesis mixture.

5. Deionized water as the solvent.

3.2.2 Recipe used

1. First, 26.4 grams of surfactant was added to ~165 grams of deionized water with moderate heating and continuous stirring.

2. While the surfactant solution was stirred on the hot plate, the vanadium source was also added slowly. The amount of vanadium to be added was determined according to the desired V/Si molar ratio in the solution. The temperature of the hot plate was kept at a suitable temperature in the range of 28-40°C to enhance the solubility of the surfactant + metal precursor system.

3. The surfactant + vanadium-precursor solution was added to 22.6 ml of the sodium silicate solution slowly with continuous stirring.

4. A gel or suspension was formed at this stage and the pH of the formed gel or suspension was around 11.4. Hence, a few drops of 4 N HCl was added to decrease the pH to 11.

5. The formed gel was mixed for an additional hour in order to get rid of any remaining impurities. When a homogeneous gel was formed, it was transferred to a teflon lined stainless steel autoclave.

6. The autoclave was placed in an etuve for the hydrothermal synthesis stage and it was kept in the etuve for 96 hours at 120°C.

7. The formed slurry was filtered and washed with deonized water till the pH of the filtrate (ideally) fell to 7.0.

8. The wet solid product was dried in a vacuum etuve for 24 h at 40°C.

9. The dried product was calcined by heating from ambient temperature to 550°C in a continuous flow of dry air with a ramp rate of 1°C/min. It was kept at 550°C for six more hours.

3.3 Synthesis of the Mo-MCM-41 Catalysts by the Alkaline Route

Molybdenum incorporated MCM-41 catalysts (Mo-MCM-41 catalysts) were also synthesized by using a modified version of the recipe given by Zhang et al [89]. The developed recipe was similar to the recipe given in Section 3.2.2 for the synthesis of the V-MCM-41 catalysts.

3.3.1 Reagents used

1. Aqueous sodium silicate solution (27 wt% SiO_2 and 14wt% NaOH, Aldrich) as the silica source.
2. CTMABr (cetyltrimethylammonium bromide), (powder, 99% pure, Sigma) as the surfactant.
3. Ammonium molybdate tetrahdrate $((NH_4)_6Mo_7O_{24}. 4H_2O$, Aldrich) as the molybdenum source.
4. 1 M NaOH to adjust the pH of the synthesis mixture.
5. Deionized water as the solvent.

3.3.2 Recipe used

1. First, a surfactant solution was prepared by dissolving 26.4 g surfactant (CTMABr) in 150 grams of deionized water with moderate heating.
2. The molybdenum source was dissolved in 15 grams of deionized water with moderate heating.
3. The molybdenum solution was added slowly to the surfactant solution with continuous stirring. The amount of molybdenum to be added was determined according to the desired Mo/Si molar ratio in the solution.
4. The surfactant + molybdenum precursor mixture was heated moderately (not exceeding 40^oC) in order to form a homogeneous solution; however, it was not possible to obtain a homogeneous solution and a suspension was formed during the syntheses of all Mo-MCM-41 samples.
5. The molybdenum+surfactant suspension was added to 22.6 ml of sodium silicate solution slowly with continous stirring to form a new suspension of the three reagents.
6. The pH value of the new suspension was below 11 and it was adjusted to 11 by adding sufficient amount of NaOH.
7. The suspension was mixed for an additional hour (with moderate heating not exceeding 40^0C); however it was not possible to dissolve the suspended species.

8. The suspension was transferred into a teflon-lined stainless steel autoclave and the autoclave was placed into an etuve. The etuve was kept at 120°C for 96 hours for the hydrothermal synthesis stage.

9. The autoclave was removed from the etuve and discharged. The obtainedslurry was filtered and washed with deionized water until the pH of the filtrate (ideally) fell to 7.

10. The washed sample was dried at room temperature for 24 hours.

11. The dried sample was calcined in a flow of N$_2$ by heating from ambient temperature to 550^{0}C with a ramp rate of 1^{0}C/min and keeping at 550^{0}C for six hours in a flow of dry air.

3.4 Synthesis of the Mo-MCM-41 Catalysts by the Acidic Route

In order to see the effect of the pH of the synthesis medium on the properties of the obtained products, Mo-MCM-41 catalysts were also synthesized by using a modified version of the one-pot acidic synthesis method given by Piquemal et al. [101-102] with the reagents and the recipe given in Sections 3.4.1 and 3.4.2., respectively.

3.4.1 Reagents used

1. Aqueous sodium silicate solution (27 wt% SiO$_2$ and 14wt% NaOH, Aldrich) as the silica source.

2. CTMACl (cetyltrimethylammonium chloride), (50 wt% solution in propanol and water) as the surfactant.

3. Ammonium molybdate tetrahydrate as the molybdenum source.

4. Hydrogen peroxide solution (35wt% solution, Merck) as the solubilizing agent.

5. HCl (37wt% solution, Merck) to provide an acidic medium.

6. Deionized water as the solvent.

3.4.2 Recipe Used

1. Sufficient amount of ammonium molybdate tetrahydrate was dissolved in a few mililiters of H_2O_2 solution (the ammonium molybdate tetrahydrate and hydrogen peroxide amounts were adjusted according to the desired Mo/Si molar ratio in the synthesis mixture) by stirring continuously at 45^oC for 1 hour.

2. To a mixture of 110 ml HCl and 350 ml deionized water was added 12 ml of CTMACl solution with continuous stirring.

3. 22.6 ml of sodium silicate solution was added to the mixture in step 2 with continuous stirring.

4. The dissolved molybdenum species in step 1 was added slowly to the acid+surfactant+silica mixture. A yellow suspension was formed at this stage.

5. The suspension was stirred moderately (200 rpm) for one more hour.

6. The precipitated product was recovered by filtration and washed with deionized water until the pH of the filtrate (ideally) fell to 7.

7. The washed product was dried at room temperature for 24 hours.

8. The dried product was calcined by heating from ambient temperature to 550^0C with a ramp rate of 1^0C/min in a flow of N_2 and keeping at 550^0C for six hours in a flow of dry air.

3.5 Characterization Techniques

MCM-41, V-MCM-41 and Mo-MCM-41 catalysts synthesized in this work were characterized by X-Ray Diffraction (XRD), Nitrogen Physisorption, Helium Pycnometry, Energy Dispersive X-Ray Spectroscopy (EDS), Atomic Absorption Spectroscopy (AAS), SEM (Scanning Electron Microscopy) and Atomic Force Microscopy (AFM) in order to determine the crystalline patterns; BET surface areas, BJH pore diameters and BJH pore volumes; solid densities; Metal/Si molar ratios in the bulk, the shapes and distributions of the particles and the dimensions of the particles, respectively.

3.5.1 X-ray diffraction (XRD)

MCM-41 has an ordered lattice consisting of a hexagonal array of pores thus XRD can be used to characterize the material structurally although it has amorphous walls. An XRD pattern for the MCM-41 material typically shows three to five reflections at low angles ($2\theta \cong 2.0^o$ to $2\theta \cong 7.0^o$).

The XRD patterns of the MCM-41 catalysts synthesized in this study are obtained using a Philips PW 3040 diffractometer with a Cu K_α radiation source (wavelength 0.15406 nm) using a step size of 0.02 and a scan speed of 0.025 (2θ/s). The scanning of the catalysts is started from the low 2θ value of 1^oC in order to obtain the low angle characteristic peaks.

3.5.2 Nitrogen physisorption

Nitrogen physisorption experiments help to determine physical properties such as pore size, pore volume, specific surface area and the distribution of pores (relative amounts of micro-, meso- and macropores) [58].

The nitrogen adsorption and desorption isotherms obtained from a nitrogen physisorption analysis can be used to calculate the Brunauer, Emmett and Teller (BET) surface areas of the samples by using the BET method. In addition, the Kelvin equation can be used to determine the pore diameter of the samples and the Barrett, Joyner and Halenda method (BJH-method) can be used to determine the pore size distributions by using the nitrogen adsorption and desorption isotherms [58].

In this study, the nitrogen physisorption experiments were carried on a Micrometrics/ASAP 2000 sorptometer. This sorptometer had two ports: The first port contained a metal loop which was immersed into a liquid nitrogen container during the experiments in order to cool the system. The sample cell, which contained the sample to be analyzed, was connected to the second port. The sample cell was also immersed into a liquid-nitrogen container in order to prevent the heating of the sample and the sample cell. The samples to be

35

analyzed were outgassed in a vacuum etuve at 110°C overnight priror to the analysis. During the nitrogen physisorption experiments, 0.1-0.2 grams of sample in powder form was put into a sample cell for the analysis.

3.5.3 Helium Pcynometry

Helium pcynometry is used to obtain the solid densities of porous materials. Helium, can enter even the smallest pores, hence, it can be used to measure the skeletal density (volume per mass) of the analyzed materials. Then the skeletal density is used in the estimation of the solid density values [117].

The solid density values of the catalysts synthesized in this study are obtained on a Micrometrics Multivolume Pcynometer 1305 and the results are given in Tables 4.1, 4.4 and 4.7.

3.5.4 Energy dispersive x-ray spectroscopy

Energy dispersive x-ray spectroscopy (EDS) identifies elemental compositions of materials imaged in a Scanning Electron Microscope (SEM) for all elements which have an atomic number greater than Boron. Most elements are detected at concentrations of order 0.1% [118]. An EDS attachment to a SEM permits the detection and identification of X-rays produced by the impact of the electron beam on the sample thereby allowing qualitative and quantitative elemental analysis. The electron beam of the scanning electron microscope is used to excite the atoms in the surface of a solid. These excited atoms produce characteristic X-rays which are readily detected. By utilizing the scanning feature of the SEM, a spatial distribution of elements can be obtained [119].

In order to apply EDS for characterization of a sample following requirements should be met: Insulating samples must be coated with a thin conductive film. The sample prepared should have diameter less than 125 mm and a height less than 40 mm. For the quantitative analysis, the standard materials of known concentrations should be available for comparison for best

results. Also, for quantitative analysis, samples should be flat, polished and homogeneous [119].

The unique advantages of using the EDS analysis involve rapid identification of particles, films, and unknown bulk materials; very fast elemental images and line scans; and excellent first look technique for new problems [119].

In a surface analysis method, microscopic chemical and physical probes are used which give information about the surface region of a sample. The probed region may be the extreme top layer of atoms (the only true surface), or it may extend up to several microns beneath the sample surface, depending on the technique used [120]. In an EDS analysis, the penetration depth of the produced electrons range between 0.3-10 microns [121]. Hence, EDS may be considered as a surface analysis method or a bulk analysis method depending on the sizes of the particles examined.

The EDS patterns of the V-MCM-41 and Mo-MCM-41 catalysts synthesized in this work are obtained on a JSM-6400 Electron Microscope (JEOL), equipped with NORAN System 6 X-ray Microanalysis System and Semafore Digitizer and the results are given in Sections 4.2.2, 4.3.3 and 4.4.2.

3.5.5 Atomic absorption spectroscopy (AAS)

Atomic absorption spectroscopy (AAS) determines the presence of various metals in liquid samples. It also measures the concentrations of the metals in the samples. Typical concentrations range in the low mg/liter range [122].

In their elemental form, metals will absorb ultraviolet light when excited by heat. Each metal has a characteristic wavelength that will be absorbed. The AAS instrument searches a particular metal by focusing a beam of UV light at a specific wavelength through a flame and into a detector. The sample of interest is aspirated into the flame. If that metal is present in the

sample, it will absorb some of the light reducing its intensity. The detector will measure this change in the intensity and a a computer data system will convert the change in the intensity into absorbance [122].

The absorbance will increase as the concentration increases. Hence, a calibration curve can be constructed for each metal by using various standards of known concentrations on the AAS and observing the absorbances. Then, the desired samples can be analyzed for their metal concentrations by using the previously-obtained calibration curves [122].

Two AAS analyses are performed on a PU9200X Philips Atomic Absorption Spectrophotometer in this study in order to determine the vanadium content of two different V-MCM-41 catalysts (see Section 4.2.3).

Before the AAS analyses, the two V-MCM-41 catalysts are dissolved in a mixture of HF and HNO_3, (a mixture with the volumetric ratio of 1:4, respectively). This mixture is placed in a teflon-lined stainless steel autoclave. The autoclave is kept in an etuve at $423^{o}K$ for 2 hours. After this acid digestion step, the mixtures are analyzed by the AAS technique to determine vanadium contents. Then, the SiO_2 contents are determined by using the gravimetric titration method. As a result of the AAS and gravimetric titration analyses, the results given in Table 4.3 in Section 4.2.3 are obtained.

3.5.6 Scanning electron microscopy (SEM)

Scanning electron microscopes use a beam of highly energetic electrons to examine objects on a very fine scale. This examination can yield the following information [123]:

Topography: The surface features of an object or "how it looks", its texture; detectable features limited to a few nanometers.

Morphology: The shape, size and arrangement of the particles making up the object that are lying on the surface of the sample or have been exposed by grinding or chemical etching; detectable features limited to a few nanometers.

Composition: The elements and compounds the sample is composed of and their relative ratios, in areas ~ 1 micrometer in diameter.

Crystallographic Information : The arrangement of atoms in the specimen and their degree of order; only useful on single-crystal particles >20 micrometers.

In all, it can be concluded that Scanning Electron Microscopy (SEM) is an analysis technique useful for the examination of the particle shapes, properties, arrangements and crystal structures (for large particles usually in the scale of micrometers). In order to examine, however, the structure of the individual particles, i.e, the pores within the particles, another method with higher magnification such as TEM (Transmission Electron Microscopy) is needed.

In this study, the SEM photographs are obtained on a Philips XL 30S FEG microscope for a purely siliceous MCM-41 catalyst and two vanadium incorporated MCM-41 catalysts as given in Sections 4.1.3 and 4.2.6.

3.5.7 Atomic force microscopy (AFM)

Atomic Force Microscopy (AFM) provide topographic information down to the Angstrom level. Additional properties of the sample, such as thermal and electrical conductivity, magnetic and electric field strength, and sample compliance can simultaneously be obtained using a specialty probe. Many applications require little or no sample preparation [124].

Data output is either a three dimensional image of the surface or a line profile with height measurements. The surface roughness parameters of Ra or RMS are also available with either of the above outputs. Other types of feature analysis include Partical Grain Size Analysis, Bearing Ratio, Fractal Dimension, Power Spectrum, and Fast Fourier Transform [124].

In this work, The AFM photographs are obtained on a MMAFM-2/1700EXL microscope and the results obtained are given in Sections 4.1.4 and 4.2.7.

3.6 Use of the Synthesized Catalysts in the Selective Oxidation of Ethanol

The V-MCM-41, MCM-41 and Mo-MCM-41 catalysts synthesized in this study are tested in the selective oxidation of ethanol which is an industrially important reaction for the production of acetaldehyde.

3.6.1 Experimental system

The catalysts synthesized in this study are tested in the selective oxidation of ethanol in a differential tubular flow reactor. The stainless steel tubular flow reactor (internal diameter 0.91 cm) is inserted into a temperature-programmed tubular furnace for the adjustment of the reaction temperature. Liquid ethanol is pumped by a syringe pump to an evaporator, placed in a constant temperature oven in which the gaseous ethanol is mixed with helium and oxygen gases. The evaporation chamber is kept at a temperature in the range of 150 ^{o}C -170°C. The gaseous mixture of ethanol, helium and oxygen leaving the evaporator enters the reactor where the reaction takes place. The products leaving the reactor go to the gas chromotograph which is connected in series with the reactor for the analysis of the product distributions. All the connection lines are heated and isolated to prevent the condensation of ethanol. (A schematic diagram of the experimental system is given in Figure 3.1).

The gas chromotograph used is a Varian CP 3800 GC equipped with a Poropak T column for the separation of the products. Helium is used as the carrier gas and a pneumatic gas sampling valve kept at 225°C is operated for the sampling of the product mixture.

3.6.2 Reagents and experimental conditions

High purity oxygen and helium gases and liquid ethanol (99% pure, Aldrich) are used in the reaction experiments.Each experiment is perfomed by using 0.2 gram of the selected catalyst. The catalyst is placed in the middle of the reactor to prevent the effects of temperature gradients and it is fixated by using glass wool.

Most of the experiments are carried out at a constant Gas Hourly Space Velocity (GHSV) of 64.7 h^{-1}. The calculation of the GHSV values using the reactor dimensions and the inlet flow rates of the reactants are given in Appendix A.
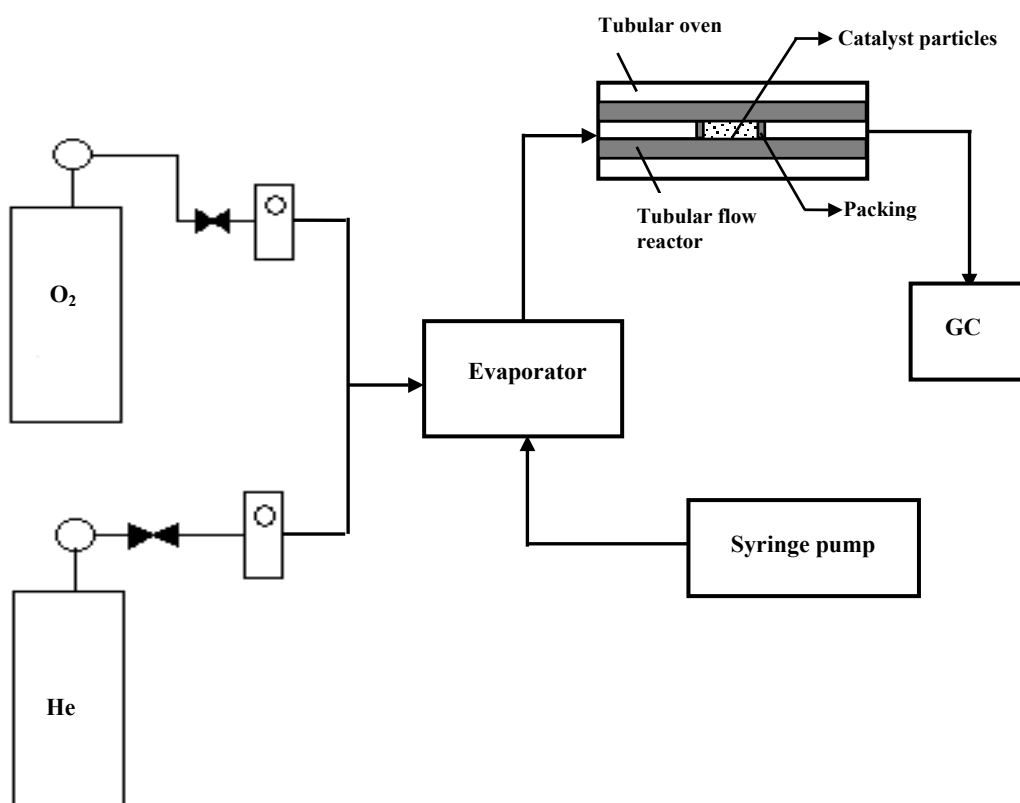
Fig. 3.1 Schematic diagram of the experimental system

The reaction temperatures varied between 150°C -400°C. The evaporation chamber is kept in the temperature range of 150°C -170°C and the heating tapes are kept at a temperature in the range of 125°C -150°C.

The TCD detector and the gas sampling valves are kept at 200°C and 225°C, respectively. A temperature-ramped program is written for the

separation of the products in the Poropak T column. The programme started at 75°C. The column is kept at this temperature for four minutes and then it is heated to 175°C with a ramp rate of 20°C/min. This program lasted nineteen minutes during which all the peaks corresponding to the main and side products are obtained. The analyses of the product samples are performed after the attainment of steady state conditions. For each data point, the sampling of the products are repeated at least twice.

The O_2/EtOH feed ratios are changed in the range of 0.083 to 2.0 in order to provide lean, stoichiometric and excess oxygen conditions.

In some experiments O_2 is not utilized and only ethanol and helium are passed over the catalysts, (i.e., non-oxidative dehydrogenation). In some other experiments, carbon dioxide is as used as the oxidant instead of oxygen.

The peaks obtained on the Gas Chromotograph are calibrated using calibration mixtures and calibration factors are evaluated experimentally. These calibration factors are given in Table B.1 in Appendix B and their values are checked from time to time during the experiments.

CHAPTER 4

RESULTS AND DISCUSSIONS

MCM-41, V-MCM-41 and Mo-MCM-41 catalysts are synthesized in this study by using the recipes given in Sections 3.1.2, 3.2.2, 3.3.2 and 3.4.2. The synthesized catalysts are named according to their synthesis methods and their Metal/Si molar ratios (in the solution) as given in Tables C.1 and C.2 in Appendix C. The nomenclature given in these tables is used throughout the following sections. The synthesized catalysts are characterized by XRD, Nitrogen Physisorption, Helium Pycnometry, EDS, AAS, SEM and AFM techniques described in Sections 3.5.1-3.5.7. Then, some selected catalysts are tested in the selective oxidation of ethanol in the temperature range of 150°C to 400°C at the O_2/EtOH feed ratios of 0.083 to 2.0.

4.1 Characterization of the MCM-41 Catalysts

Two purely siliceous MCM-41 catalysts (see Table C.1 in Appendix C for the nomenclature) are synthesized using the one-pot alkaline synthesis recipe given in Section 3.1.2. These catalysts are characterized by XRD, Nitrogen Physisorption, Helium Pycnometry, SEM and AFM methods.

4.1.1 XRD patterns

The XRD patterns corresponding to sample 1 and sample 2 (see Table C.1 in Appendix C for the properties of these samples) are given in Figure 4.1. It is seen that; the characteristic peak corresponding to $2\theta \cong 2.5^{\circ}$ is obtained for both samples along with some secondary peaks. The secondary
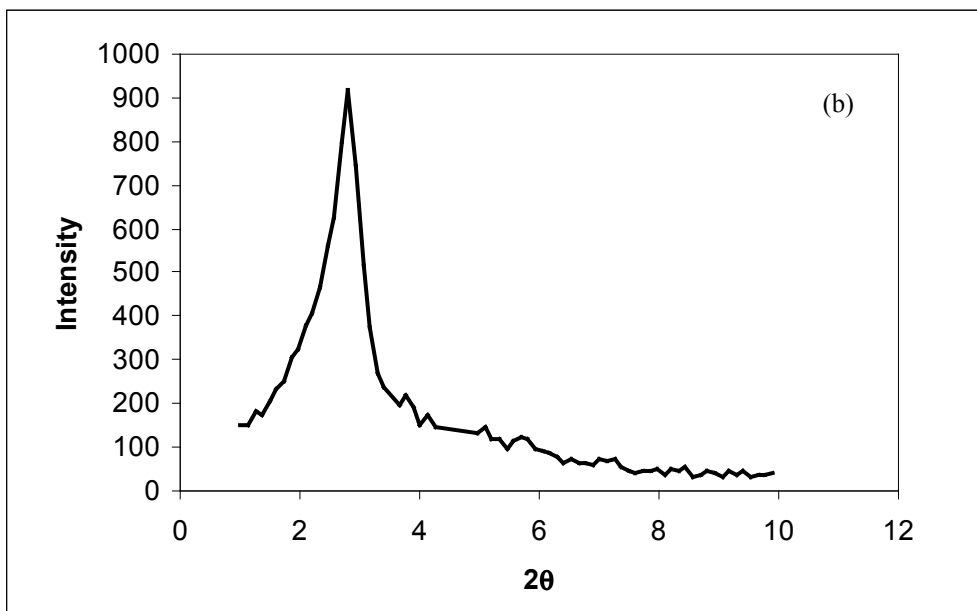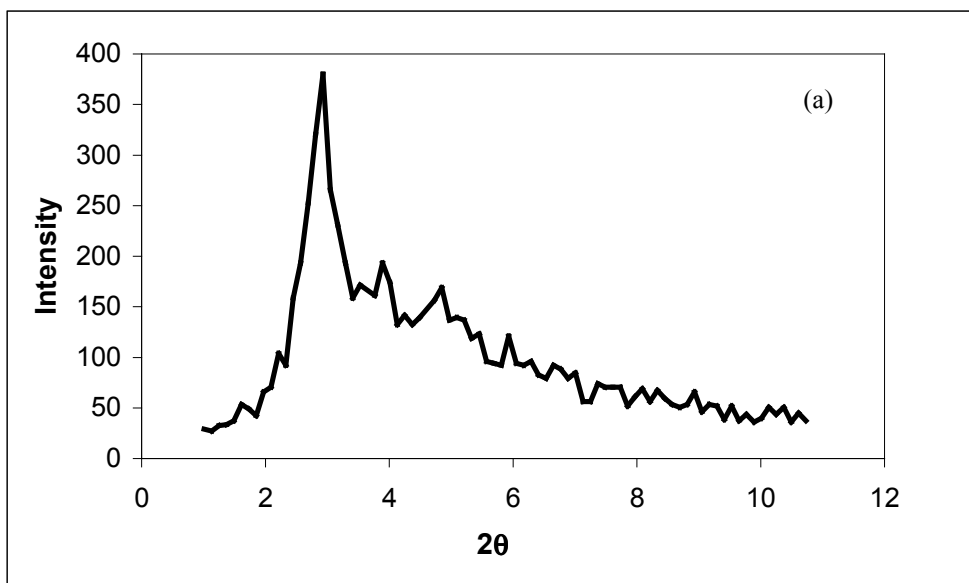
Fig. 4.1 XRD patterns of (a) sample 1 and (b) sample 2

peaks are obtained at the 2θ values of 3.89°, 4.85° and 5.93° for sample 1. For sample 2, on the other hand, the secondary peaks are obtained at the 2θ values of 3.77°, 4.13° 5.09° and 5.81° for Cu K_α radiation of wavelength 0.15406 nm.

A typical MCM-41 material synthesized should have three reflections corresponding to 2.49°, 4.27° and 4.93°. A fourth peak corrresponding to 6.50° may sometimes be present. If the synthesized material is of high quality a fifth peak corresponding to 7.35° may also be present, [125], (all these 2θ values also correspond to Cu K_α radiation of wavelength 0.15406 nm).

The 2θ values obtained for the synthesized samples and the expected 2θ values (listed in the paragraph above) do not match very well with each other especially for the secondary peaks. This is due to the fact that during the syntheses of sample 1 and sample 2, teflon bottles, which allowed the escape of water vapor, were used instead of autoclaves. Thus, the initial gel composition could not be preserved and a crystalline structure could not be obtained.

The XRD data obtained for MCM-41 materials is useful in two senses: First of all, it is used to identify the material synthesized and secondly, the 2θ values corresponding to the most intense peaks may be used in the Bragg's law (Equation 4.1) to calculate the d-spacing, d_{100}, values. The d_{100} values may then be used to determine the lattice parameter "a" (the distance between two pore centers) and the pore wall thickness δ as shown in Appendix D.

$$n\lambda = 2d\sin(\theta) \quad\text{...(4.1)}$$

4.1.2 Physical properties

The BET specific surface areas, BET S.A., the BJH adsorption pore diameters, d_p, and the BJH adsorption pore volumes, V_p, of the synthesized MCM-41 catalysts are found using their nitrogen adsorption isotherms (In Appendix D, detailed information about the nitrogen isotherms of MCM-41 type materials is given) . The results given in Table 4.1 are obtained.

Table 4.1 Physical Properties of the Synthesized MCM-41 Catalysts

Sample ID	BET S.A. (m^2/g)	ρ_s (g/cm^3)	ρ_{app} (g/cm^3)	Porosity $\in$	BJH Ads. V_p (cm^3/g)	BJH Ads. d_p (nm)	$d_{(100)}$ (nm)	lattice param. "a" (nm)	Pore wall thickness δ (nm)
Sample 1	1400	1.9	0.66	0.66	1.00	2.7	3.03	3.49	0.94
Sample 2	1452	2.0	0.67	0.67	1.01	2.7	3.08	3.56	0.96

Table 4.1 also contains the solid density, ρ_s, apparent density, ρ_{app}, d-spacing, d_{100}, lattice parameter, a, and pore wall thickness, δ, values.

The d-spacing, d_{100}, values are estimated using the Bragg's Law given in Equation 4.1. The ρ_s values are estimated using helium pycnometry data. The estimation of the apparent density, ρ_{app}, porosity, $\in$, lattice parameter, a, and pore wall thickness, δ, values are given in Appendix D.

It is seen by observing the values given in Table 4.1. that; the produced samples have high porosities around 70%. The solid density and apparent density values are very close to each other for the two samples. The pore diameters are around 3 nm as expected due to the surfactant used, i.e., CTMABr. The pore wall thickness values are $\cong$ 1.0 nm as again expected due to the surfactant used, i.e., CTMABr, [126].

It is concluded that the one-pot alkaline synthesis method is a succesful procedure that results in the synthesis of high surface area MCM-41 materials with reproducible properties.

4.1.3 SEM photographs

In Figures 4.2-4.4, the SEM photographs of sample 1 are given. In these figures, the particle shapes and distributions are seen. It is also seen that the particles have porous structures, however, the individual pores are not detectable due to the magnification limitations.

Fig 4.2 SEM photographs of sample 1 at the 2 µm scale
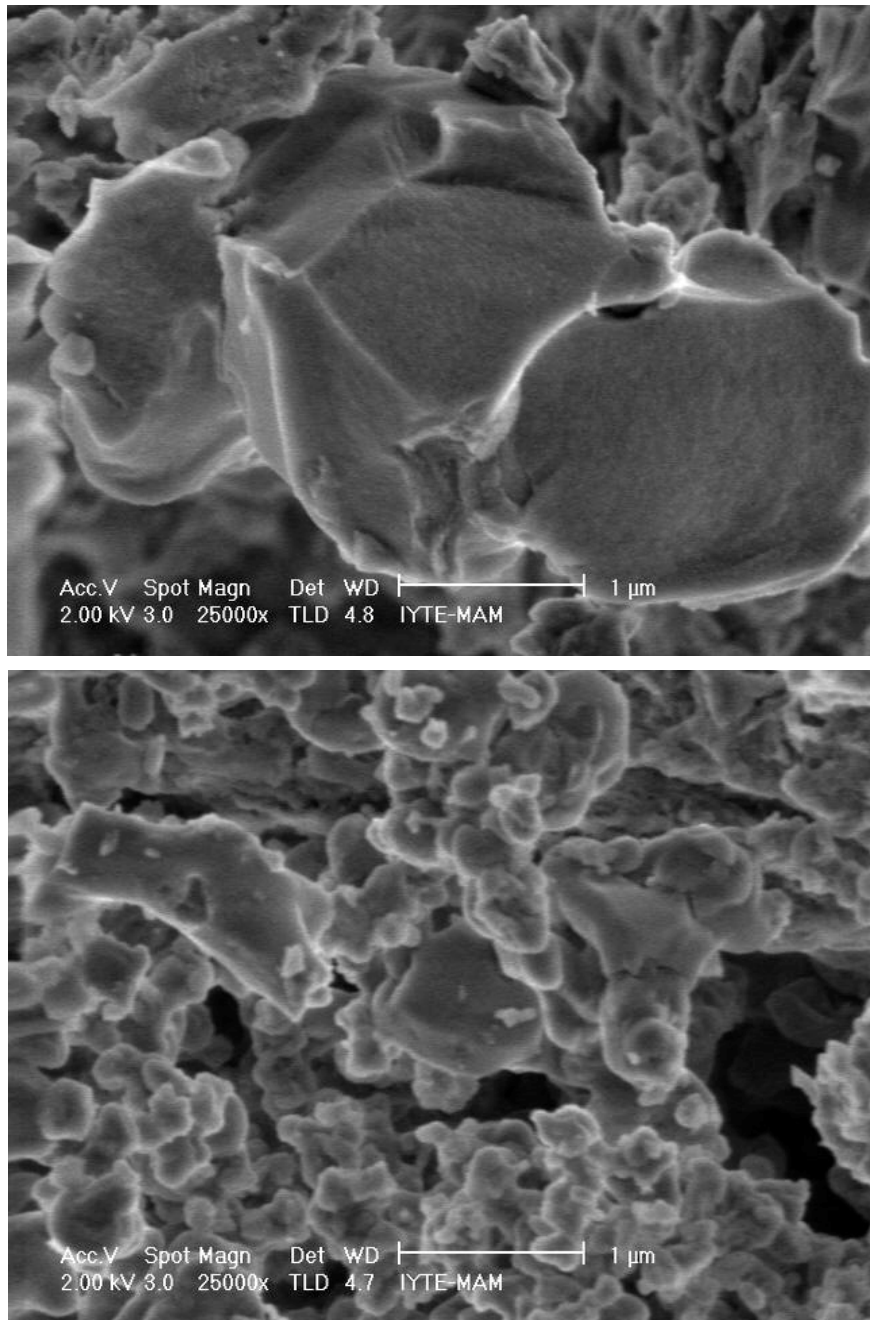
Fig 4.3 SEM photographs of sample 1 at the 1 μm scale
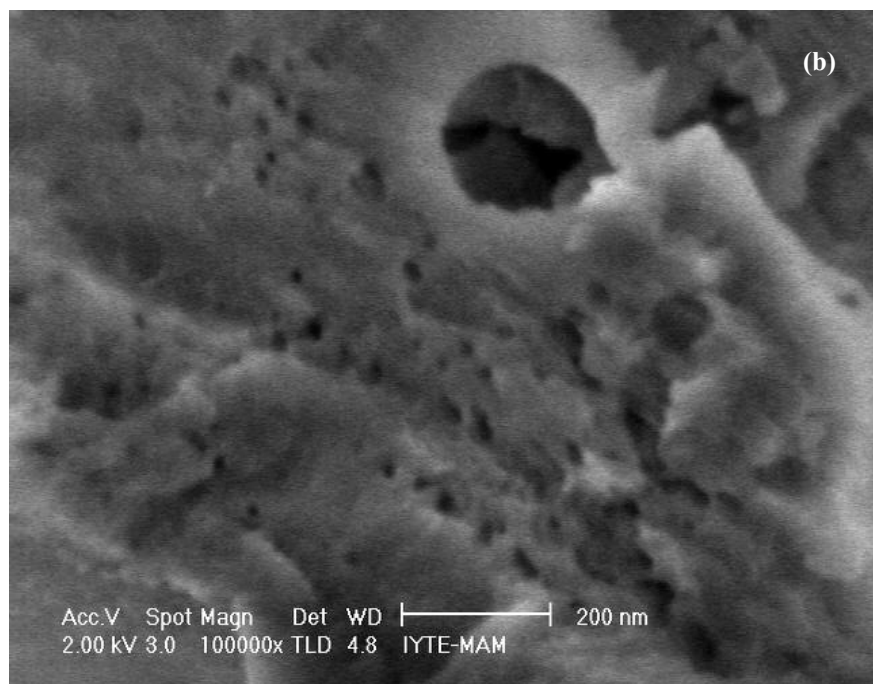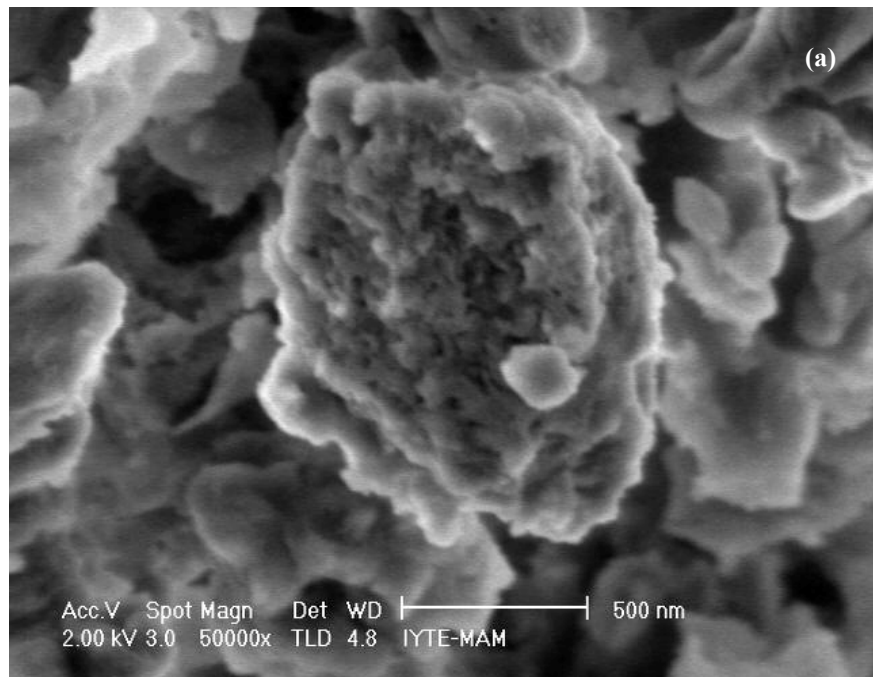
Fig 4.4 SEM photographs of sample 1 at the (a) 500 nm and (b) 200 nm scales

4.1.4 AFM photographs

The AFM photographs of sample 1 are given in Figures 4.5-4.7. These figures illustrate the shapes and dimensions of the catalyst particles and the surface topography. The magnification limitations prevent the detection of the pores within individual particles. However, a close examination of the figures suggest that the catalyst is made up of particles which has a size around 100 nm.

4.2 Characterization of the V-MCM-41 Catalysts

The V-MCM-41 catalysts synthesized in this study were characterized by XRD, EDS, AAS, N_2 adsorption, helium pycnometry, SEM and AFM techniques and the results given in Sections 4.2.1-4.2.7 are obtained.

4.2.1 XRD patterns

Figure 4.8 illustrates the XRD patterns of the V-MCM-41 samples synthesized using vanadyl sulfate hydrate as the vanadium source with V/Si molar ratios (in the solution) of 0.01 and 0.03 (see the nomenclature in Table C.1). Figure 4.9 illustrates the V-MCM-41 samples synthesized using vanadyl sulfate hydrate as the vanadium source with the V/Si molar ratio (in the solution) of 0.09 synthesized with different flow rates of dry air at the calcination stage. In this figure, sample V_3 is synthesized using a dry air flow rate of 1 l/min at the calcination stage and sample V_4 is synthesized using a dry air flow rate of 1 > l/min at the calcination stage. Figure 4.10 illustrates the V-MCM-41 samples synthesized with a V/Si ratio of 0.09 (in the solution) using ammonium vanadate as the vanadium source. In this figure there are two V-MCM-41 samples; sample V_5 and sample V_6. The only difference between these samples is the fact that a suspension is formed during the synthesis of sample V_5 and a non-homogeneous gel is formed during the synthesis of sample V_6; the rest of the experimental conditions are the same for the two samples.
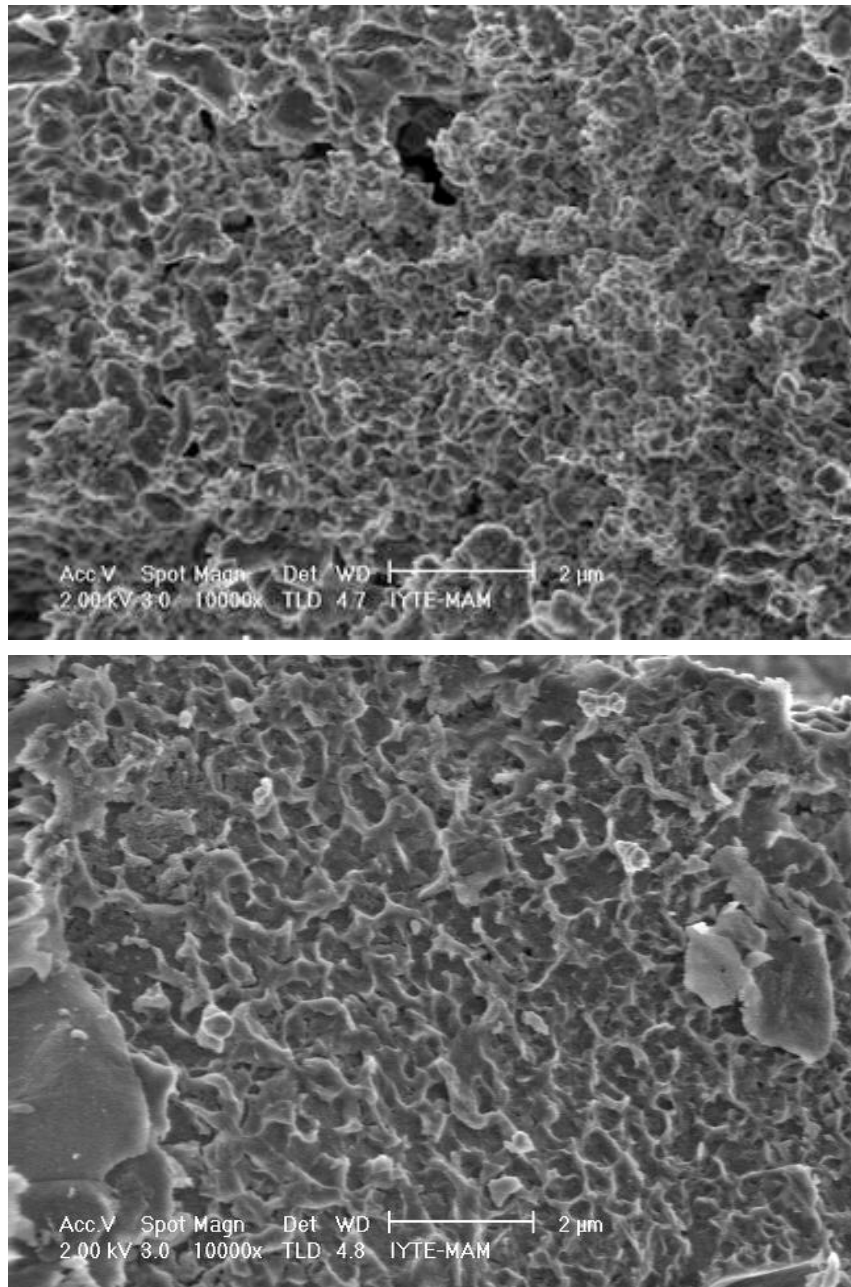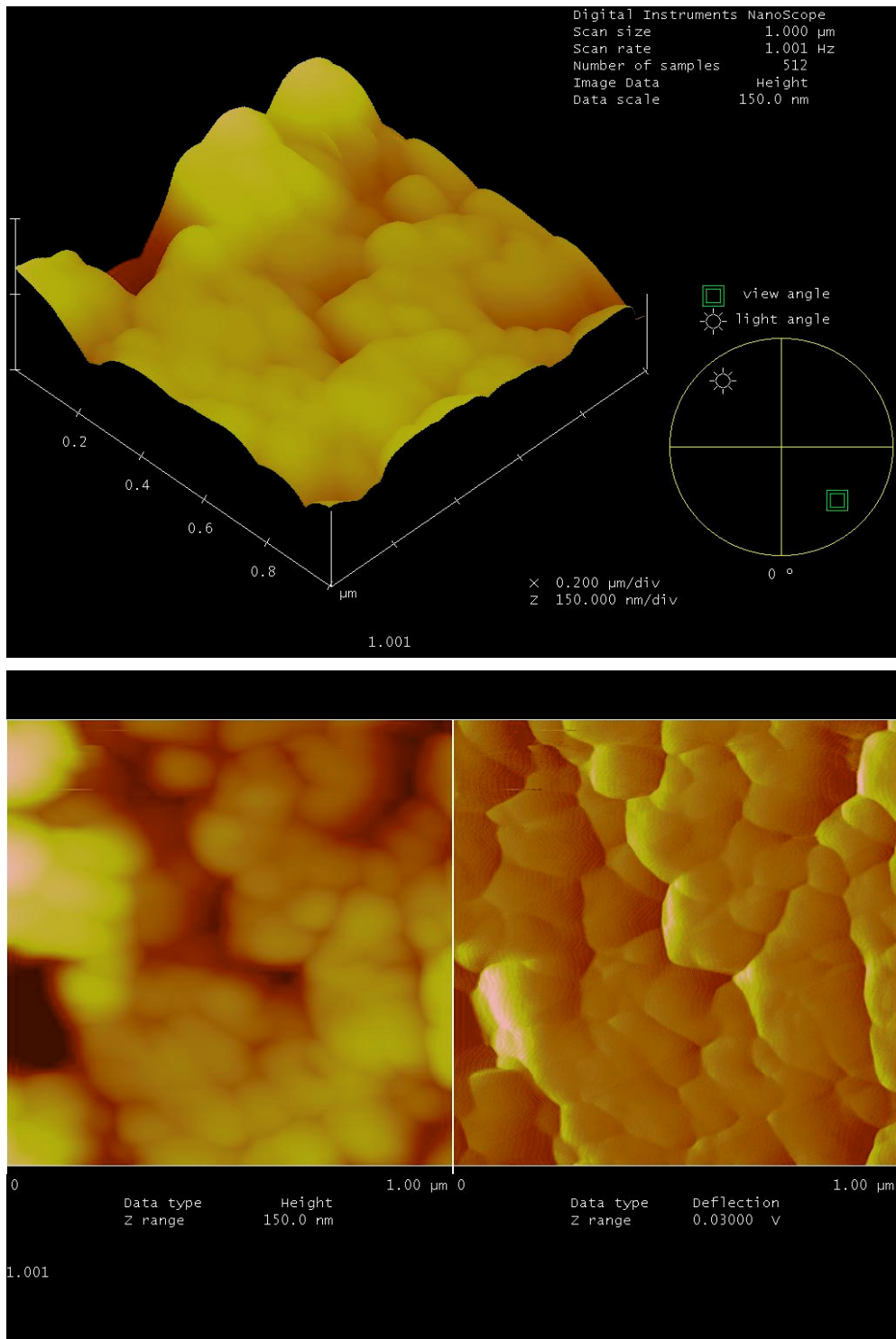
Fig. 4.5 AFM photographs of sample 1 at the 1µm scale-1
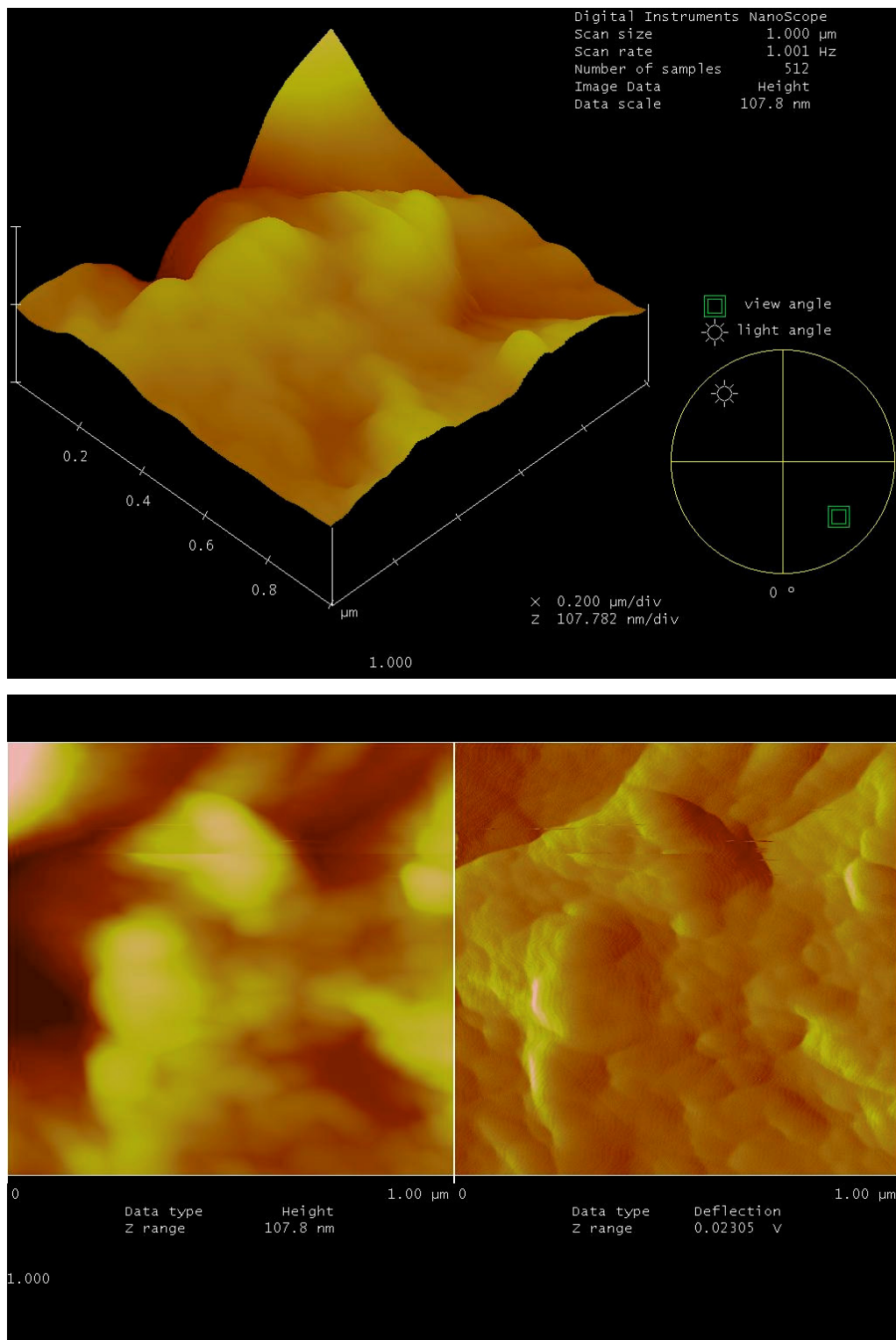
Fig. 4.6 AFM photographs of sample 1 at the 1µm scale-2
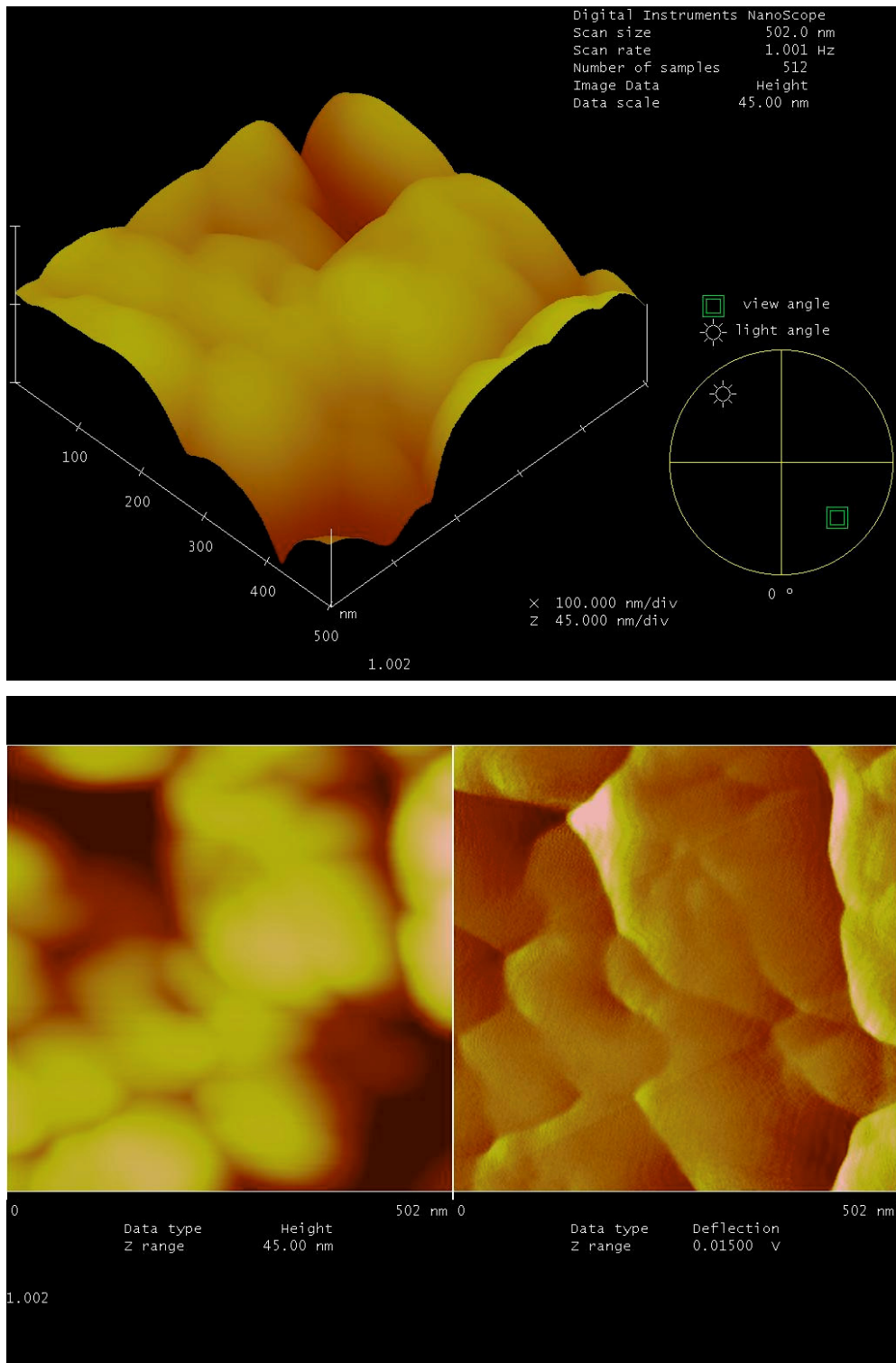
Fig. 4.7 AFM photographs of sample 1 at the 500 nm scale
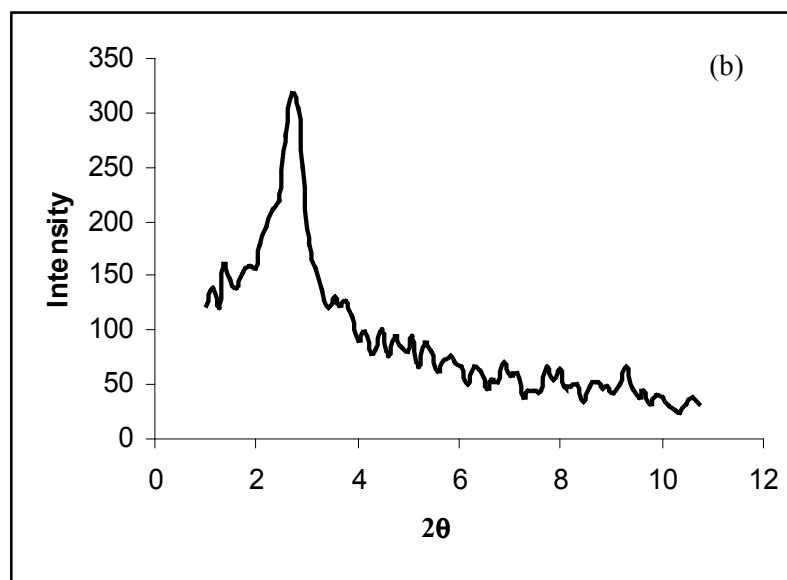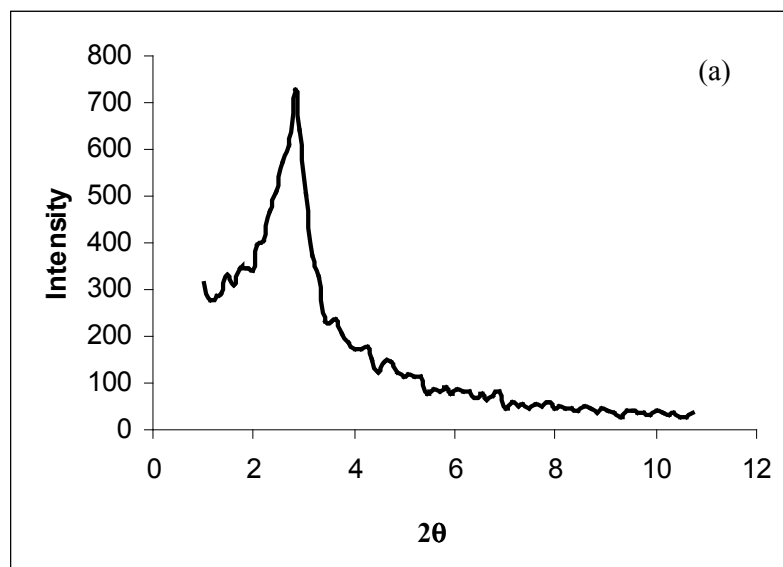
Fig. 4.8 XRD patterns of (a) sample V_1 and (b) sample V_2
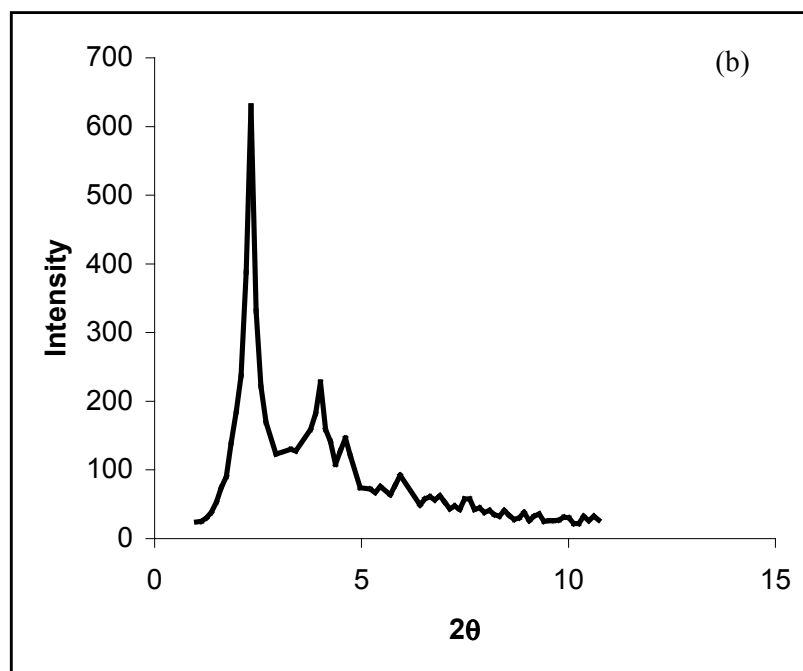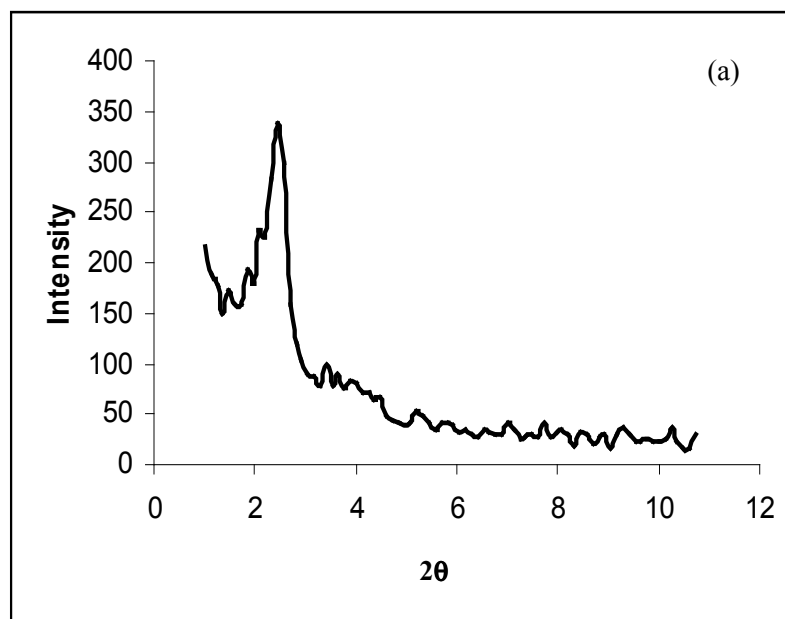
Fig. 4.9 XRD patterns of (a) sample V_3 and (b) sample V_4
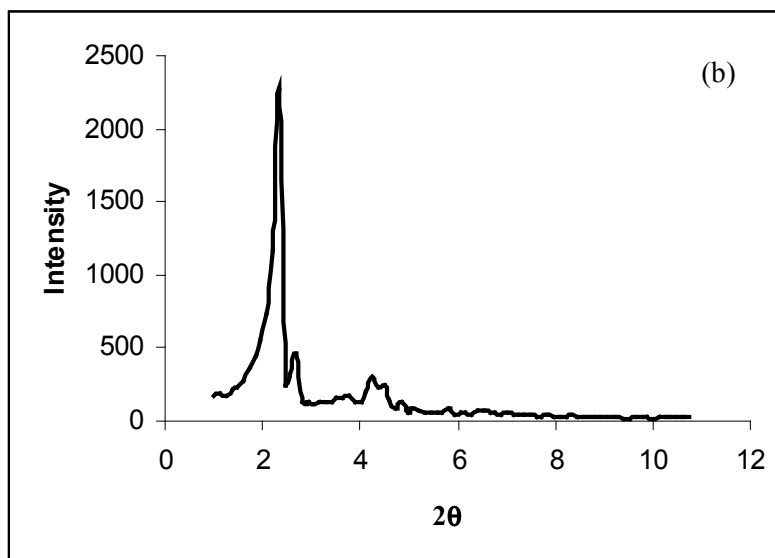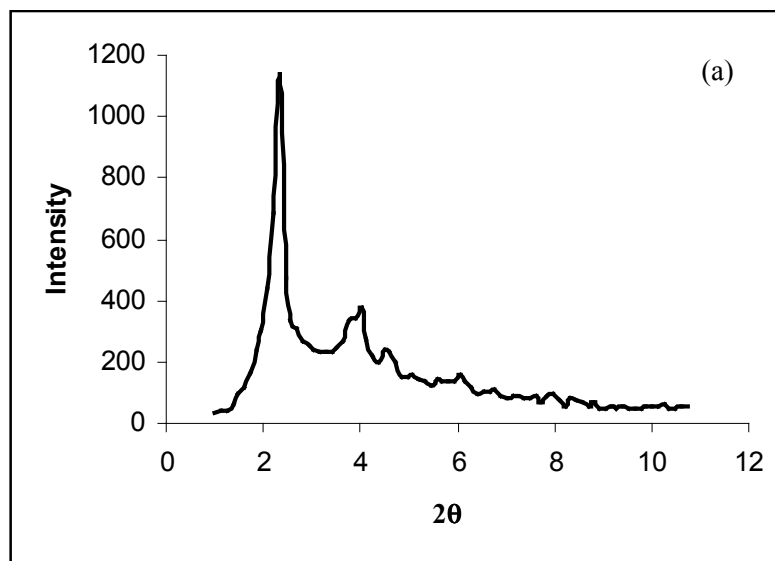
Fig. 4.10 XRD patterns of (a) sample V_5 and (b) sample V_6

As seen in Figures 4.8-4.10, the characteristic peak of MCM-41 (around $2\theta \cong 2.5^{\circ}$) is retained in all the synthesized V-MCM-41 samples. This suggests that the introduction of vanadium by a direct alkaline synthesis method does not destroy the MCM-41 structure up to a V/Si atomic ratio of 0.09 (in the solution) and the samples preserve the crystalline properties.

In addition to the sharp Bragg peaks corresponding to d_{100}, two to three other reflections are also detected for the V-MCM-41 catalysts. For instance, for sample V_3, the main XRD peaks obtained are at the 2θ values of 2.45, 3.77, 4.25 and 4.97°; and for sample V_5, they are at the 2θ values of 2.33, 4.01 and 4.97°. A small shift in both the main and secondary peaks with respect to the peaks of the MCM-41 structure are observed for all the synthesized V-MCM-41 catalysts. These shifts are the evidence of the incorporation of vanadium into the walls of the MCM-41 materials [127].

The XRD patterns reveal that the samples synthesized using ammonium vanadate have better structures than those synthesized using vanadyl sulfate hydrate. However, EDS results are also important to determine whether ammonium vanadate is a better source for the incorporation of vanadium into the MCM-41 structure. It is also seen through the XRD patterns that sample V_4 which is calcined in excess of dry air has a better XRD pattern than sample V_3 although both samples have the same V/Si molar ratio of 0.09 and the same vanadium source, i.e., vanadyl sulfate hydrate.

4.2.2 EDS results

In Figures 4.11 and 4.12, the EDS patterns of samples V_1-V_4, synthesized using vanadyl sulfate hydrate as the vanadium source, are given. In Figure 4.13, the EDS patterns of samples V_5 and V_6, synthesized using ammonium vanadate as the vanadium source, are given. In these figures, the corresponding atomic concentrations of vanadium and silicon as found in the solid product are also given so that the corresponding V/Si ratios (in the bulk) can be calculated.
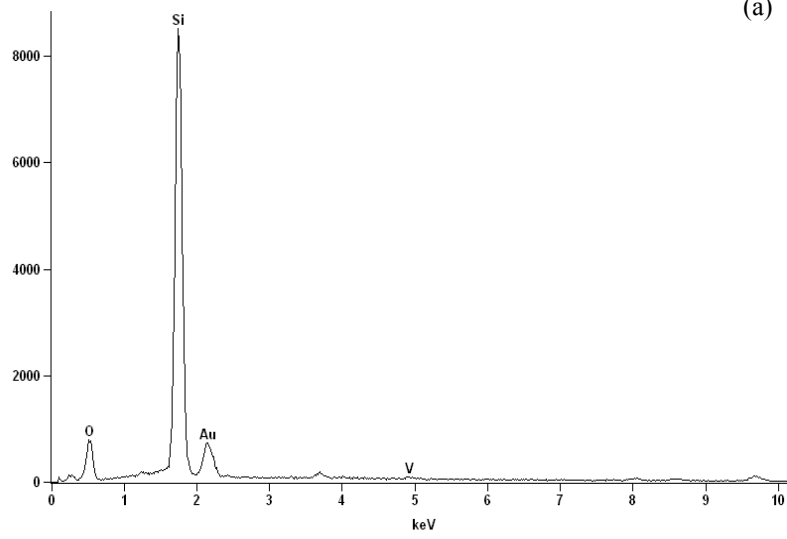
Element	Weight Conc %	Atom Conc %
Si	98.87	99.37
V	1.13	0.63
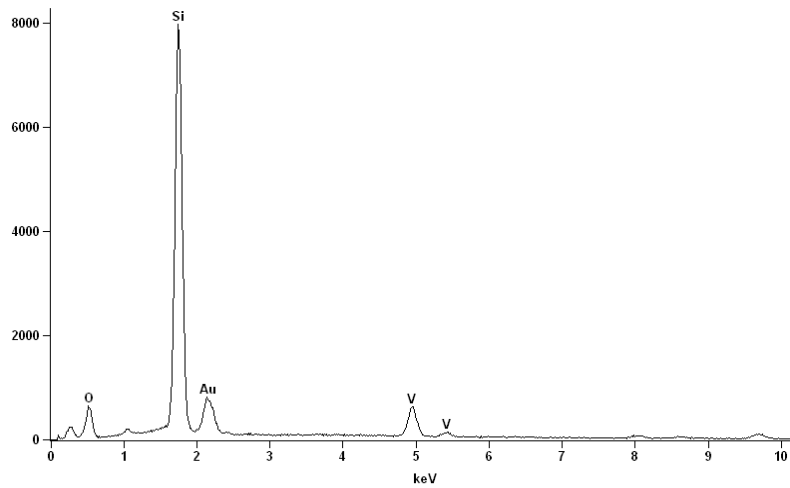
Element	Weight Conc %	Atom Conc %
Si	80.61	88.29
V	19.39	11.71

Figure 4.11 EDS patterns of samples (a) V_1 and (b) V_2
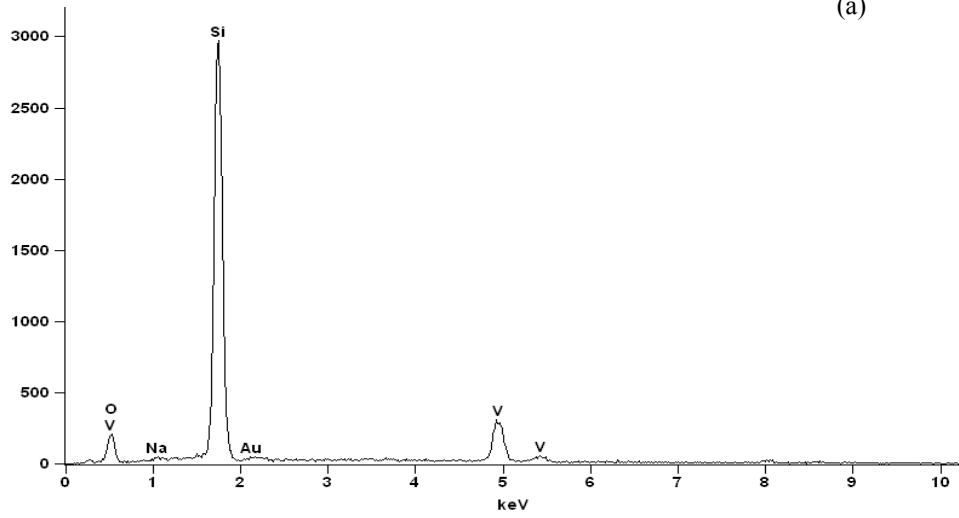
Element	Weight Conc %	Atom Conc %	Compnd Conc %	Formula
O	51.21	67.08	0.00	
Na	0.71	0.64	0.95	Na_2O
Si	37.32	27.85	79.83	SiO_2
V	10.76	4.43	19.22	V_2O_5
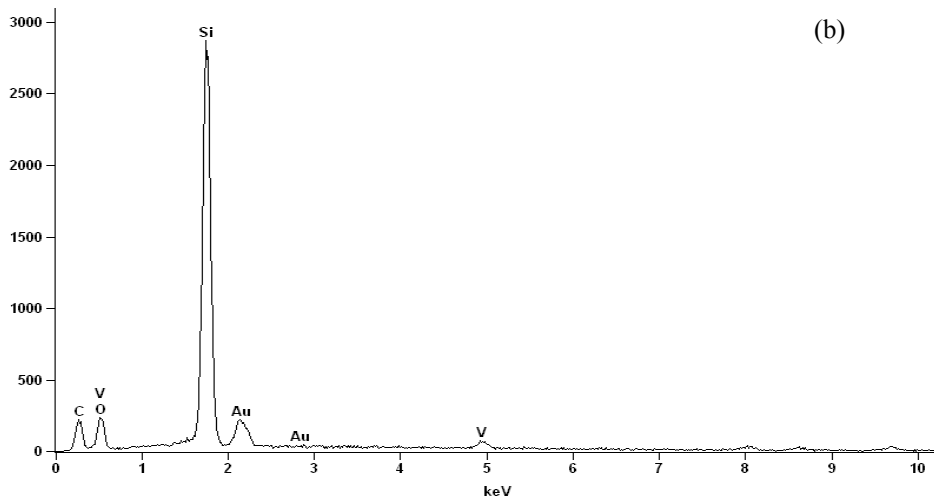
Element	Weight Conc %	Atom Conc %
Si	93.30	96.19
V	6.70	3.81

Fig. 4.12 EDS patterns of samples (a) V_3 and (b) V_4

Full scale counts: 4391

(a)
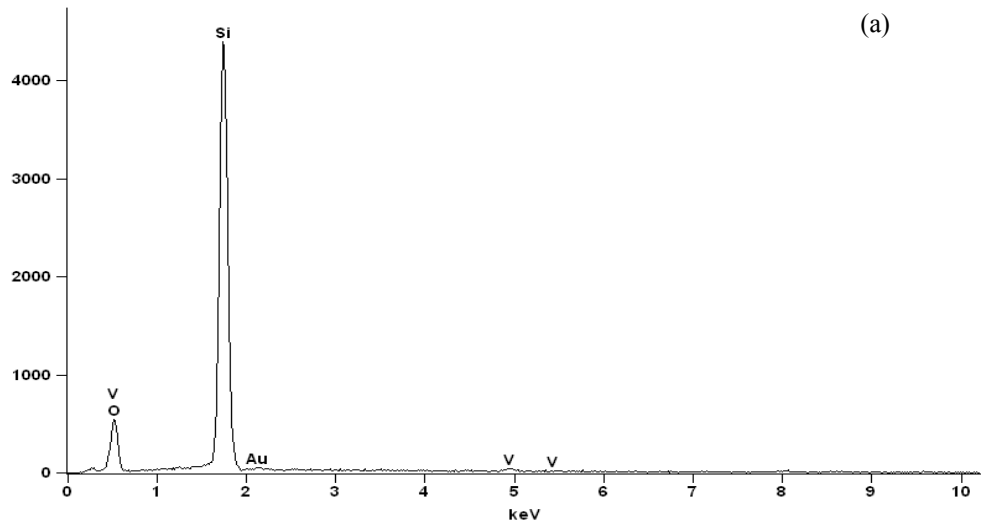
Element	Weight Conc %	Atom Conc %	Compnd Conc %	Formula
O	52.84	66.83	0.00	
Si	44.65	32.17	95.53	SiO_2
V	2.50	0.99	4.47	V_2O_5

Full scale counts: 4391

(b)
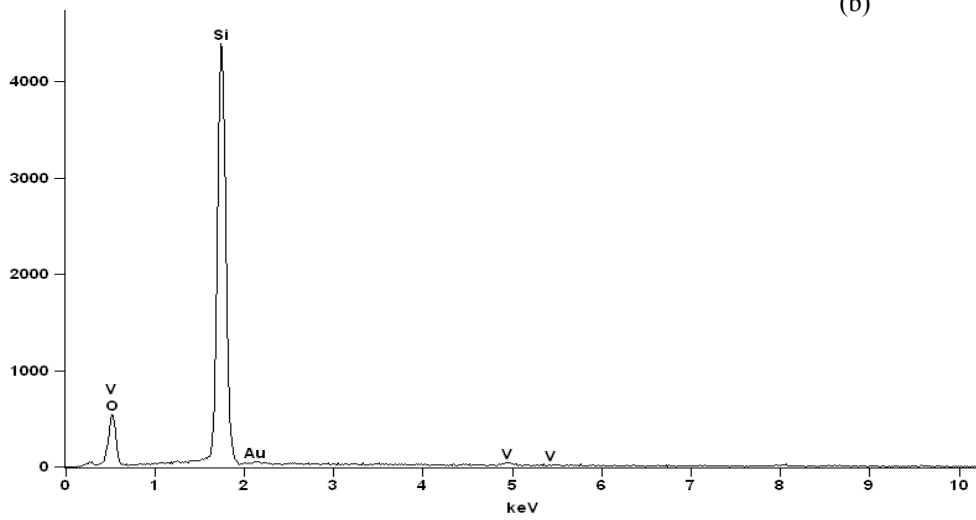
Element	Weight Conc %	Atom Conc %	Compnd Conc %	Formula
O	53.12	66.72	0.00	
Si	46.07	32.96	98.56	SiO_2
V	0.81	0.32	1.44	V_2O_5

Fig. 4.13 EDS patterns of samples (a) V_5 and (b) V_6

For example, for sample V_3, the atomic concentration of vanadium incorporated into the structure is 4.43% and the atomic concentration of Si found in the sample is 27.85% (see the composition table in Fig. 4.12.a). Hence, the V/Si molar ratio in the bulk of the sample is:

$$V/Si = 4.43 / 27.85$$

$$= 0.159$$

The other V/Si ratios in the bulk of the synthesized catalysts calculated from the EDS data are given in Table 4.2.

The results in Table 4.2 illustrate that in general; the V/Si molar ratios in the bulk of the V-MCM-41 catalysts synthesized using vanadyl sulfate hydrate (samples V_2 and V_3) are much higher than the corresponding ratios for the samples synthesized using ammonium vanadate. For instance, the amount of vanadium incorporated into sample V_3 using vanadyl sulfate hydrate is

Table 4.2 V/Si Molar Ratios (in the bulk) Calculated from the EDS Data

Sample ID	Vanadium Source	V/Si Molar Ratio in the Solution	V/Si Molar Ratio in the Bulk
V_1	Vanadyl sulfate hydrate	0.01	0.006
V_2	Vanadyl sulfate hydrate	0.03	0.133
V_3	Vanadyl sulfate hydrate	0.09	0.159
V_4	Vanadyl sulfate hydrate	0.09	0.040
V_5	Ammonium vanadate	0.09	0.041
V_6	Ammonium vanadate	0.09	0.010

four times as much as the vanadium incorporated into sample V_5 and sixteen times as much as the amount of vanadium incorporated into sample V_6 which were synthesized using ammonium vanadate. This observation suggets that the

use of vanadyl sulfate hydrate is more advantageous than the use of ammonium vanadate as the vanadium source when incorporating vanadium into the MCM-41 structure (Sample V_4 which has the same V/Si bulk molar ratio as sample V_5 is an exception since it was calcined in excess of dry air). This observation about the differences between the two vanadium salts is also justified by the subsequent Atomic Absorption Spectroscopy (AAS) analysis as given in Section 4.2.3.

4.2.3 AAS results

The Atomic Absorption Spectroscopy (AAS) analyses of samples V_3 and V_5 are carried out by a method suggested by Grubert et al. [93]. The vanadium content is determined by using this method as follows: Catalysts V_3 and V_4 are dissolved in a mixture of HF and HNO_3, (a mixture with the volumetric ratio of 1:4, respectively). This mixture is placed in a teflon-lined stainless steel autoclave. The autoclave is kept in an etuve at $423^{o}K$ for 2 hours. After this acid digestion step, the mixtures are analyzed by Atomic Absorption Spectroscopy for their vanadium contents. Then, the SiO_2 contents are determined by using the gravimetric titration method. As a result of these analyses, the results given in Table 4.3 are obtained. (Since AAS analysis is a bulk analysis method, the V/Si molar ratios in Table 4.3 are the bulk molar V/Si ratios).

Table 4.3 depicts that the V/Si bulk molar ratio of sample V_3 is 7 times as large as that of V_5. This trend is in agreement with the results obtained by the EDS analysis; i.e., more vanadium is incorporated into the MCM-41 structure when vanadyl sulfate hydrate is used as the vanadium source rather than ammonium vanadate.

4.2.4 Nitrogen physisorption results

The nitrogen physisorption results are illustrated in Figures 4.14 and 4.15. The type IV isotherm specific to mesoporous materials (see Appendix E)

Table 4.3 V/Si Molar Ratios (in the bulk) for Samples V_3 and V_5 Calculated from the AAS Data

Sample ID	Vanadium source	V/Si ratio in the solution	moles Vanadium	moles Silicon	V/Si ratio in the bulk
V_3	Vanadyl sulfate hydrate	0.09	0.309	1.46	0.212
V_5	Ammonium vanadate	0.09	0.035	1.21	0.029

is obtained for all the synthesized samples. The narrow capillary condensation steps (especially displayed for sample V_5) seen in Figures 4.14 and 4.15 indicate that the as-synthesized samples have narrow pore size distributions. This observation is justified in Figure 4.16 where the pore size distributions calculated by the BJH method are displayed.

4.2.5 Physical properties

The multi-point BET surface areas, BJH pore volumes, V_{pore}, BJH pore diameters, d_p, solid densities, ρ_s, apparent densities, ρ_{app} and porosities, ε, of the V-MCM-41 catalysts are given in Table 4.4. The BET, V_{pore} and d_p values are obtained from the nitrogen adsorption isotherms of the physisorption data whereas the solid density, ρ_s, values are obtained by utilizing helium pcynometry data. The ρ_{app} and ε values are calculated as described in Appendix D.
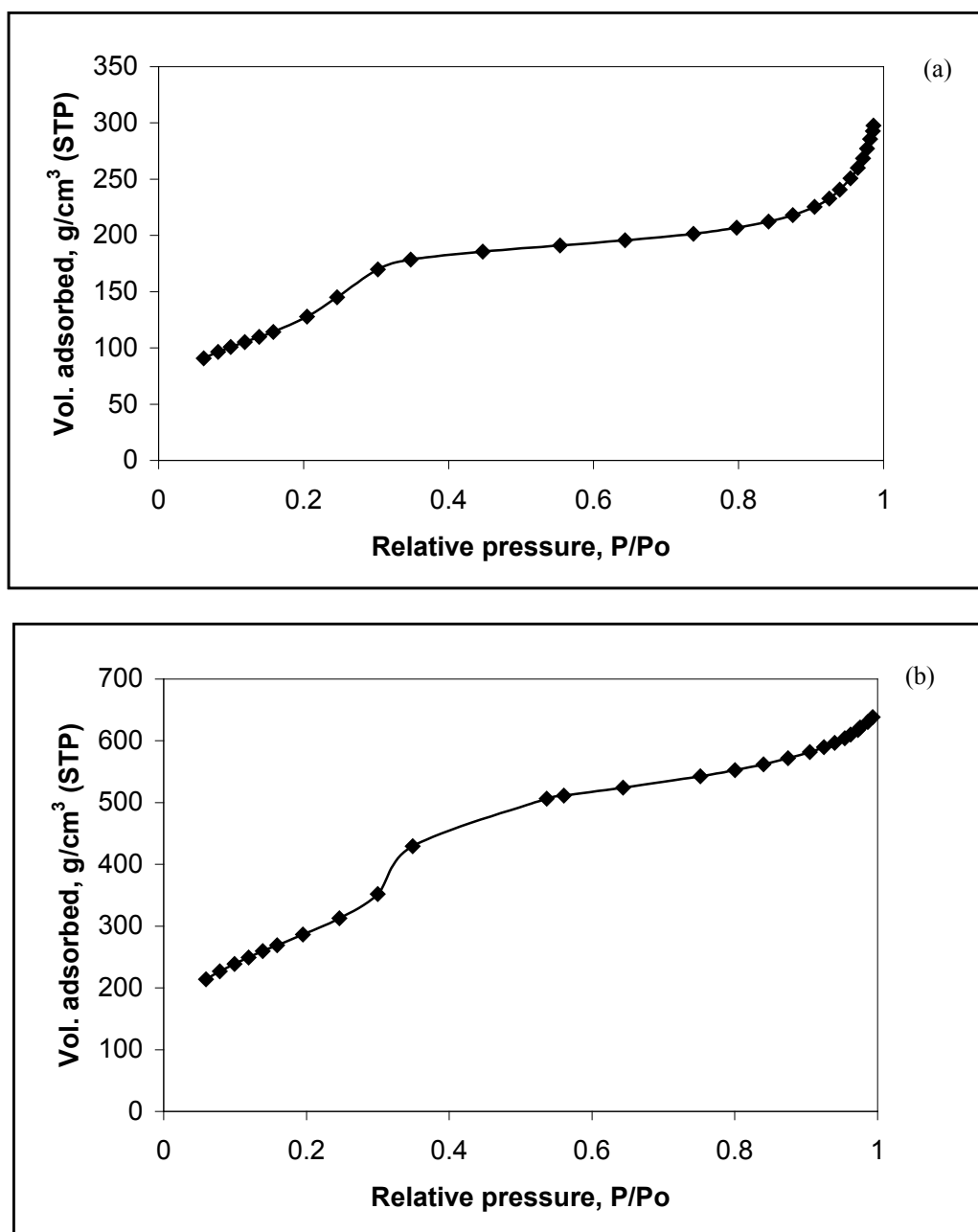
Fig. 4.14 Nitrogen adsoption isotherms of samples (a) V_3 and (b) V_4
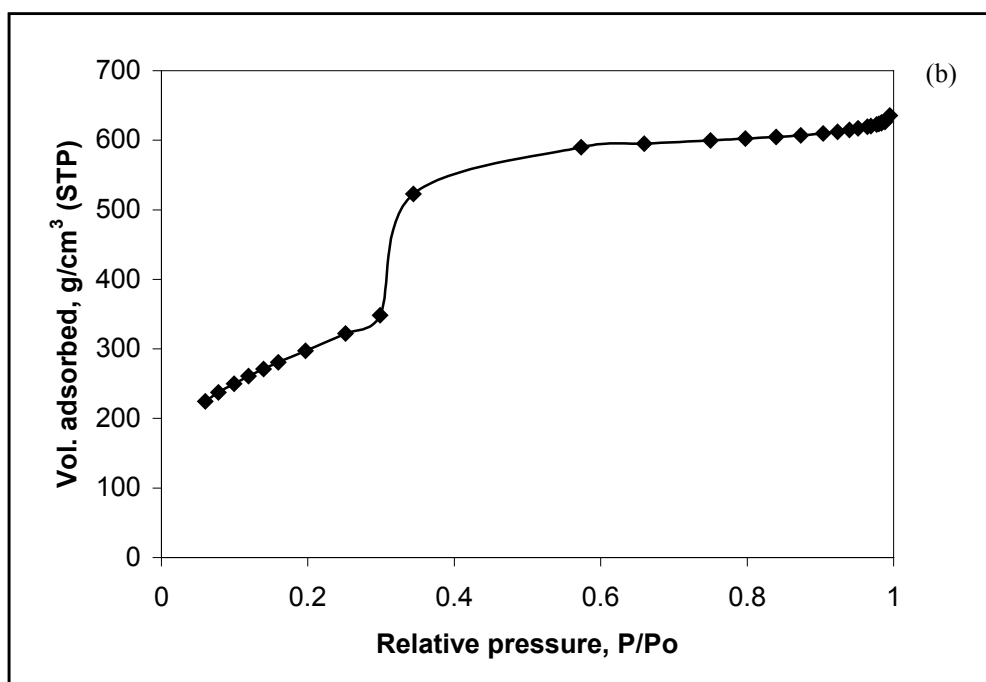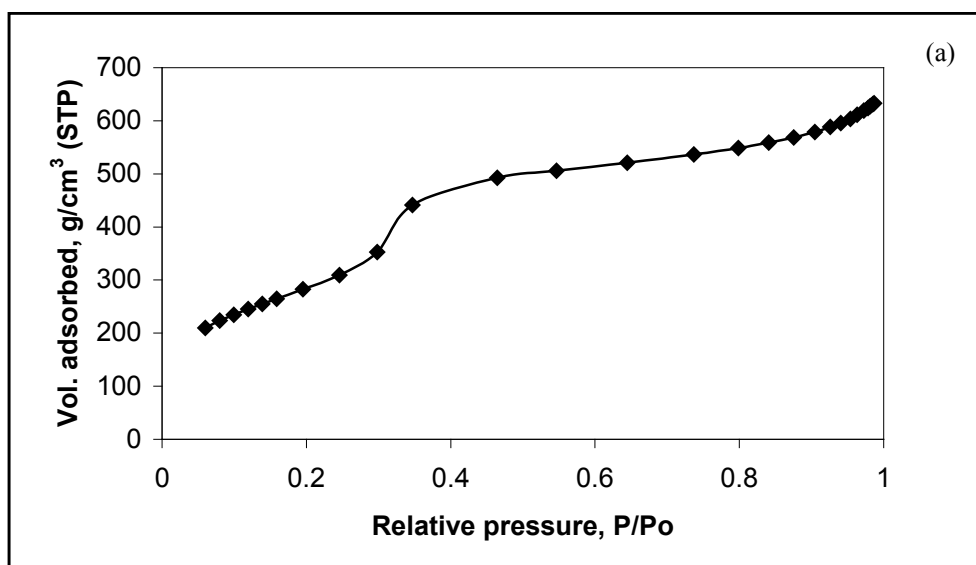
Fig. 4.15 Nitrogen adsorption isotherms of samples (a) V_5 and (b) V_6
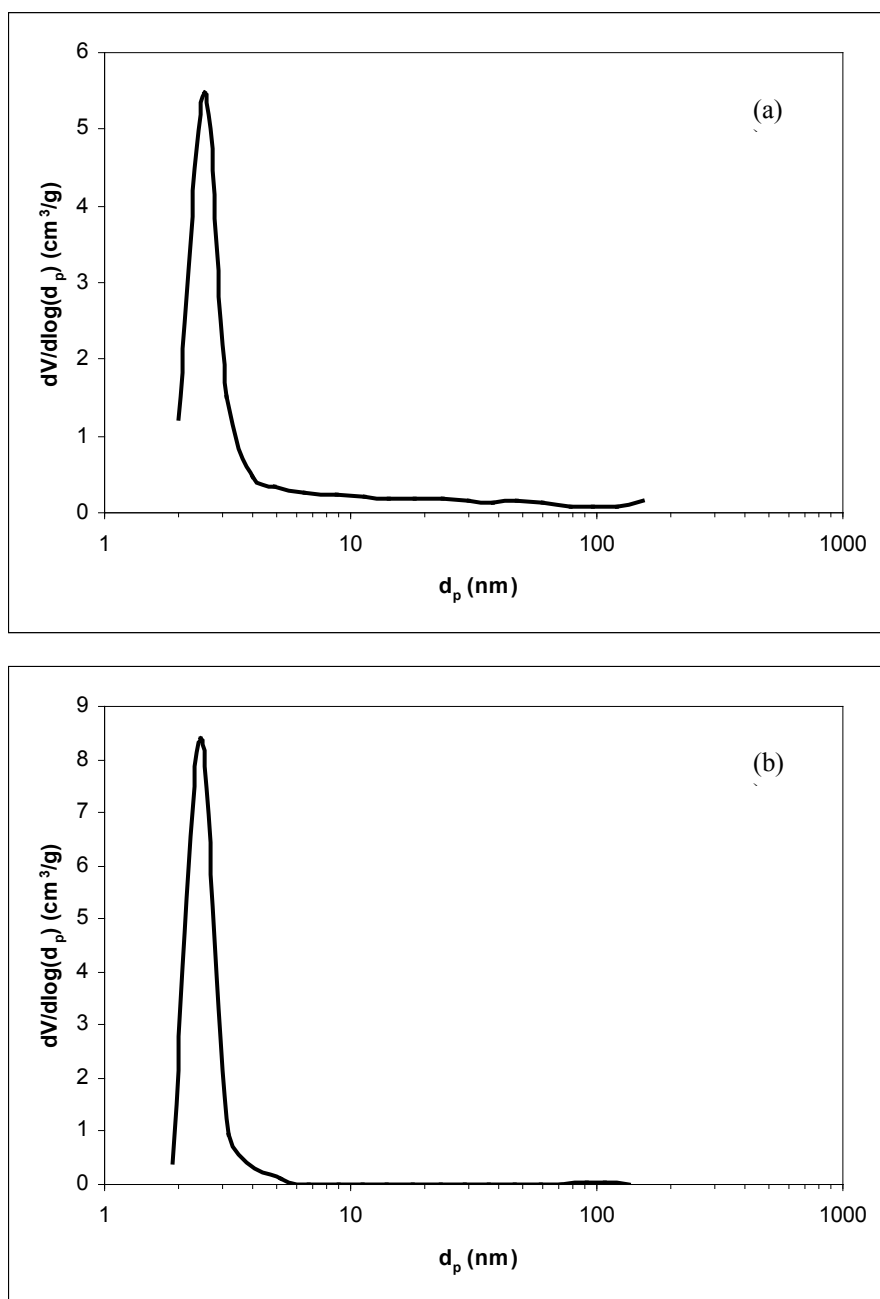
Fig. 4.16 Pore size distributions of samples (a) V_5 and (b) V_6

Table 4.4 Physical Properties of the Synthesized V-MCM-41 Catalysts

Sample ID	Vanadium salt	V/Si in solution	BET (m^2/g)	V_{pore} (cm^3/g) (*)	d_p (nm) (*)	ρ_s (g/cm^3)	ρ_{app} (g/cm^3)	ϵ
V1	$VOSO_4$	0.01	1315	0.92	2.7	2.06	0.71	0.66
V2	$VOSO_4$	0.03	813	0.44	2.9	2.24	1.13	0.50
V3	$VOSO_4$	0.09	481	0.53	3.7	3.11	1.17	0.62
V4	$VOSO_4$	0.09	1062	1.09	3.2	1.90	0.62	0.67
V5	NH_4VO_3	0.09	1053	1.08	3.2	2.96	0.71	0.76
V6	NH_4VO_3	0.09	1094	1.06	2.7	2.45	0.68	0.72

* Pore volume and pore diameter values are calculated from the nitrogen adsorption data using the BJH method.

The results in Table 4.4 show that, a decreasing trend is observed in the BET surface area of samples V_1, V_2 and V_3, synthesized using vanadyl sulfate hydrate ($VOSO_4$), with an increase of the V/Si ratio (in the solution). This decrease in specific surface area is accompanied with an increase in the apparent density and a decrease in the pore volume as expected due to the increase of the amount of vanadium added [23]. The average pore diameters of the V-MCM-41 materials having V/Si ratios of 0.01 and 0.03 in the solution are around 2.8 nm. A somewhat higher average pore diameter is observed for samples V_3, V_4 and V_5. It is interesting to observe that the V-MCM-41 materials prepared by using ammonium vanadate (NH_4VO_3) as the vanadium source (samples V_5 and V_6) have higher BET surface areas and higher pore volumes than the corresponding V-MCM-41 materials prepared by using $VOSO_4$ as the vanadium source (except for sample V_4 which was calcined in excess air). This is due to the fact that less vanadium is incorporated into the structure when ammonium vanadate is used as the vanadium source and the structure is more close to the purely siliceous MCM-41 structure.

In Table 4.5, the d-spacing, d_{100}, the lattice parameter, a, and the pore wall thickness, δ, values of samples V_1-V_6 are given. The increase of the pore wall thickness, δ, values above 1 nm for samples V_1, V_4, V_5 and V_6 indicate the successful incorporation of vanadium into the MCM-41 walls.

Table 4.5 Structural Properties of the Synthesized V-MCM-41 Catalysts

Sample ID	Vanadium Salt	V/Si bulk ratio	$d_{(100)}$ (nm)	lattice parameter "a" (nm)	Pore wall thickness δ (nm)
V_1	$VOSO_4$	0.01	3.14	3.63	1.06
V_2	$VOSO_4$	0.03	3.14	3.63	0.92
V_3	$VOSO_4$	0.09	3.60	4.16	0.67
V_4	$VOSO_4$	0.09	3.76	4.34	1.30
V_5	NH_4VO_3	0.09	3.79	4.38	1.38
V_6	NH_4VO_3	0.09	3.78	4.37	1.81

4.2.6 SEM Photographs

The SEM photographs of samples V_3 and V_6 are given in Figures 4.17-4.20 and 4.21-4.23, respectively. It is seen that both samples have a high density of pores; however, the individual pores are not detectable due to the limitations in the magnification scales. The photographs also show that sample V_6 has a more homogeneous and regular structure than sample V_3 as expected since the vanadium loading in sample V_6 is too low compared to sample V_3.

4.2.7 AFM photographs

The AFM photographs of sample V_3 are given in Figures 4.24-4.26. These figures illustrate the shapes and dimensions of the catalyst particles. The magnification limitations prevent the detection of the individual pores and only the shapes and distributions of the particles which have dimensions in the μm scale are detected.

4.3 Characterization of the Mo-MCM-41 Catalysts Synthesized by the Alkaline Route

The Mo-MCM-41 catalysts synthesized by the one-pot alkaline synthesis method are characterized by XRD, nitrogen physisorption, EDS
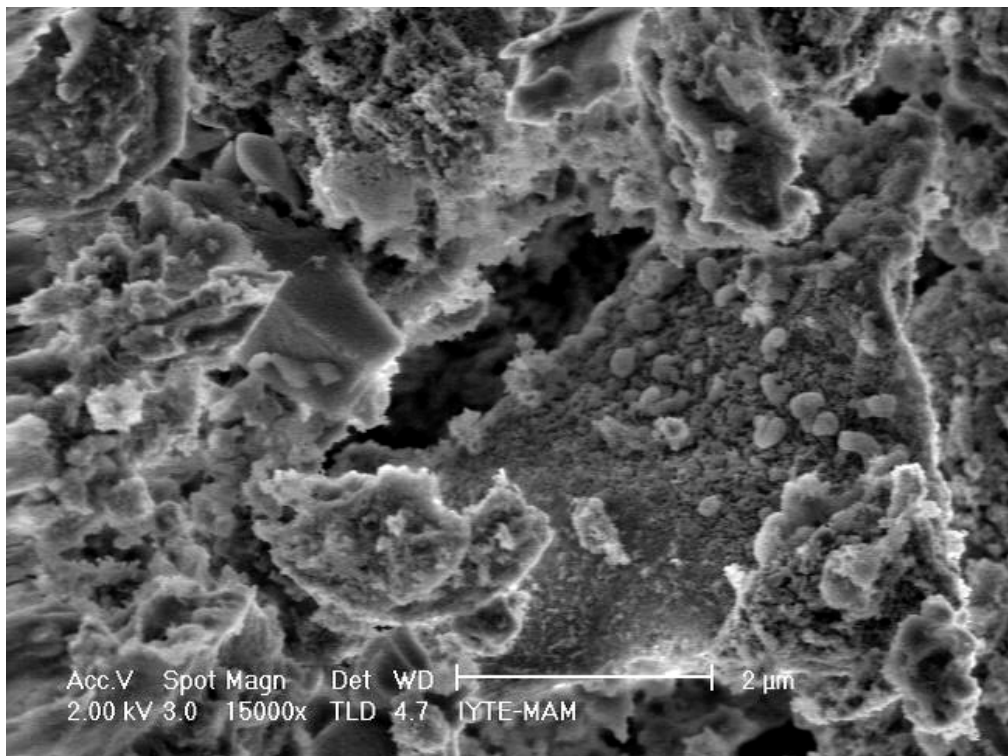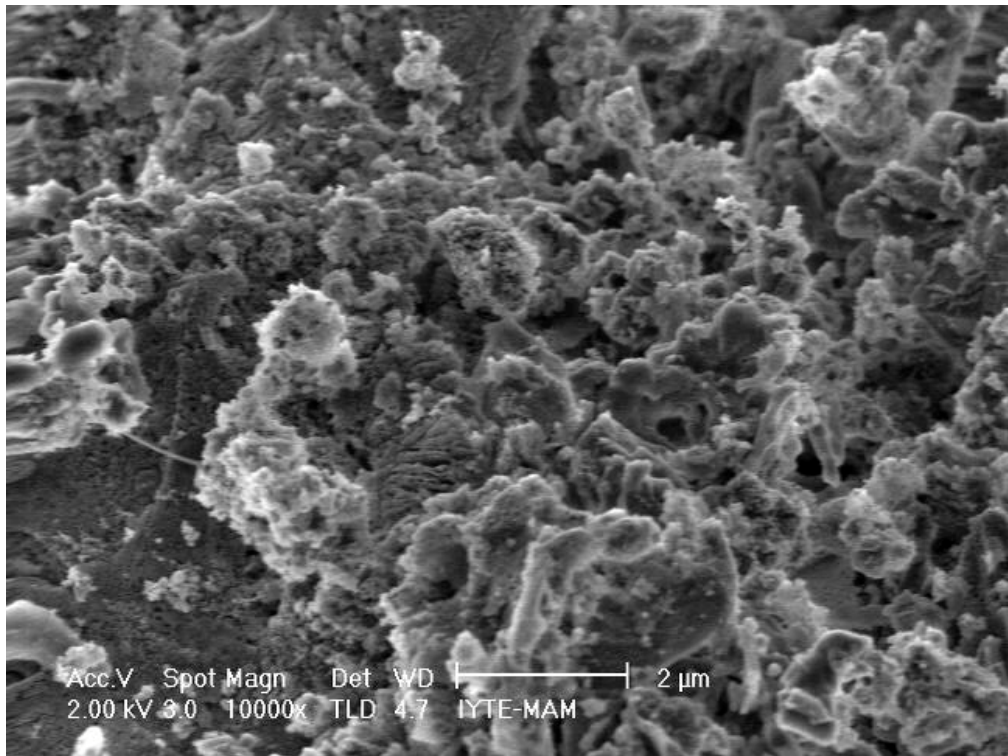
Fig. 4.17 SEM photographs of sample V$_3$ at the 2 µm scale
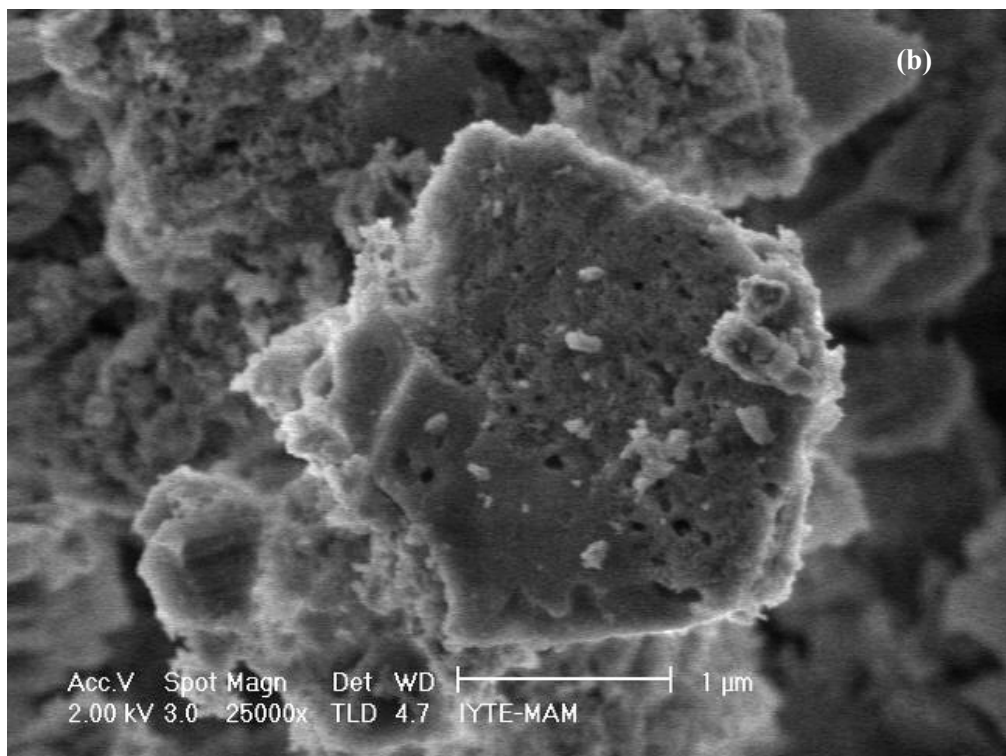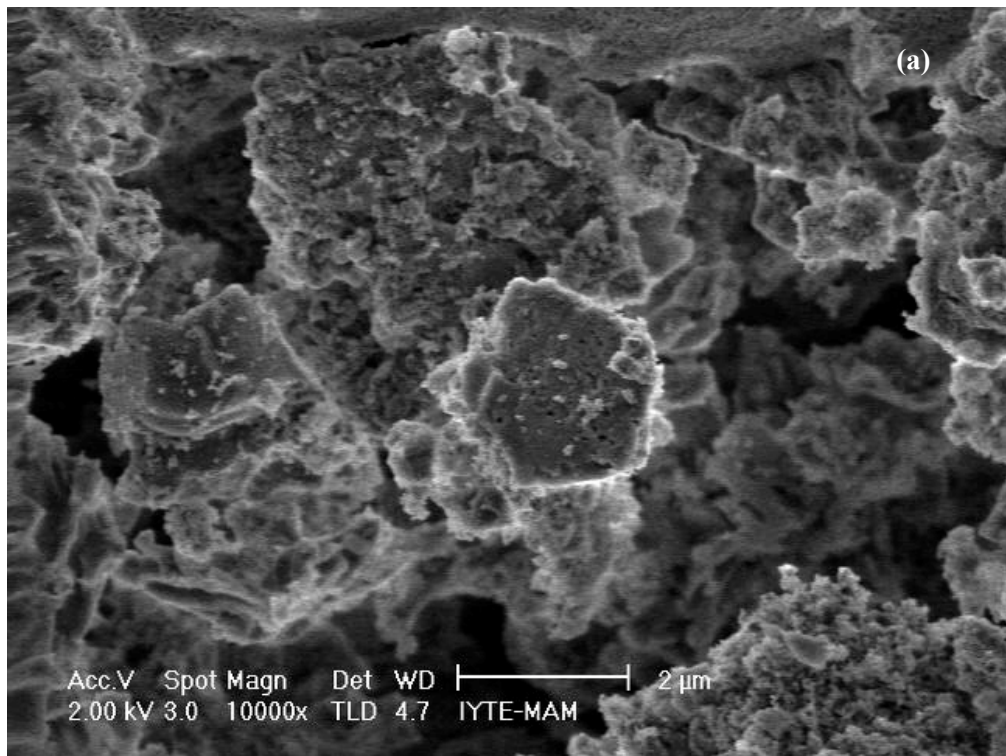
Fig. 4.18 SEM photographs of sample V_3 at the (a) 2 µm and (b) 1 µm scales
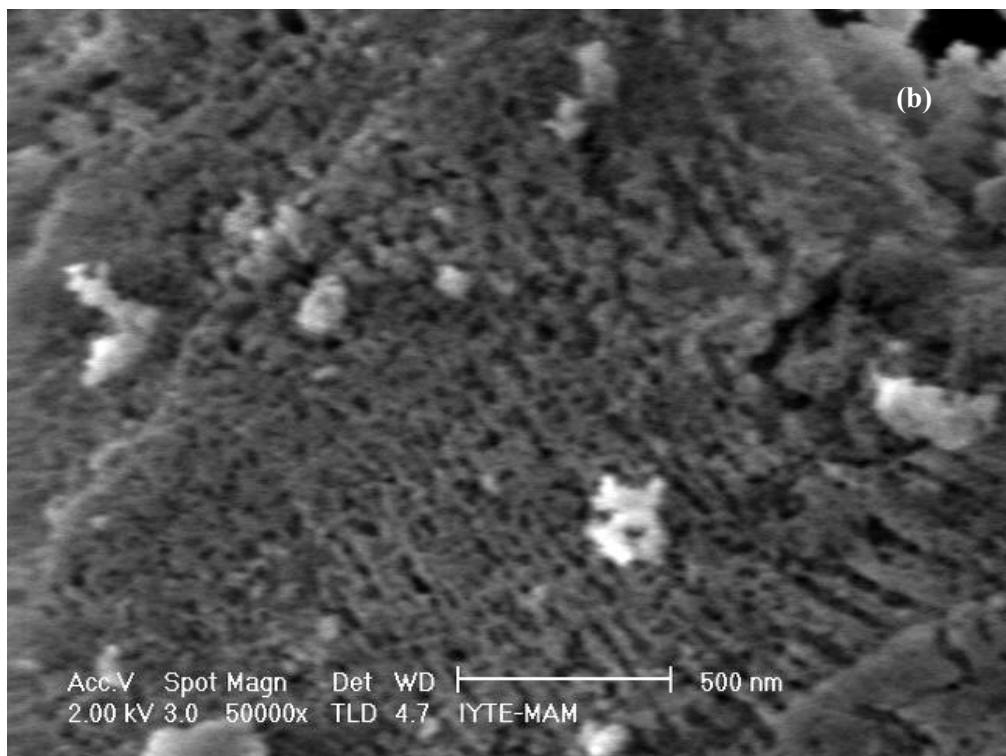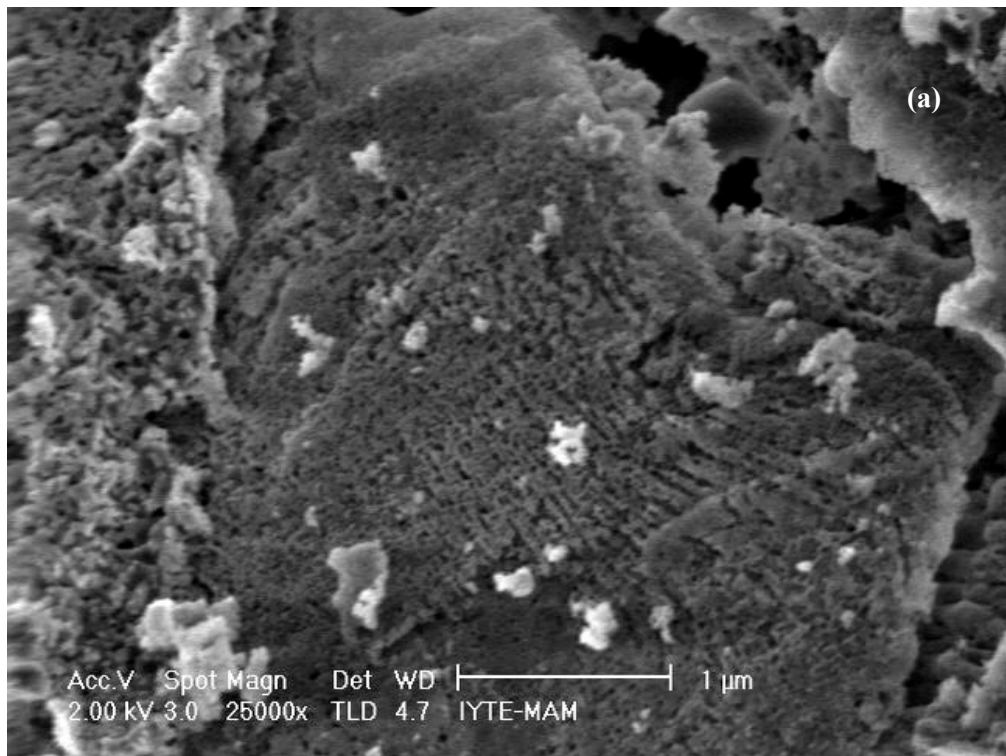
Fig. 4.19 SEM photographs of sample V_3 at the (a) 1 µm and (b) 500 nm scales
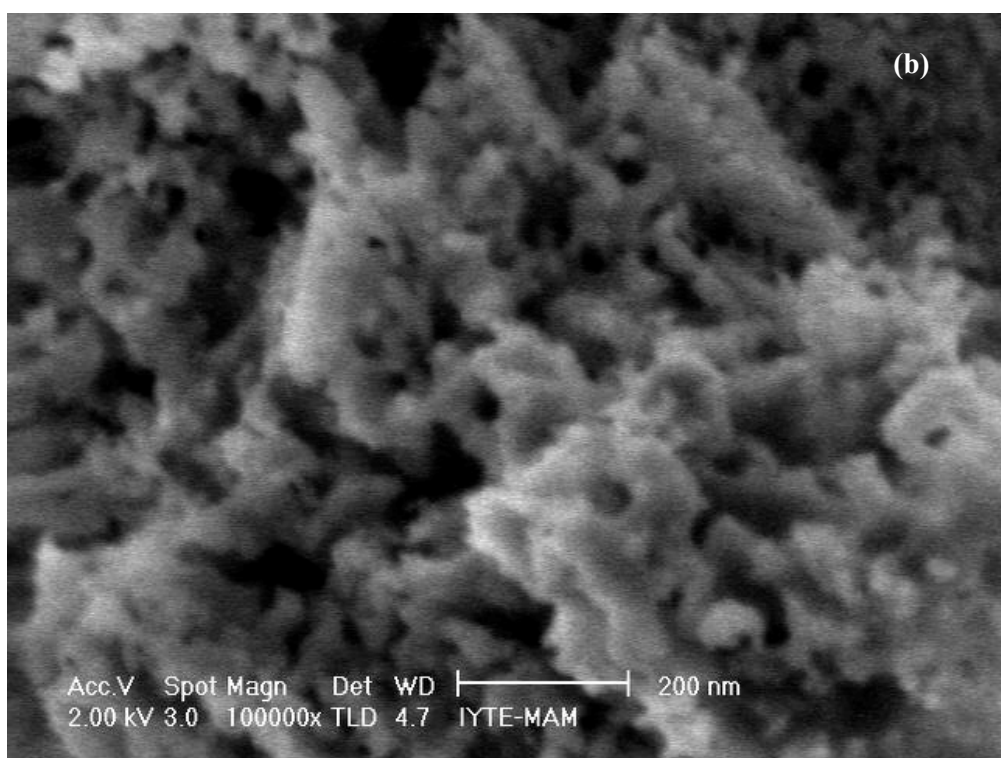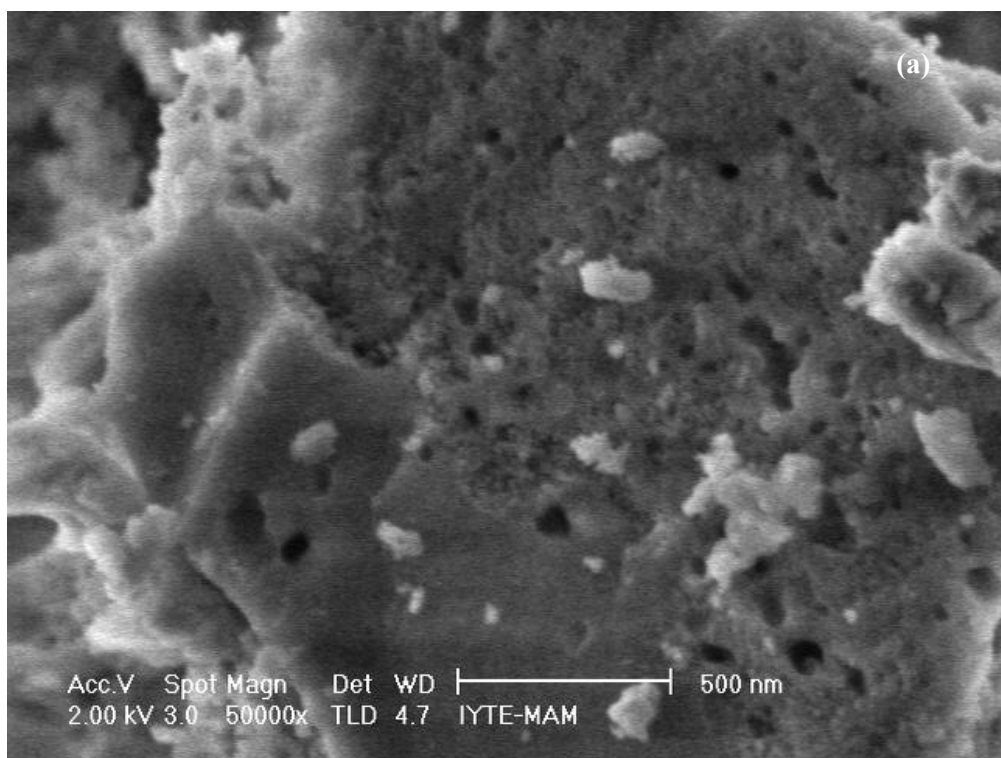
Fig. 4.20 SEM photographs of sample V$_3$ at the (a) 500 nm and (b) 200 nm scales
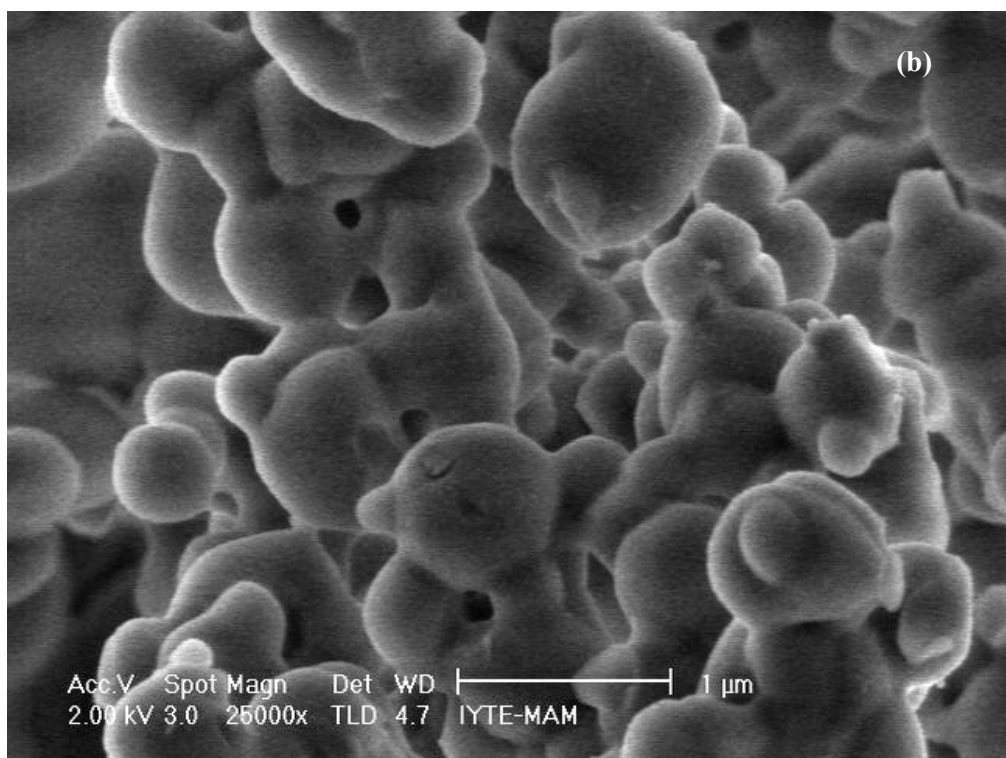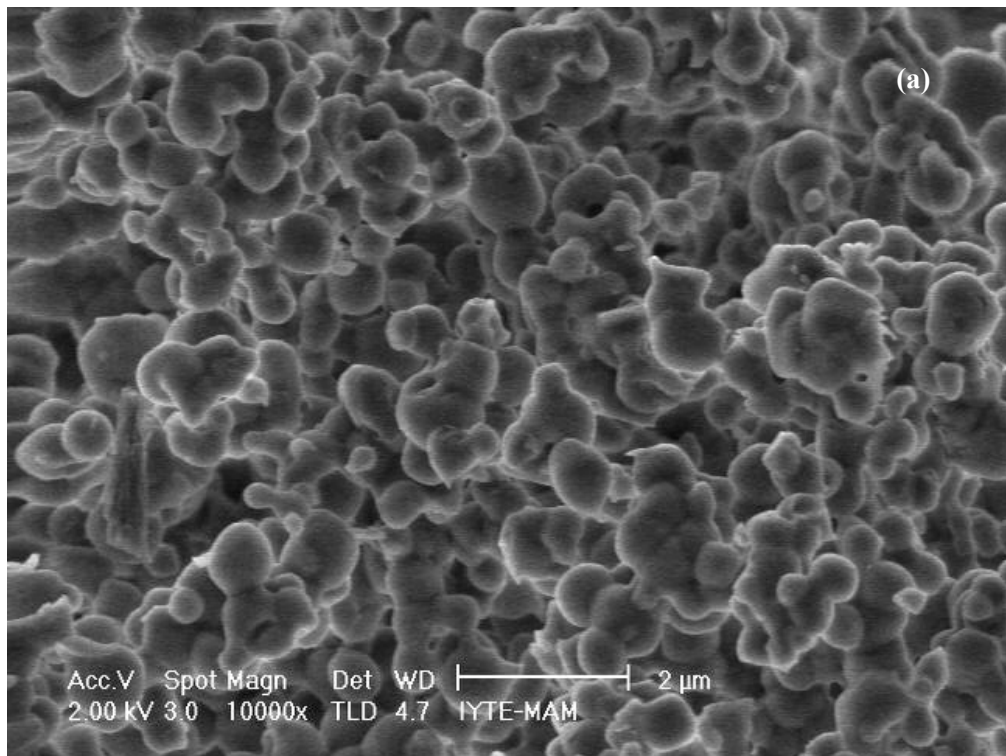
Fig. 4.21 SEM photographs of sample V_6 at the (a) 2 µm and (b) 1µm scales
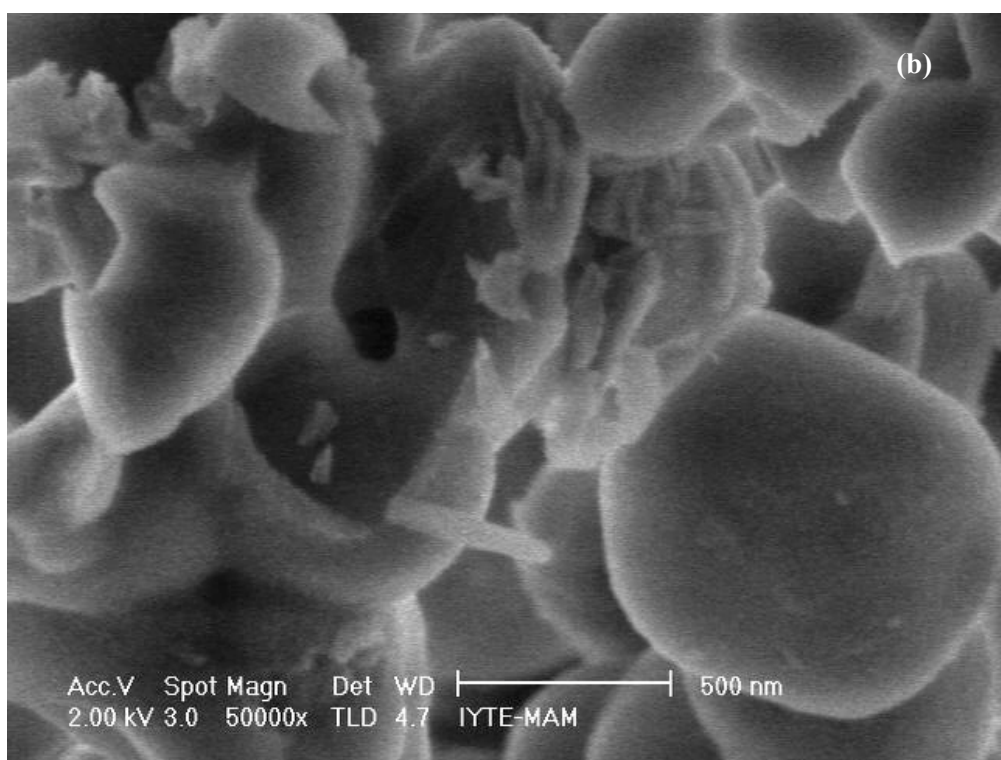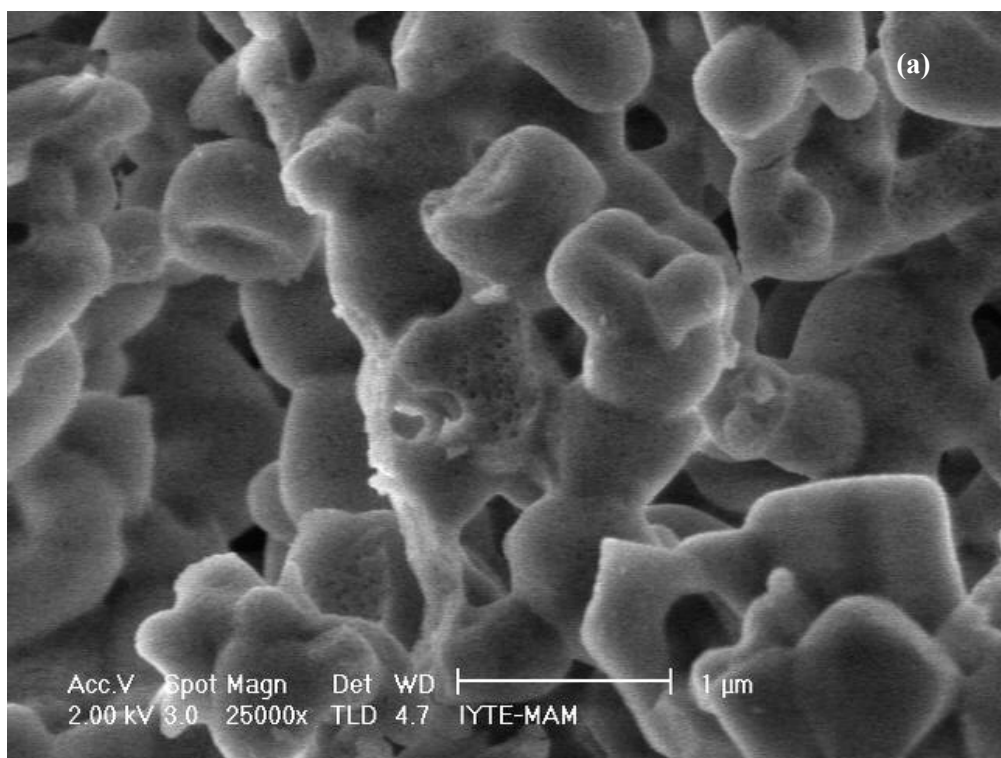
Fig. 4.22 SEM photographs of sample V_6 at the (a) 1 µm and (b) 500 nm scales
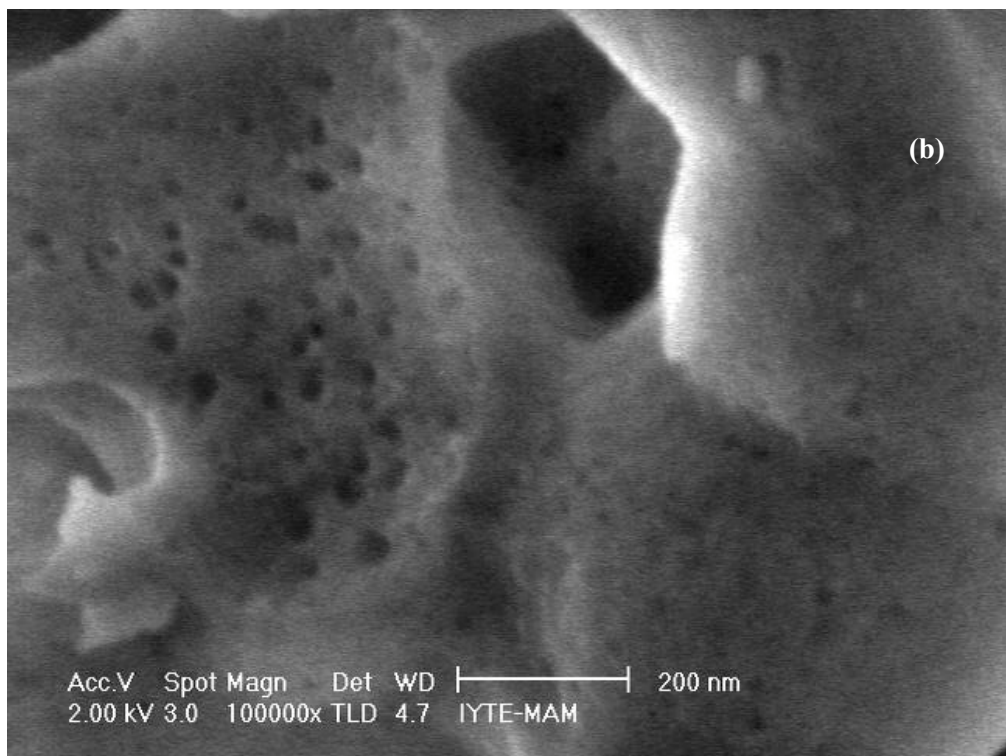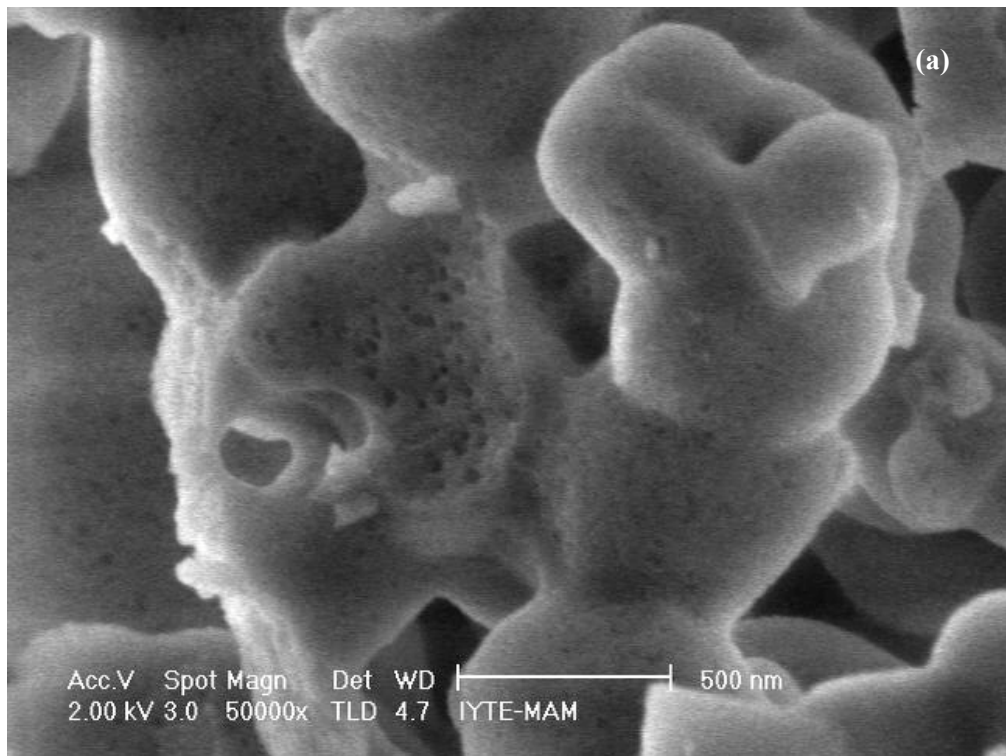
Fig. 4.23 SEM photographs of sample V_6 at the (a) 500 nm and (b) 200 nm scales
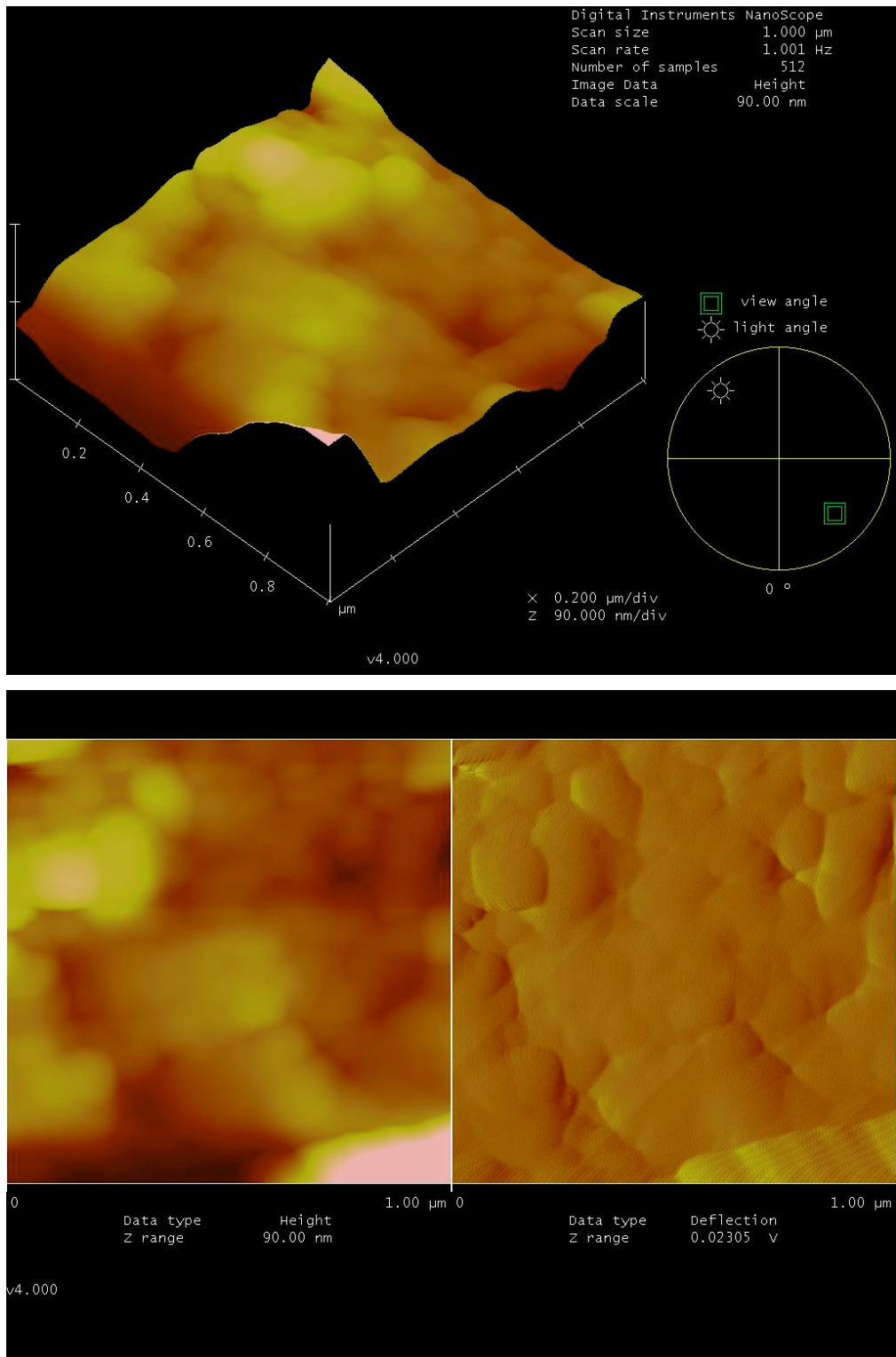
Fig. 4.24 AFM photographs of sample V_3 at the 1 μm scale-1

Fig. 4.25 AFM photographs of sample V$_3$ at the 1 µm scale-2

Digital Instruments NanoScope
Scan size   502.0 nm
Scan rate   1.001 Hz
Number of samples   512
Image Data   Height
Data scale   60.00 nm

view angle
light angle

X 100.000 nm/div
Z 60.000 nm/div

0 °

v4.002

Data type   Height
Z range   60.00 nm

Data type   Deflection
Z range   0.01500 V
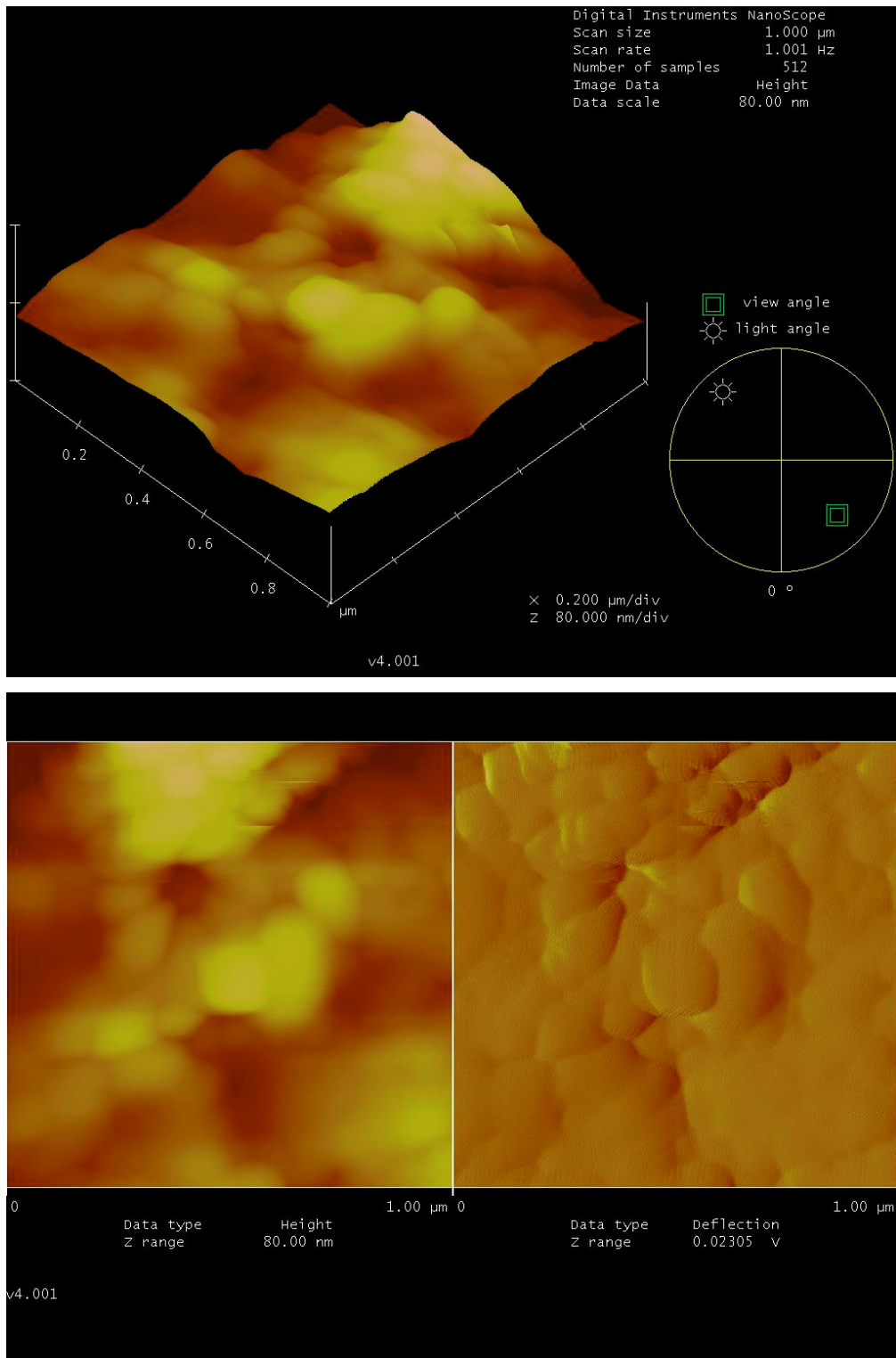
v4.002
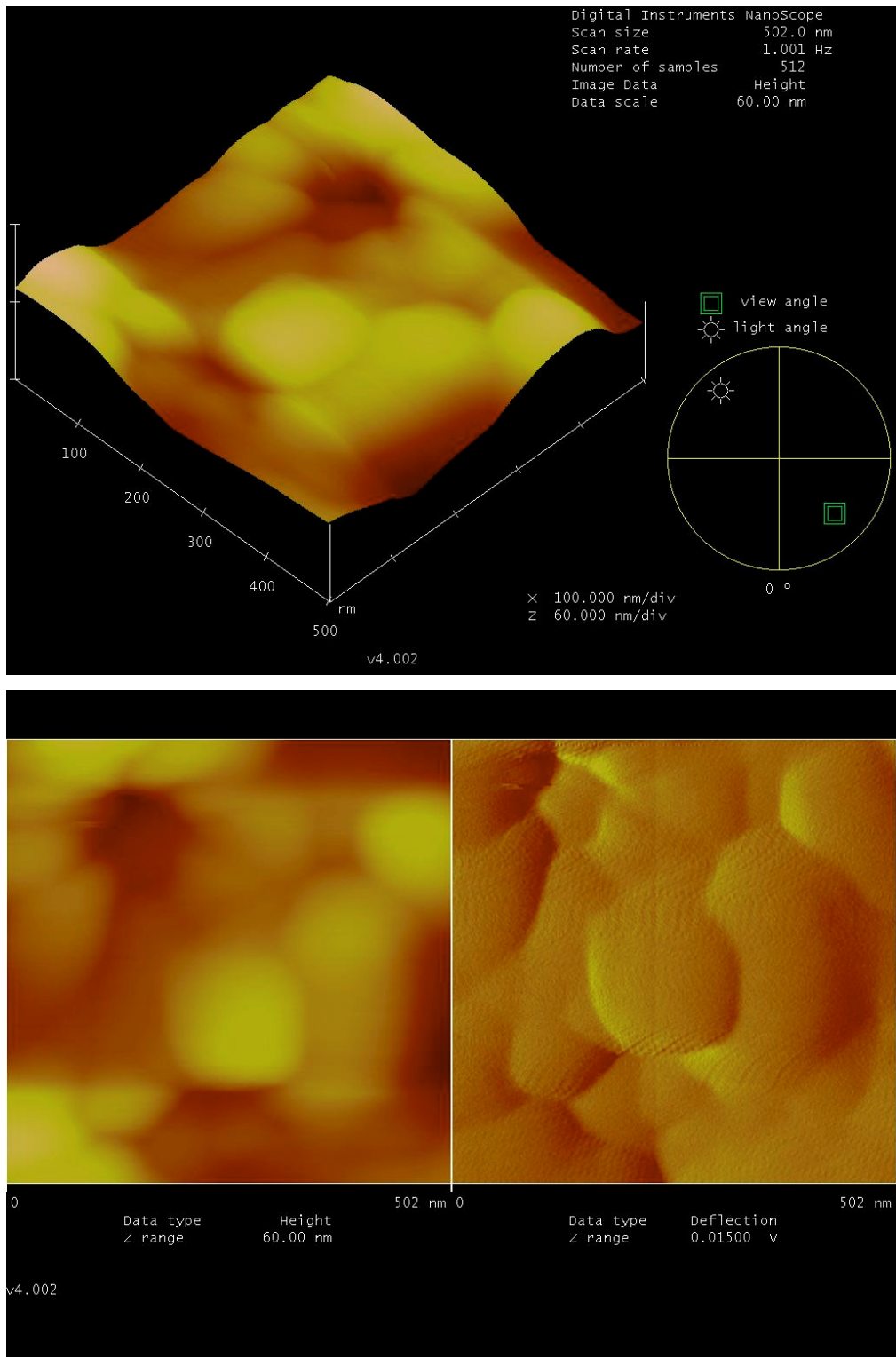
Fig. 4.26 AFM photographs of sample V_3 at the 500 nm scale

and helium pycnometry techniques and the results obtained are given in Sections 4.3.1 to 4.3.4.

4.3.1 XRD patterns

The XRD patterns of the Mo-MCM-41 samples synthesized by the one-pot alkaline synthesis route are given in Figure 4.27. In figure 4.27, the XRD patterns of samples Mo_1, Mo_2 and Mo_3 are given (see the nomenclature in Table C.2. in Appendix C for the properties of these samples).

It is seen that all the samples, except for sample Mo_1, retain the properties of the MCM-41 structure with significant secondary peaks. Hence, no loss of crystallinity seems to have ocurred for samples Mo_2 and Mo_3 upon addition of molybdenum. However, without the EDS results, it is not possible to decide whether molybdenum is sucessfully incorporated into the MCM-41 structure or not.

4.3.2 Nitrogen physisorption results

The nitrogen adsorption isotherms given in Figure 4.28 depict that all the synthesized materials have the type IV adsorption isotherms. The pore size distributions obtained (especially for sample Mo_1), on the other hand, show that all the samples have narrow pore size distributions. Sample Mo_1, different from other samples, also has a small peak corresponding to 50 nm so that it has some macropores in its structure as well as mesopores.

4.3.3 EDS results

The EDS patterns obtained for samples Mo_1, Mo_2 and Mo_3 are given in Figures 4.30 and 4.31. The Mo/Si molar ratios (in the bulk) for these samples are determined by using the composition data given in the same figures. It is seen that for all the synthesized samples; the Mo/Si molar ratio in the product is around 0.01 and is lower than the corresponding ratio in the solution (see Table 4.6). Hence, contrary to the results obtained with the V-MCM-41
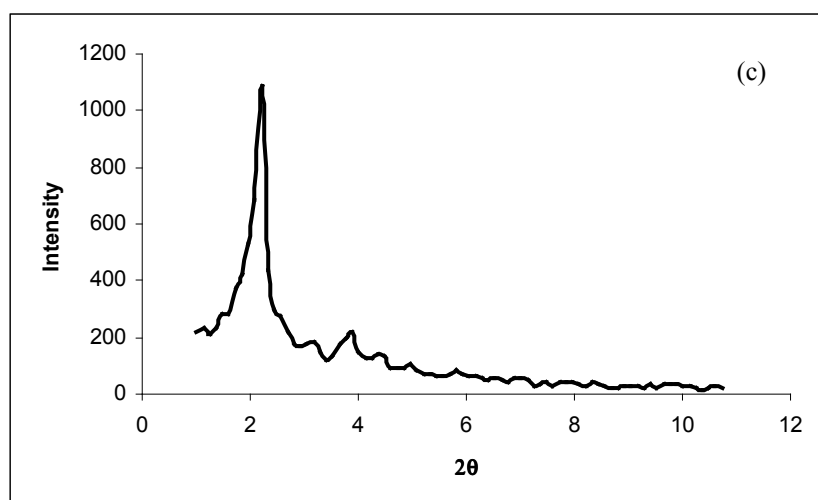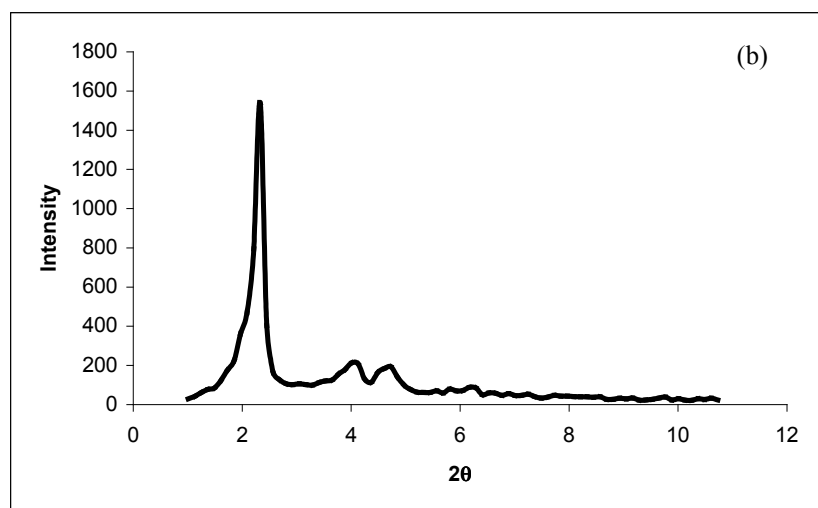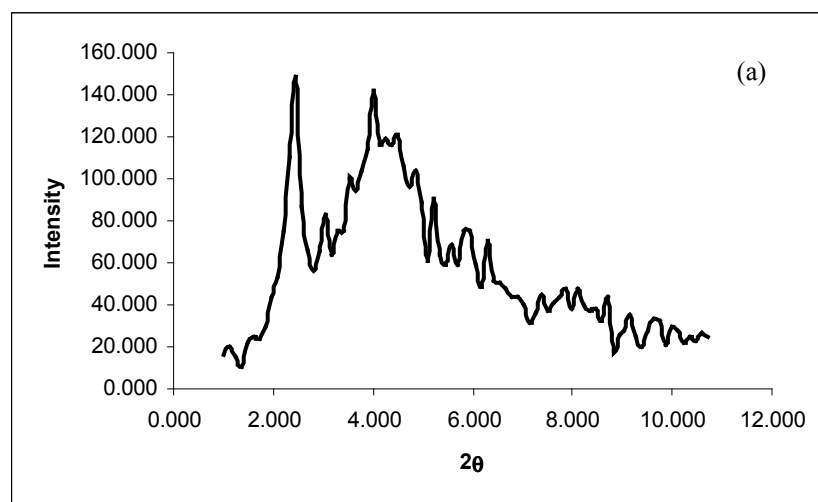
Fig. 4.27 XRD patterns of samples (a) Mo_1, (b) Mo_2 and (c) Mo_3
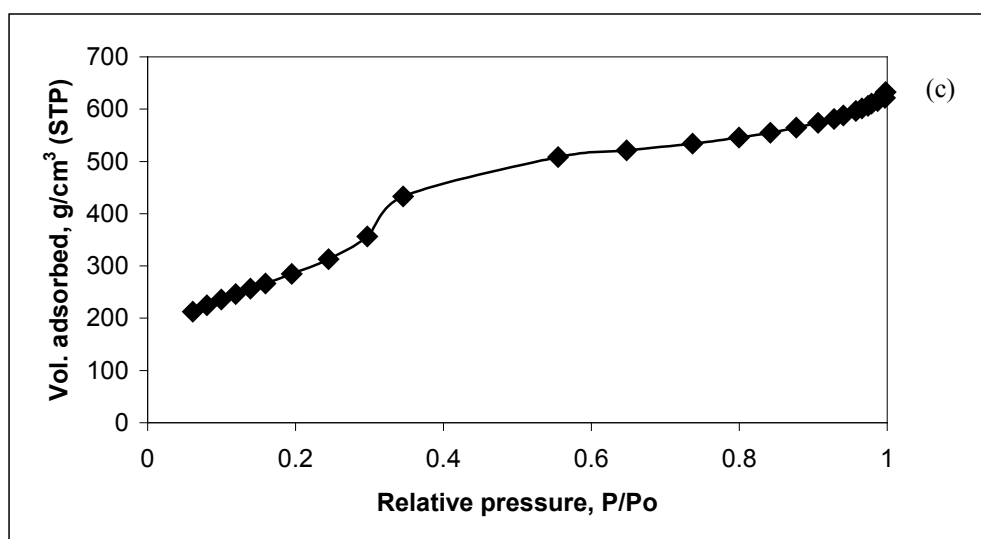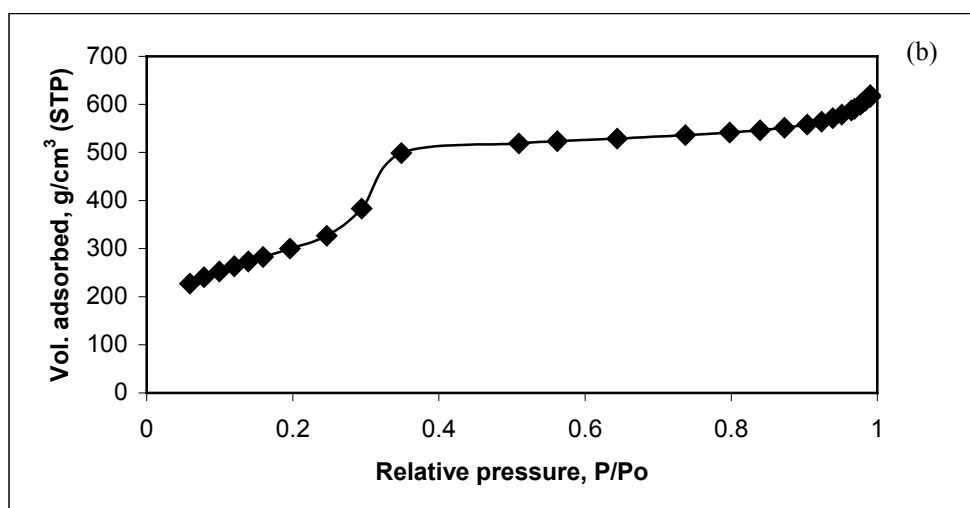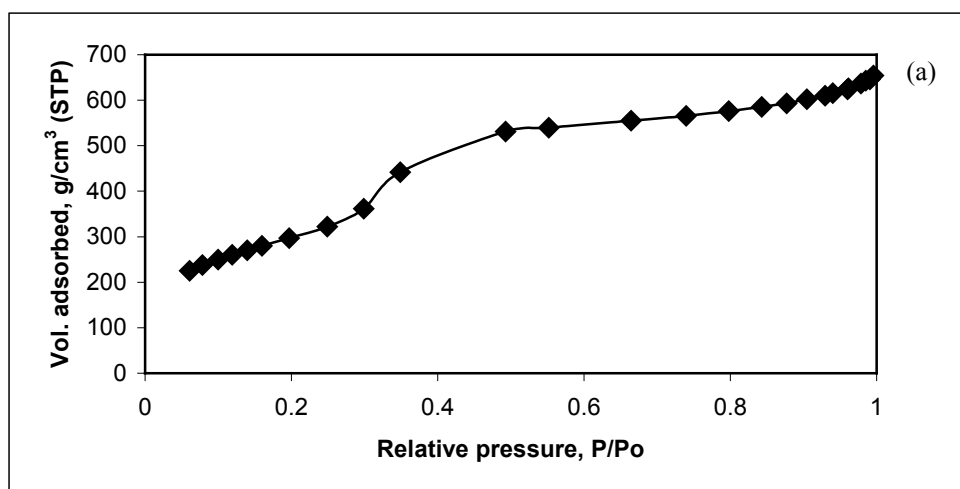
Fig. 4.28 Adsorption isotherms of samples (a) Mo_1, (b) Mo_2 and (c) Mo_3
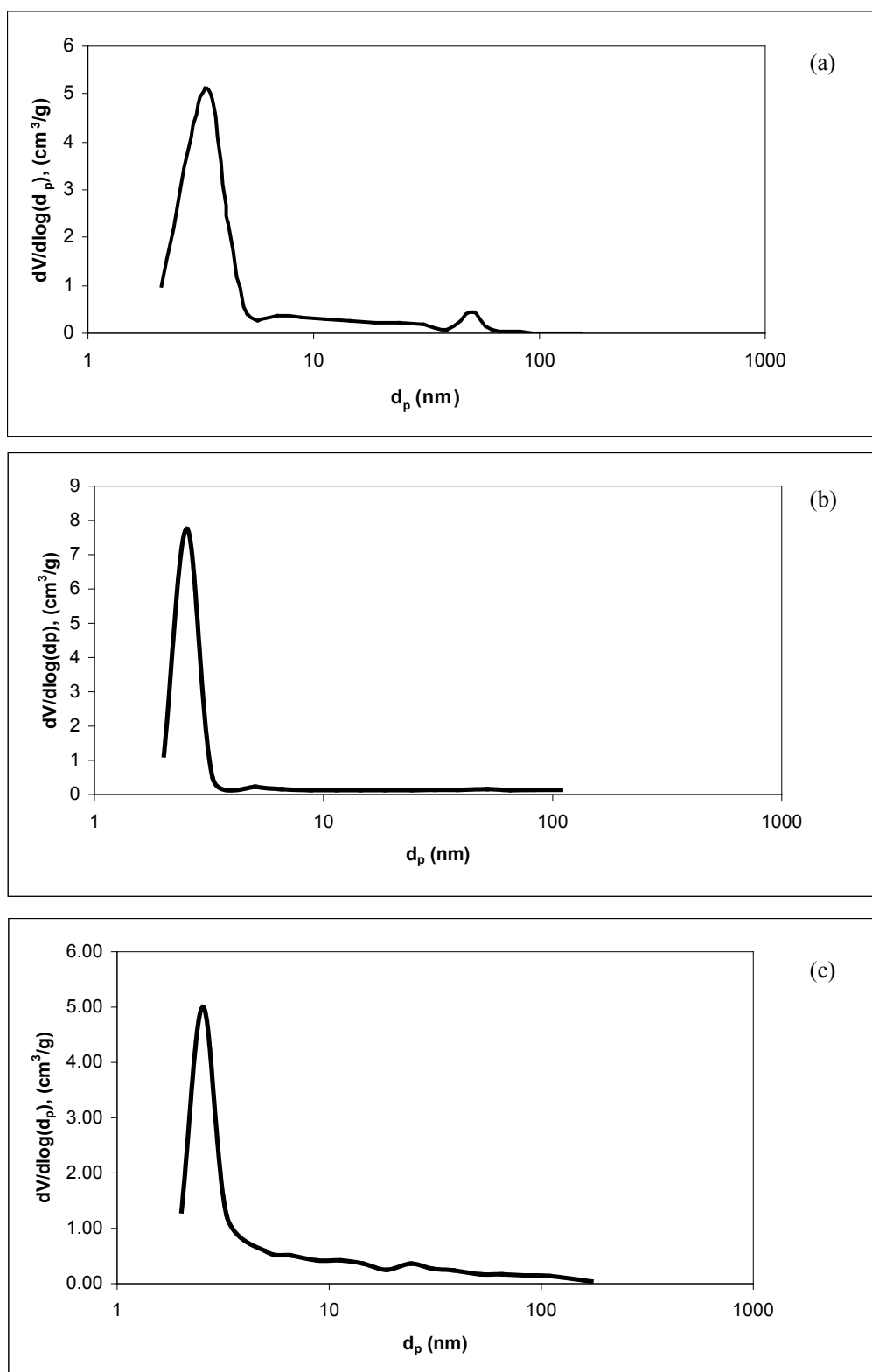
Fig. 4.29 Pore size distributions of samples (a) Mo_1, (b) Mo_2 and (c)Mo_3

(a)
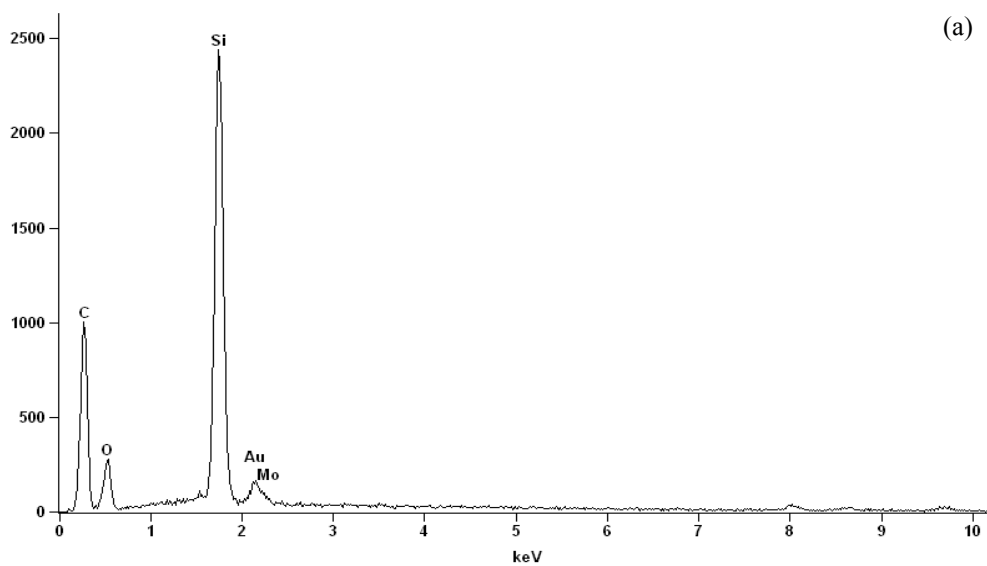
Element	Weight Conc %	Atom Conc %
Si	98.47	99.55
Mo	1.53	0.45

(b)
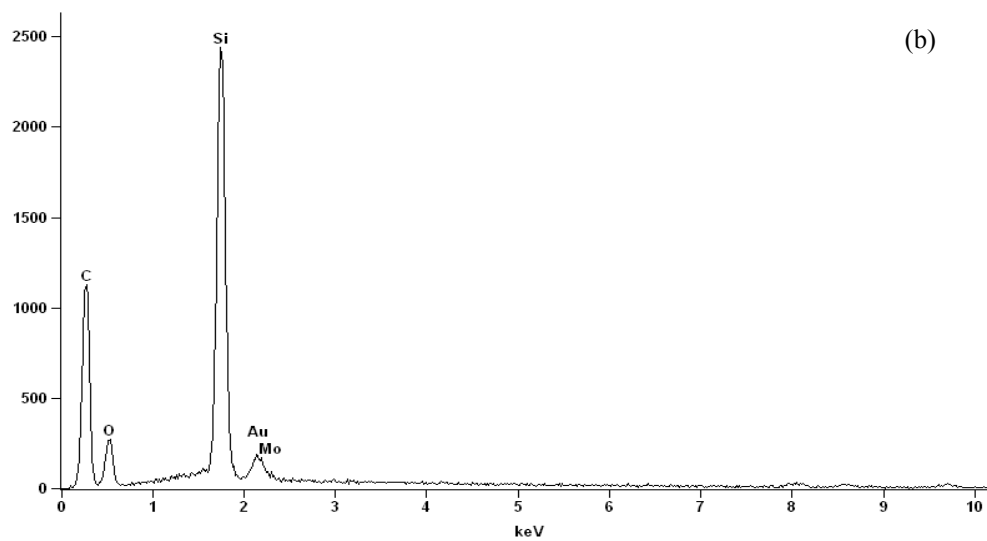
Element	Weight Conc %	Atom Conc %
Si	96.97	99.09
Mo	3.03	0.91

Fig. 4.30 EDS patterns of (a) sample Mo_1 and (b) sample Mo_2

Element	Weight Conc %	Atom Conc %
Si	99.51	99.86
Mo	0.49	0.14
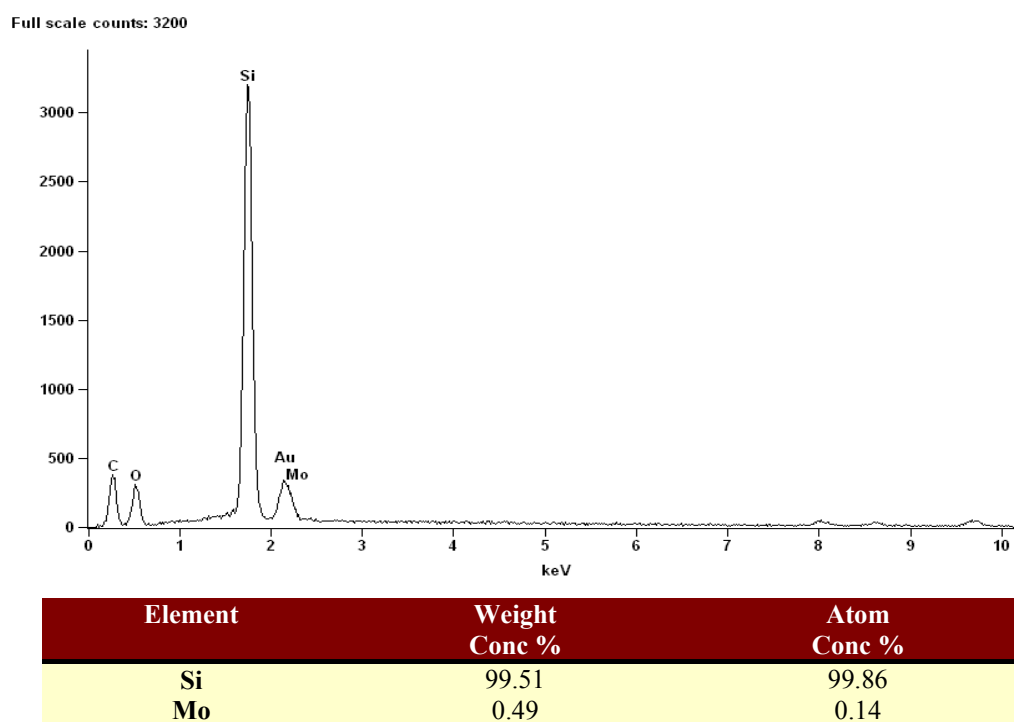
Fig. 4.31 EDS pattern of sample Mo_3

catalysts, the one-pot alkaline synthesis route is not a very successful method for the incorporation of the molybdenum metal into the structure.

Table 4.6 Mo/Si Molar Ratios (in the bulk) Calculated from the EDS Data for the Samples Synthesized with the Alkaline Route

Sample ID	Mo/Si molar ratio in the solution	Mo/Si molar ratio in the solid
Mo_1	0.03	0.005
Mo_2	0.06	0.009
Mo_3	0.09	0.014

4.3.4 Physical properties

All synthesized samples had high surface areas, high pore volumes and porosities (see Table 4.7). However, the pore diameters did not change

considerably with the increasing Mo/Si ratio since only low amounts of molybdenum were incorporated.

Table 4.7 Physical Properties of the Mo-MCM-41 Catalysts Synthesized with the Alkaline Route

Sample ID	Mo/Si bulk ratio	BET (m^2/g)	Vpore (cm^3/g) (*)	D_{pore} (nm) (*)	ρ_s (g/cm^3)	ρ_{app} (g/cm^3)	$\in$
Mo_1	0.03	1088	1.10	3.2	3.20	0.71	0.78
Mo_2	0.06	1101	1.07	2.9	3.78	0.75	0.80
Mo_3	0.09	1367	1.06	3.1	3.36	0.74	0.78

4.4 Characterization of the Mo-MCM-41 Catalysts Synthesized by the Acidic Route

The Mo-MCM-41 catalysts were also synthesized through a one-pot acidic synthesis route in order to see the effect of the pH on the final product properties. These catalysts are characterized by the XRD, EDS and BET techniques as given in Sections 4.4.1 to 4.4.3.

4.4.1 XRD patterns

Initially, two Mo-MCM-41 catalysts designated Mo_4 and Mo_5 are synthesized using the acidic synthesis route (see the nomenclature in Table C.2 in Appendix C). The XRD patterns corresponding to these samples are given in Figure 4.32. It is seen that the characteristic peaks obtained for the samples have broadened when compared to the Mo-MCM-41 samples synthesized through the alkaline route. Further, the secondary peaks which verify the hexagonal geometry are not easily detectable. These problems are thought to be due to the absence of the aging (hydrothermal synthesis) step in the one-pot acidic synthesis recipe. Hence, two more samples (Mo_6 and Mo_7), are synthesized by adding a one-day aging step to the synthesis procedure. The XRD patterns obtained for these new samples are given in Figure 4.33. These
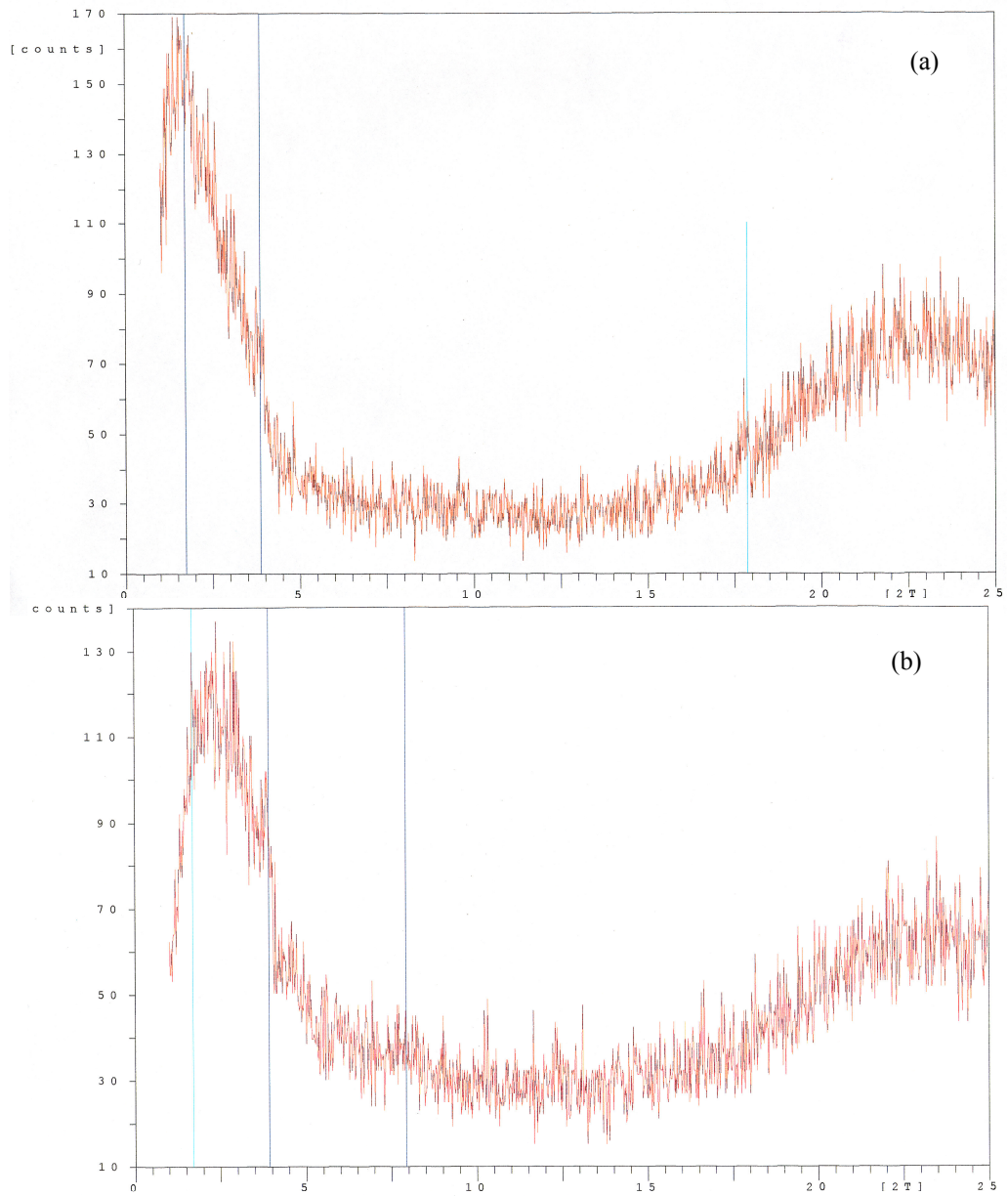
Fig. 4.32 XRD patterns of sample (a) Mo_4 and (b) Mo_5

86
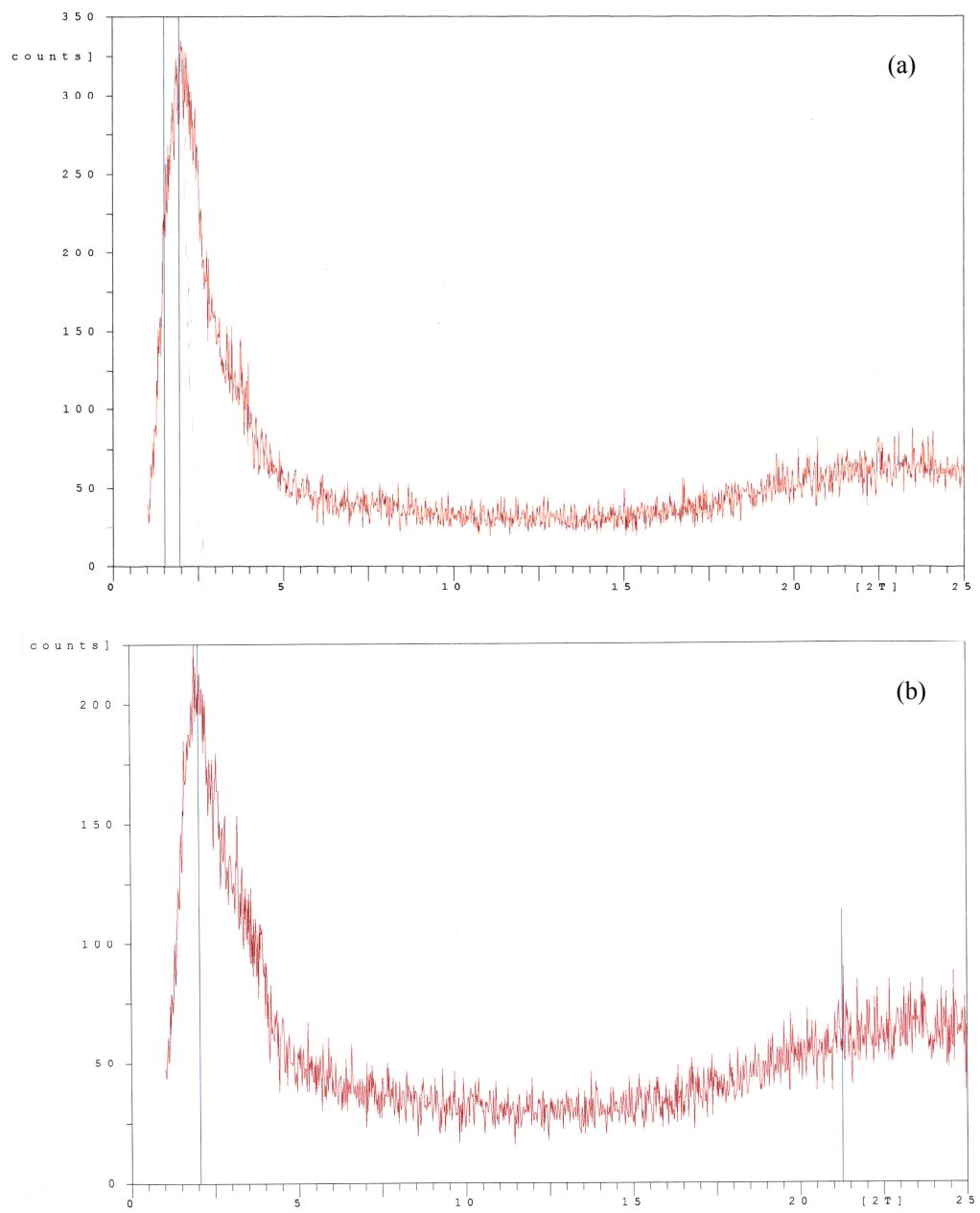
Fig 4.33 XRD patterns of samples (a) Mo$_6$ and (b) Mo$_7$

samples are found to have narrower characteristic peaks than samples Mo_4 and Mo_5; hence the addition of the aging step has improved the structure.

4.4.2 EDS results

Table 4.8 displays the Mo/Si molar ratios (in the bulk) obtained for samples Mo_4-Mo_7 (see the nomenclature in Table C.2 in Appendix C for the properties of these samples) as calculated from their EDS results. In general, all the samples synthesized by the acidic route have higher Mo/Si molar ratios (in the bulk) than the samples synthesized by the alkaline route.

Table 4.8 Mo/Si Molar Ratios (in the bulk) Calculated from the EDS Data
for the Mo-MCM-41 Samples Synthesized with the Acidic Route

Sample ID	Mo/Si molar ratio in the solution	Mo/Si molar ratio in the solid
Mo_4	0.03	0.021
Mo_5	0.09	0.027
Mo_6	0.03	0.039
Mo_7	0.09	0.031

On the other hand, if the samples Mo_6 and Mo_7 synthesized with the aging step are compared with the samples Mo_5 and Mo_6 synthesized without the aging step; the addition of the aging step seems to increase the amount of molybdenum incorporated to the structure.

4.4.3 Physical properties

Mo-MCM-41 catalysts synthesized with the acidic route have lower BET surface areas compared to those synthesized with the alkaline route (see Table 4.9). This is due to two reasons: First of all, higher amounts of molybdenum are added to the MCM-41 structure through the acidic route than through the alkaline route and secondly, the MCM-41 structure is destroyed more in the case of the acidic route compared to the alkaline route.

(a)
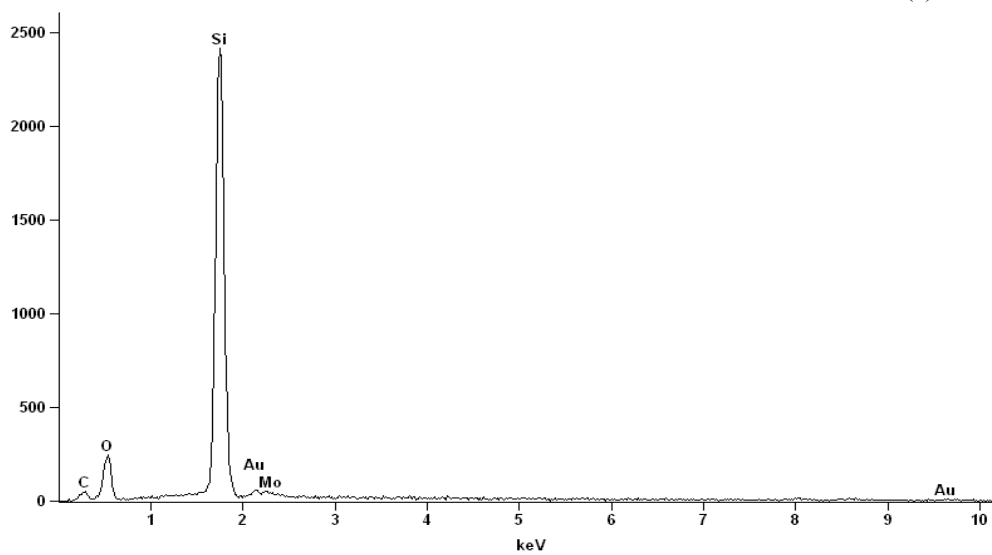
Element	Weight Conc %	Atom Conc %
Si	93.36	97.96
Mo	6.64	2.04

(b)
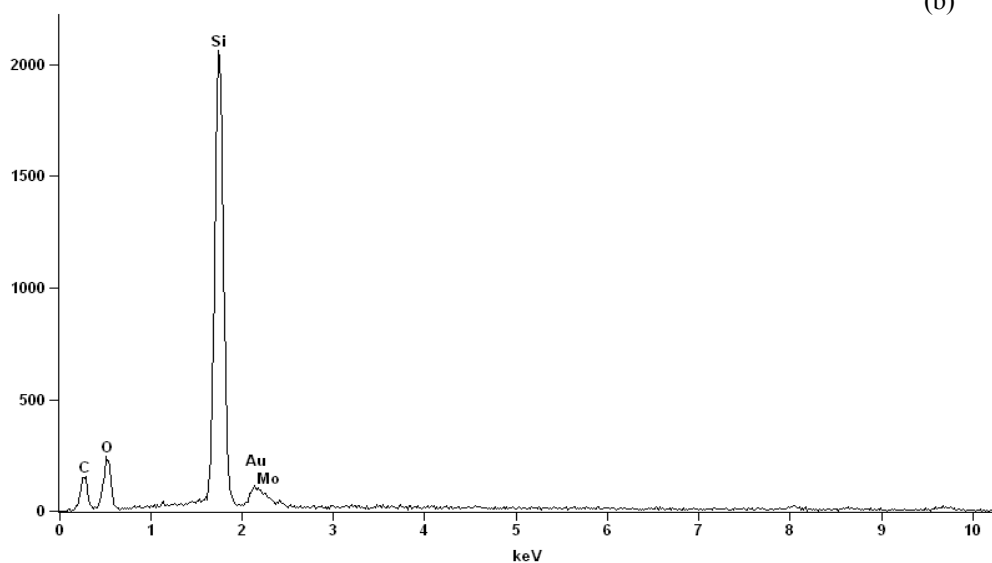
Element	Weight Conc %	Atom Conc %
Si	91.42	97.33
Mo	8.58	2.67

Fig. 4.34 EDS patterns of (a) sample Mo_4 and (b) sample Mo_5

Full scale counts: 2249

(a)
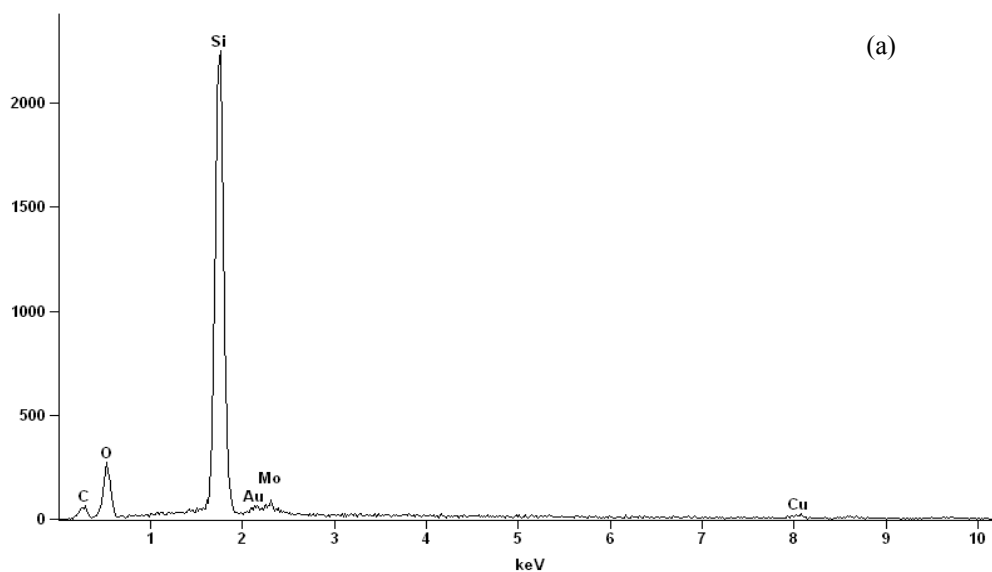
Element	Weight Conc %	Atom Conc %
Si	88.34	96.28
Mo	11.66	3.72

Full scale counts: 4443

(b)
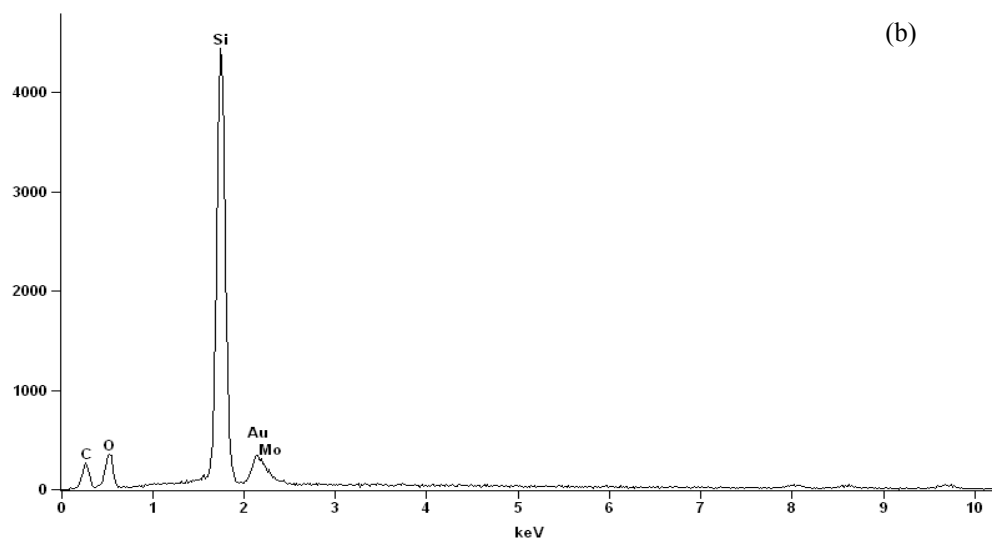
Element	Weight Conc %	Atom Conc %
Si	90.35	96.97
Mo	9.65	3.03

Fig 4.35 EDS patterns of samples (a) Mo_6 and (b) Mo_7

Table 4.9 BET Surface Areas of the Mo-MCM-41 Catalysts Synthesized with the Acidic Route

Sample ID	Mo/Si ratio in the solution	BET Specific Surface Area (m^2/g)
Mo_4	0.03	433
Mo_5	0.09	549
Mo_6	0.03	470
Mo_7	0.09	488

4.5 Use of the Synthesized Catalysts in the Selective Oxidation of Ethanol

The first catalyst tested in the selective oxidation experiments was the catalyst V_4. This catalyst had a high BET surface area of 1062 m^2/g, a high quality XRD pattern with significant secondary peaks and aV/Si molar ratio in the bulk of 0.04. The high value of the BET surface area and the high quality of the XRD pattern indicated that V_4 was a successfully-prepared catalyst, however, the V/Si molar ratio of 0.04 seemed to be moderate. Would this be a handicap or an advantage? This question is answered in the following sections.

4.5.1 Experiments with the catalyst V_4

The first group of experiments performed with the catalyst V_4 were the reaction experiments at different temperatures with different $O_2/EtOH$ ratios. The results corresponding to this set of experiments are given in Figures 4.36 to 4.43.

It is seen, by observing Figures 4.36-4.41, that, as expected conversions increase with increasing temperature at every value of the $O_2/EtOH$ ratio.

For the low $O_2/EtOH$ ratios of 0.083 and 0.17 (Figure 4.36.a and b), the increase of conversion with temperature is not significant. The maximum conversion values obtained at the $O_2/EtOH$ ratios of 0.083 and 0.17 are 0.19 and 0.25, respectively. For these cases, oxygen is the limiting reactant.

Figure 4.37.a indicates that when the O_2/EtOH ratio increases to 0.28, the increase of converison with temperature is still not very significant, however, the maximum conversion (at $400^{o}C$) value now reaches to 0.49.

In Figure 4.37.b, the results obtained with the stoichiometric O_2/EtOH ratio of 0.5 are shown. It is seen that at the stoichiometric ratio, the conversion suddenly jumps from a value of 0.24 at $300^{o}C$ to a value of 0.96 at $375^{0}C$. Hence it seems that the catalyst is activated at a temperature between $300^{o}C$ to $375^{o}C$. Considering the selectivity to acetaldehyde, this product has a selectivity of 1.00 at the temperatures of $150^{o}C$ and $200^{o}C$. When the temperature raises to $250^{o}C$, its selectivity falls to 0.82 and when the temperature raises to $300\ ^{o}C$, it falls further to 0.49. However, when the yield versus temperature graph corresponding to the stoichiometric ratio (Figure 4.40.b) is observed, it is seen that the highest yield of acetaldehyde is obtained at $375^{0}C$ due to the high conversion there although the selectivity is moderate at that temperature. Hence, for optimum acetaldehyde production, the reaction can be operated at $375^{0}C$ at the O_2/EtOH ratio of 0.5.

Considering the carbon dioxide production; carbon dioxide selectivity is not considerable even at the high temperature of $400^{o}C$ at the stoichiometric O_2/EtOH ratio of 0.5.

Figure 4.37.b displays another very important feature. It is seen that; along with acetaldehyde, significant amounts of ethylene are produced as well. For instance at $375^{o}C$, the selectivity to ethylene is 0.64 and at $400^{o}C$, it is 0.67. Interestingly, these selectivity values are much higher than the selectivities of acetaldehyde at $375^{o}C$ and $400^{o}C$ (0.28 and 0.26, respectively). Hence, contrary to the literature findings where ethylene is always listed as a side product of the ethanol partial oxidation, the catalyst V_4 produces ethylene as the major product at temperatures higher than $300^{o}C$ at the stoichiometric O_2/EtOH ratio of 0.5.

Fig. 4.38.a displays the results obtained in excess oxygen medium with the O_2/EtOH feed ratio of 1.2. This figure has the same trend as Figure 4.37.b
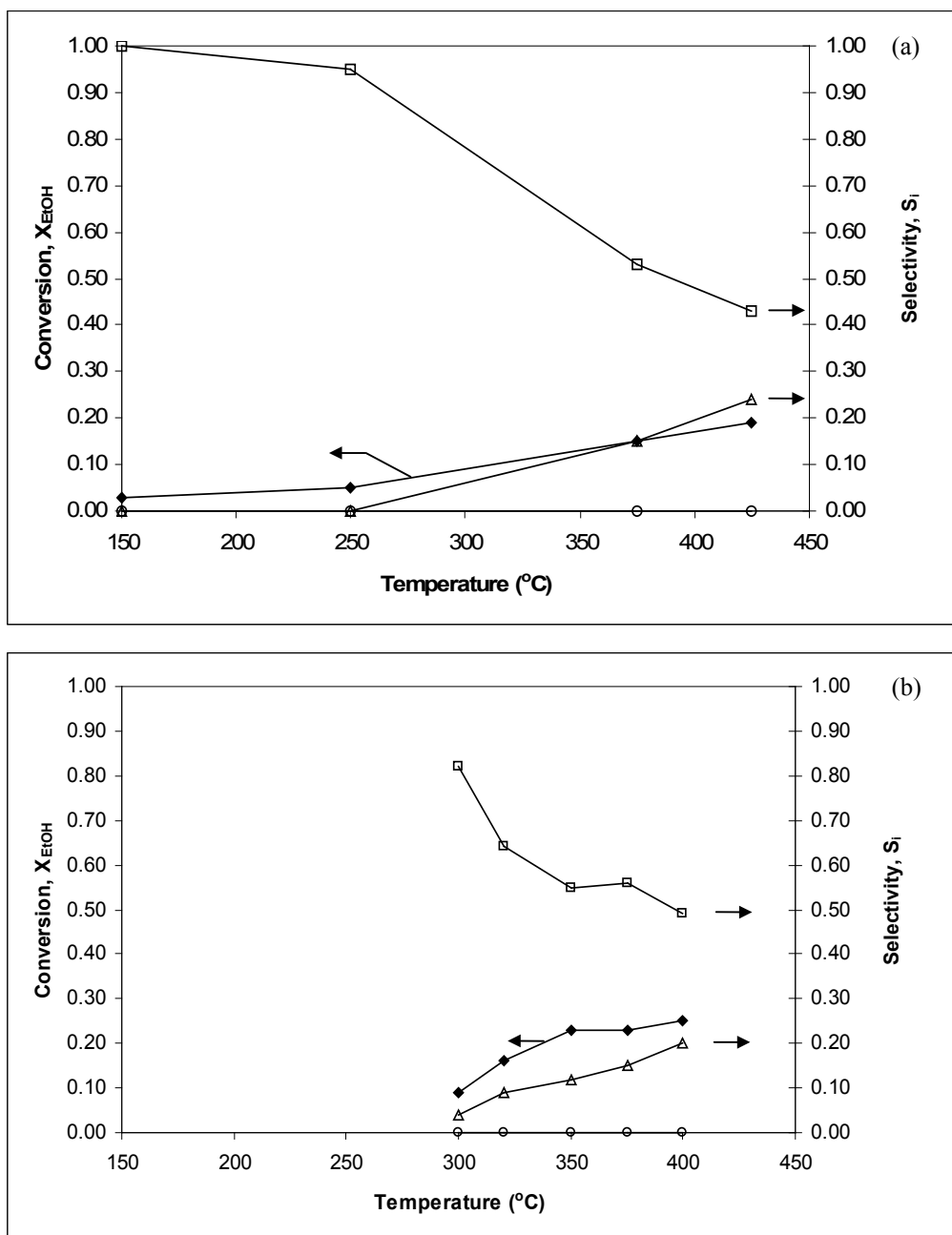
Fig. 4.36. Conversion and selectivity values obtained on the catalyst V_4.
  (c) for GHSV = 44.6 h^{-1} at an O_2/EtOH feed ratio of 0.083.
  (d) for GHSV= 37.8 h^{-1} at an O_2/EtOH feeed ratio of 0.17.
  (♦) EtOH conversion, (□) acetaldehyde selectivity, (△) ethylene selectivity,
  (○) carbon dioxide selectivity.
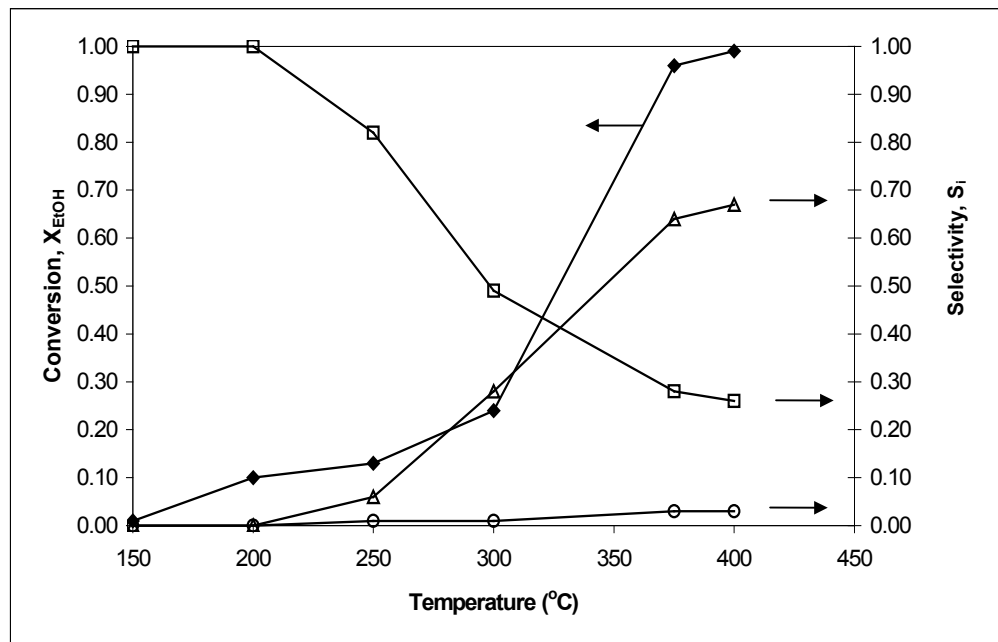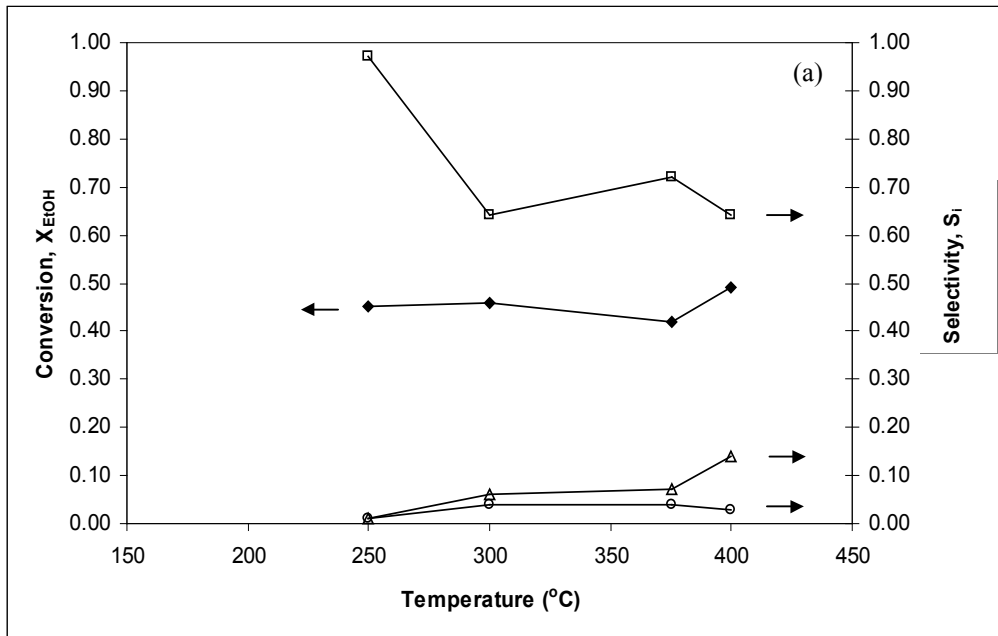
Fig. 4.37 Conversion and selectivity values obtained on the catalyst V_4. for the GHSV of 64.7 h^{-1} at an $O_2/EtOH$ feed ratio of (a) 0.28 and (b) 0.50. (♦) EtOH conversion, (□) acetaldehyde selectivity, (△) ethylene selectivity, (○) carbon dioxide selectivity.
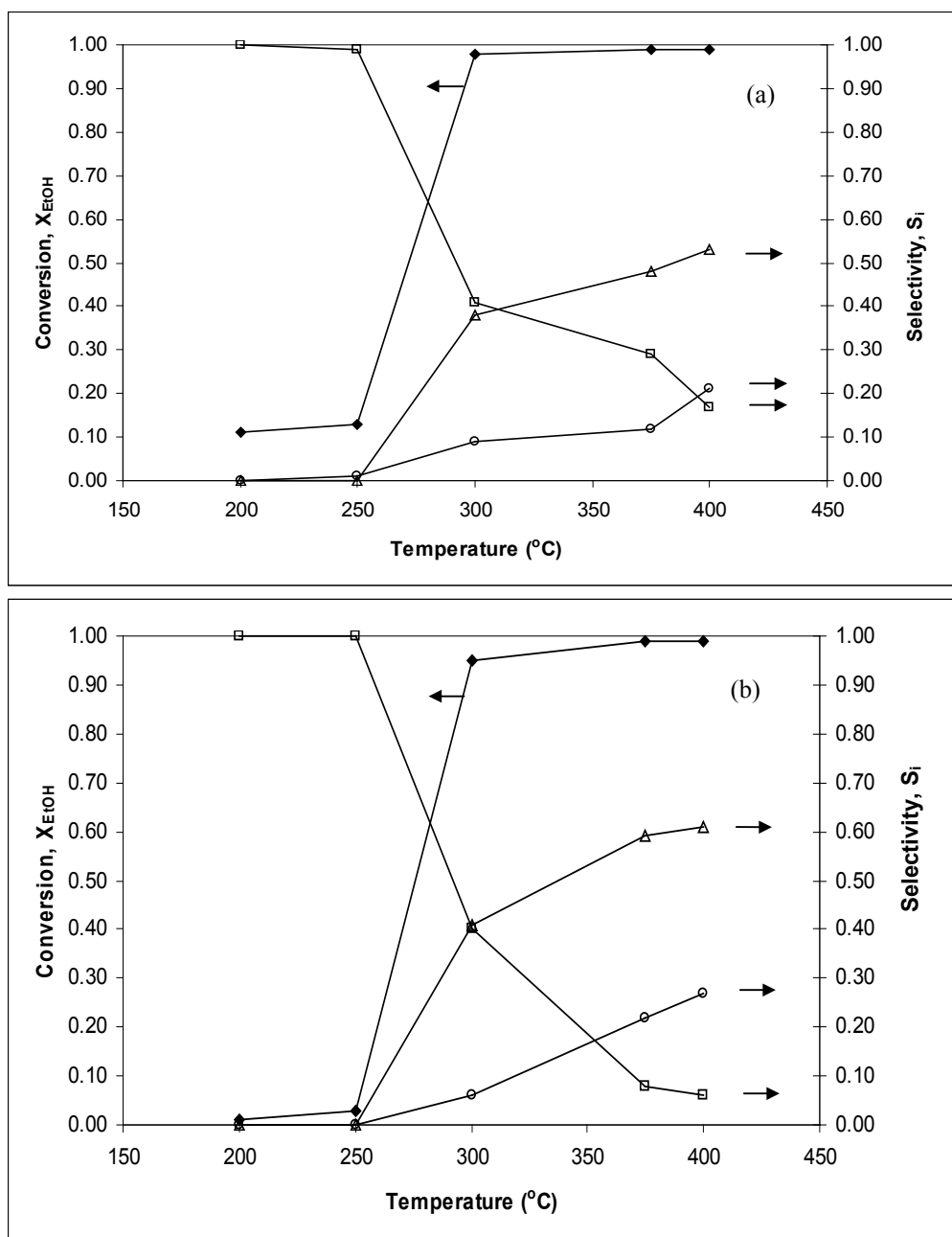
Fig. 4.38 Conversion and selectivity values obtained on the catalyst V_4 for the GHSV of 64.7 hr^{-1} at an O_2/EtOH feed ratio of (a) 1.20 and (b) 2.00. (♦) EtOH conversion, (□) acetaldehyde selectivity, (△) ethylene selectivity and (○) carbon dioxide selectivity.

where the $O_2/EtOH$ ratio was 0.5. However, the jump in the conversion now occurs at 300°C (considering the yield values, Figure 4.41.a displays that the highest yield of acetaldehyde also occurs at 300°C). The carbon dioxide selectivity is now more significant due to the use of excess oxygen and its maximum value is 0.21 at 400°C.

Fig. 4.38.b displays the results obtained in the excess oxygen medium with an $O_2/EtOH$ feed ratio of 2.0. The same trend as in Figures 4.37.b and 4.38.a are displayed. However, the acetaldehyde selectivities at 375°C and 400°C are now too low . The ethylene selectivities obtained are higher than those obtained at the $O_2/EtOH$ ratio of 1.2 but lower than those obtained at the stoichiometric $O_2/EtOH$ ratio of 0.5. The maximum carbon dioxide selectivity is now 0.27 at 400°C.

Figures 4.39-4.41 show the conversion and yield versus temperature graphs for the different $O_2/EtOH$ ratios. In Figure 4.39 (a) and (b), at the low $O_2/EtOH$ ratios of 0.083 and 0.17, the yields of acetaldehyde and ethylene are also low.

When the $O_2/EtOH$ ratio raises to 0.28, the maximum acetaldehyde yield becomes 0.44, however, the ethylene yield still remains low (Figure 4.40.a).

When the $O_2/EtOH$ ratio is raised to the stoichiometric value of 0.5 (Figure 4.40.b), the ethylene and acetaldehyde yields show a significant increase and the maximum ethylene yield bypasses the maximum acetaldehyde yield. The acetaldehyde yield gives a maximum at 375°C and then decreases somewhat at 400°C since its low selectivity at 400°C can not be compensated by the high conversion at that temperature. However, the ethylene yield increases with increasing temperature since its selectivity also increases with increasing temperature.

The results obtained with $O_2/EtOH$ ratios of 1.2 and 2.0 (Figure 4.41.a and 4.41.b, respectively) show that use of excess oxygen is not favourable for acetaldehyde production especially at high temperatures.
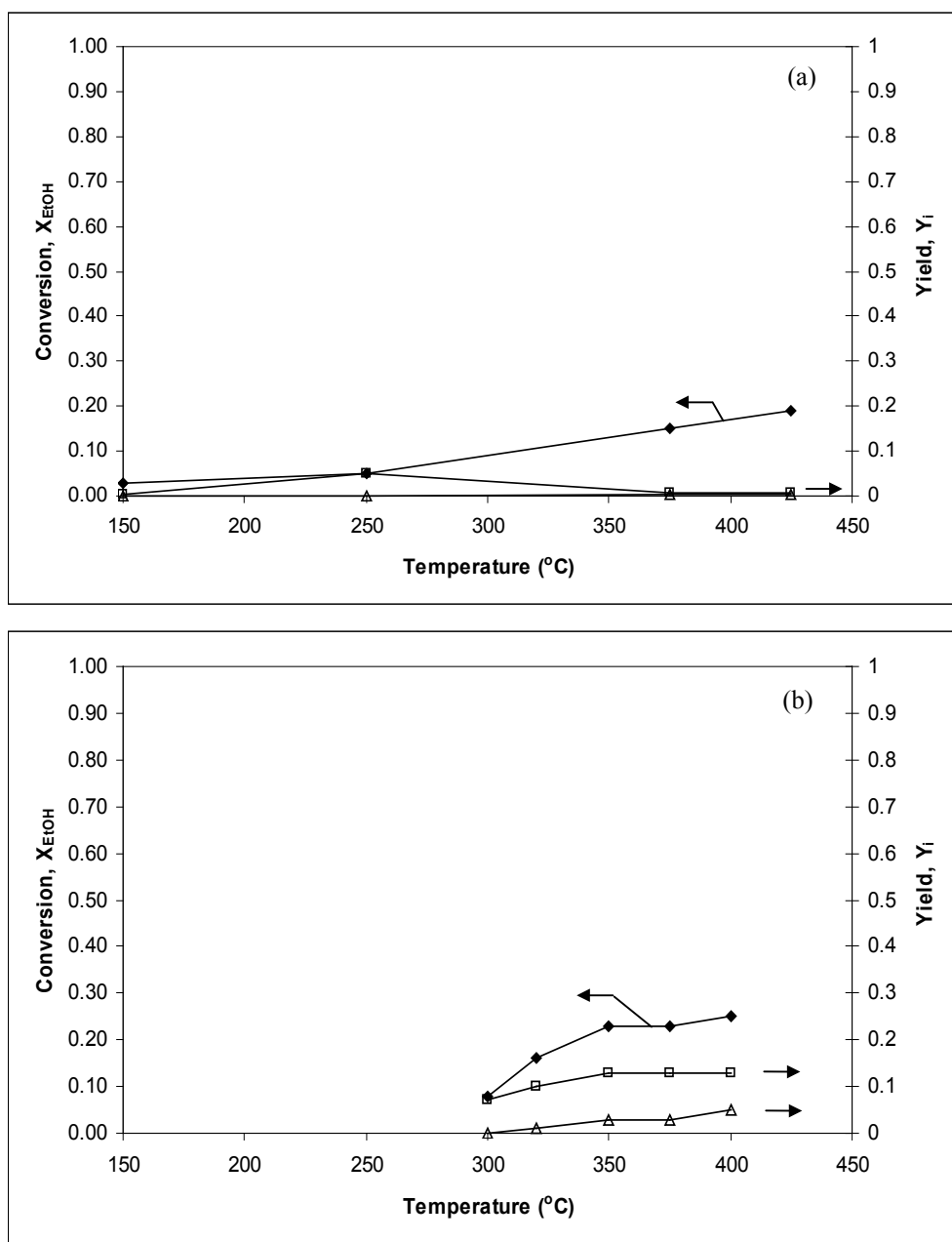
Fig. 4.39 Conversion and yield values obtained on the catalyst V_4.
(a) for GHSV = 44.6 h^{-1} at an O$_2$/EtOH feed ratio of 0.083
(b) for GHSV = 37.8 h^{-1} at an O$_2$/EtOH feeed ratio of 0.17.
($\blacklozenge$) EtOH conversion, ($\square$)acetaldehyde yield, ($\triangle$) ethylene yield.
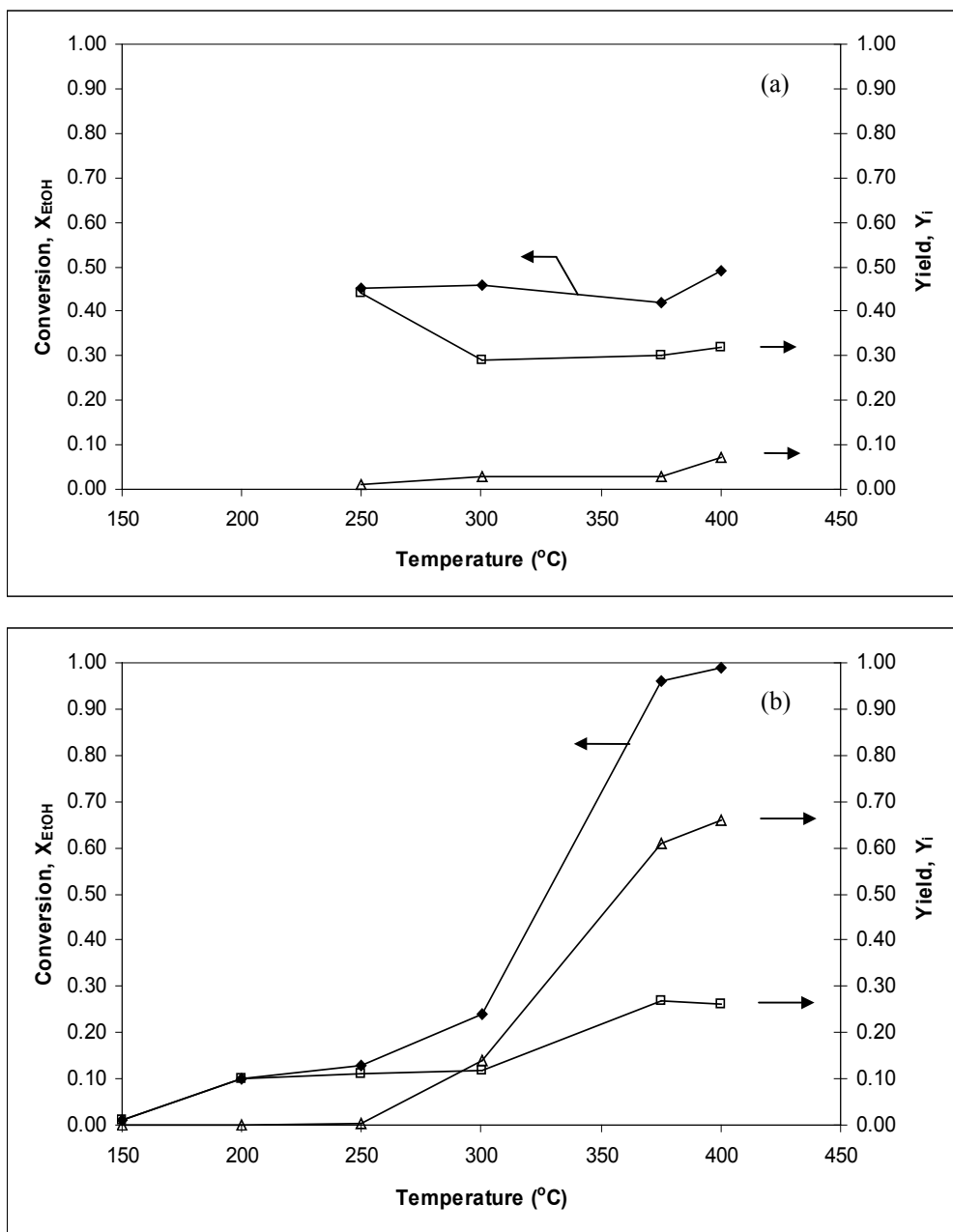
Fig. 4.40 Conversion and yield values obtained on the catalyst V_4 for the GHSV of 64.7 h^{-1} at an O$_2$/EtOH feed ratio of (a) 0.28 and (b) 0.50. (♦) EtOH conversion, (□) acetaldehyde yield, (△) ethylene yield.
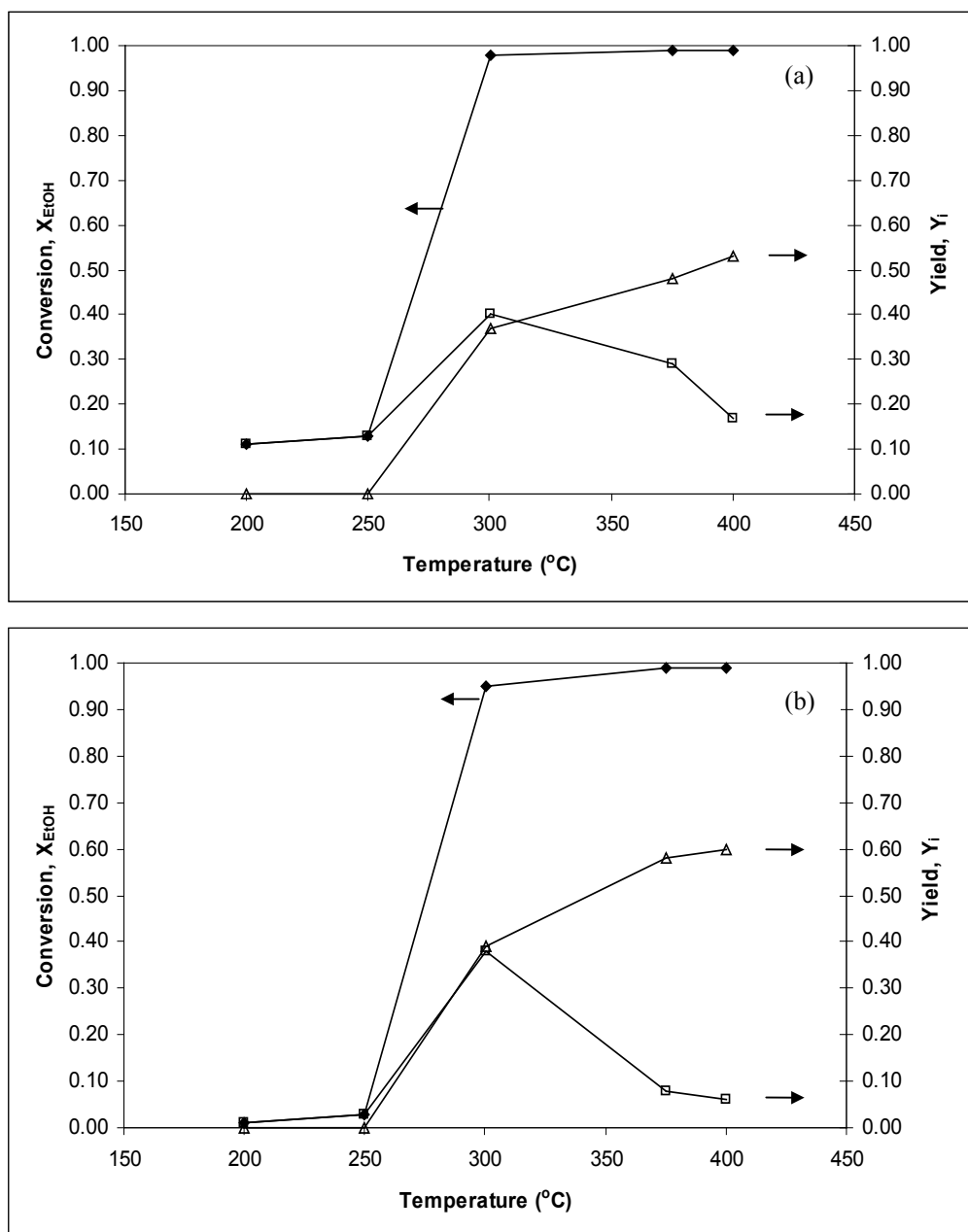
Fig. 4.41 Conversion and yield values obtained on the catalyst V_4 for the GHSV of 64.7 hr^{-1} at an O_2/EtOH feed ratio of (a) 1.20 and (b) 2.00. (♦) EtOH conversion, (□) acetaldehyde yield, (△) ethylene yield.

The use of excess oxygen brings about a small decrease in the yield values of ethylene, as well. The maxium ethylene yield decreases from 0.66 to 0.53 when the O_2/EtOH ratio increases from the stoichiometric value of 0.5 to 1.2. When the O_2/EtOH ratio increases further to 2.0, the maximum ethylene yield becomes 0.61 however it is still less than the value (0.66) obtained at the stoichiometric ratio.

In general, Figures 4.36-4.41 bring about very important results. First of all, it is seen that acetaldehyde selectivity and yield decreases with increasing temperature. Contrarily, ethylene selectivity and yield increases with increasing temperature. The reaction attains a conversion value of 0.96-0.99 at around 350^oC which means that it can be run at moderate temperatures to obtain high conversions. In general, lean oxygen conditions favour acetaldehyde production whereas the ethylene production is most favoured at the stoichiometric O_2/EtOH ratio of 0.5. The excess oxygen conditions also give high ethylene yields however the yield values are somewhat lower than those obtained at the stoichiometric O_2/EtOH ratio of 0.5. For excess oxygen conditions, further oxidation of the reaction products and especially acetaldehyde causes the formation of carbon dioxide. The last and the most important result is that by using a high surface area V-MCM-41 catalyst, which has a moderate V/Si molar ratio in the product, it is possible to produce ethylene with yield values as high as 0.66 in the selective oxidation of ethanol. Hence, a new method of ethylene production can be developed by using the selective oxidation of ethanol over high surface area V-MCM-41 catalysts.

Following these important results, Figures 4.42 and 4.43 are also plotted to see the effects of the different O_2/EtOH ratio on the selectivity, conversion and yield values of the reaction more clearly at the temperatures of 300^oC, 375^oC and 400^oC.

In Figure 4.42.a , it is seen that at 300^oC, the conversion values increased with increasing O_2/EtOH feed ratios. The ethylene selectivities also
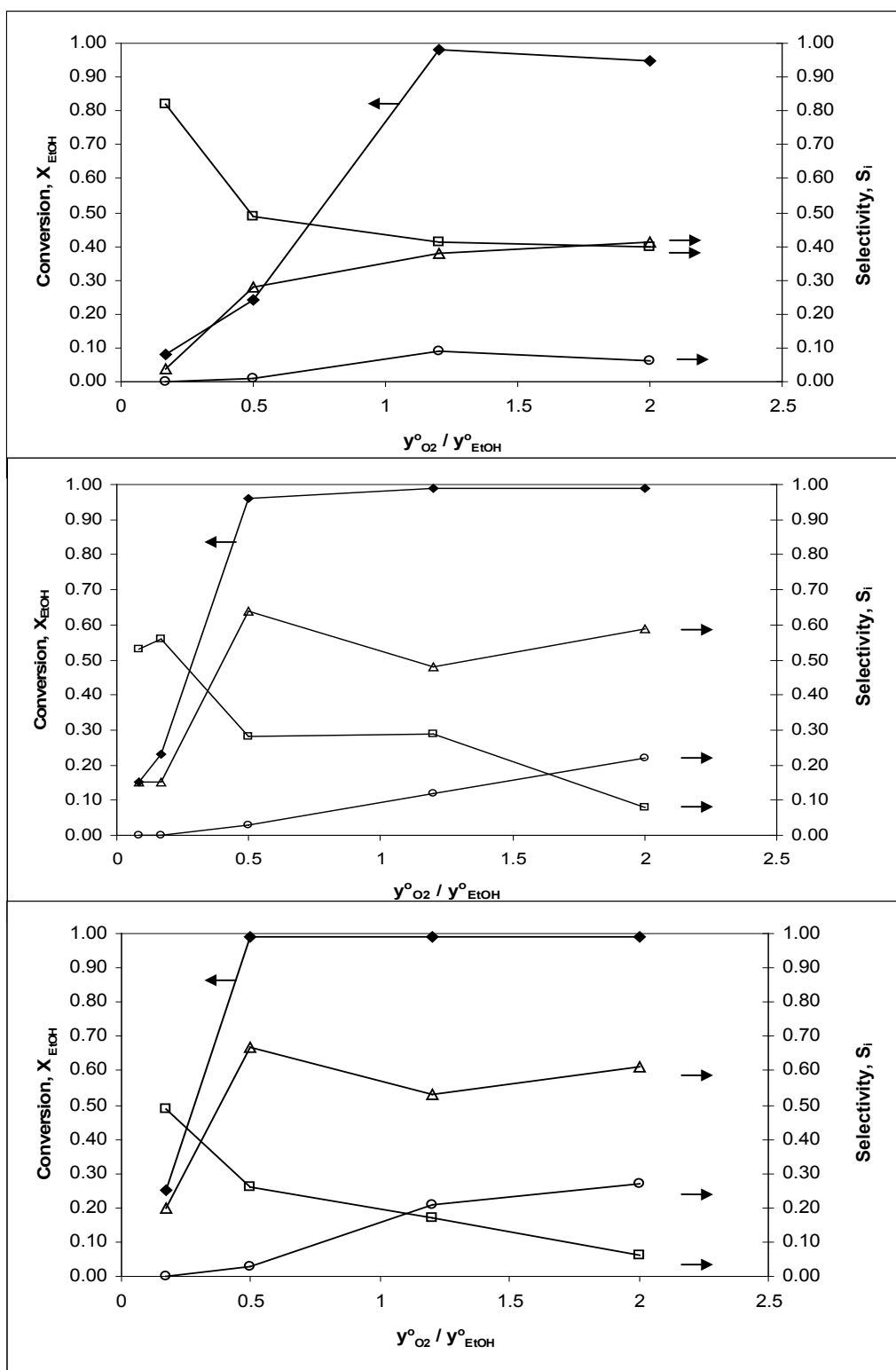
Fig 4.42. Conversion and selectivity values obtained with different y^o_{O2}/ y^o_{EtOH} ratios at (a) 300°C, (b) 375°C and (c) 400°C. (♦) EtOH conversion, (□) acetaldehyde selectivity, (△) ethylene selectivity, (○) carbon dioxide selectivity.

increased with increasing O_2/EtOH ratios while the acetaldehyde selectivities decreased with increasing O_2/EtOH ratios. This indicates, as mentioned previously, that ethylene production is favoured by stoichiometric and excess O_2 conditions whereas acetaldehyde production is favoured by lean oxygen conditions.

The conversion values increase with increasing O_2/EtOH ratios at the temperatures of 375^oC and 400^oC as well as seen in Figures 4.42.b and 4.42.c, respectively. This increase in conversion is partly due to the increased production of carbon dioxide at the O_2/EtOH ratios of 1.2 and 2.0. The acetaldehyde selectivities decrease with increasing O_2/EtOH ratios. In the case of the ethylene selectivities, the maximum selectivities occur at the stochiometric ratio and then the selectivities decrease as the excess oxygen conditions are used.

Figure 4.43 displays the yield values obtained at the different O_2/EtOH ratios at the temperatures of 300, 375 and 400^oC. This figure shows a similar trend as Figure 4.42. The maximum ethylene yield (0.66) occurs at the stoichiometric O_2/EtOH ratio of 0.5 at 400^oC and the maximum acetaldehyde yield (0.4) occurs at the O_2/EtOH ratio of 1.2 (at 300^oC) due to the high conversion there.

The second set of experiments performed with the catalyst V_4 is the non-oxidative dehydrogenation of ethanol. That is, no oxygen is sent to the reactor for this set of experiments and ethanol is dehydrogenated over the catalyst V_4 without oxygen. The results of this set of experiments can be used to discuss the deactivation behaviour of the catalyst V_4. Figure 4.44 depicts that the conversion decreases, as expected, with time as the catalyst is deactivated. The deactivation rate of the catalyst is not very fast as observed from the shallow slope of the curve and the conversion seems to remain fixed at around 0.07 as time goes to infinity. This suggests that the catalyst uses the oxygen found in its structure and hence the conversion does not fall to zero as time goes to infinity.
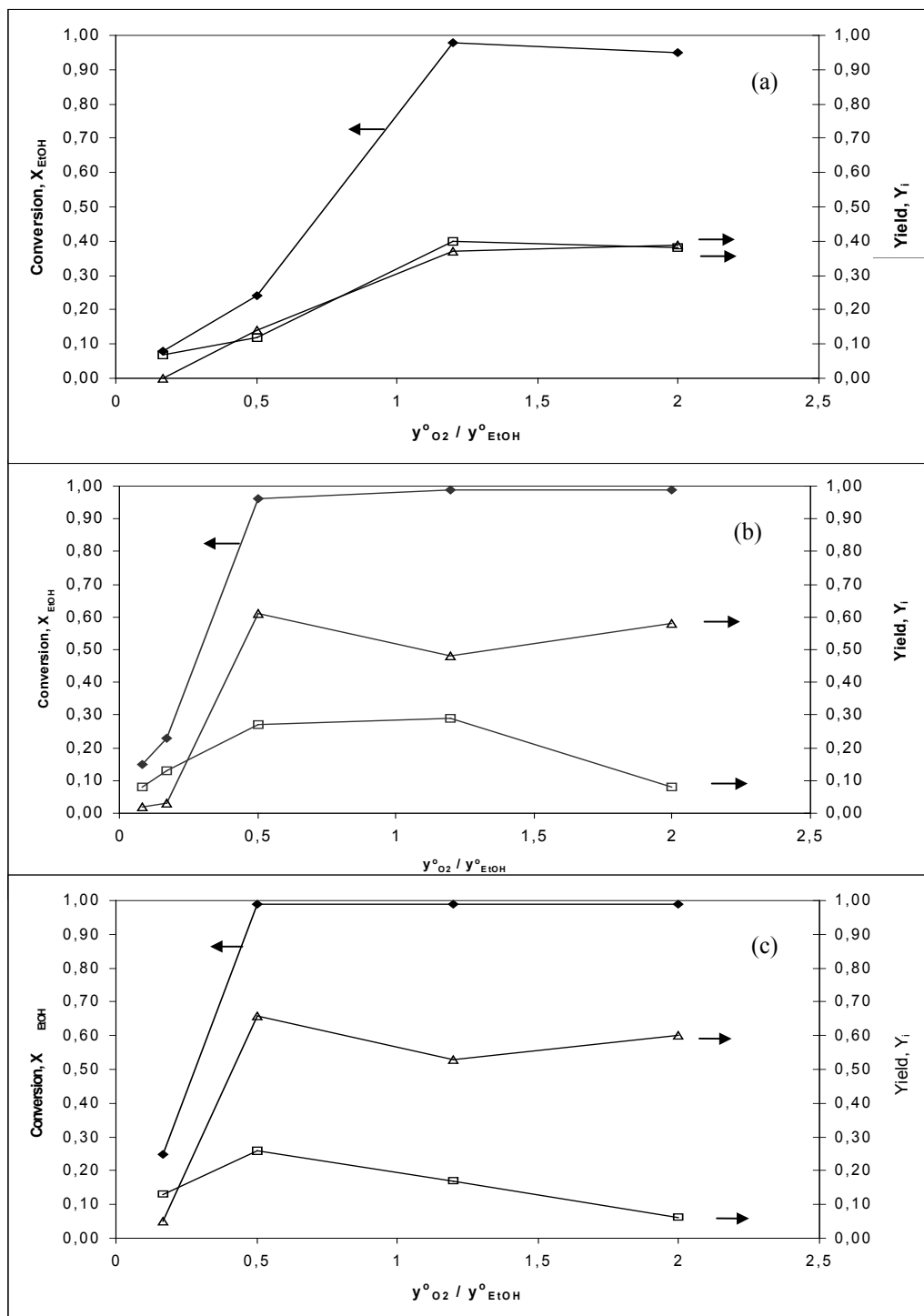
Fig 4.43 Conversion and yield values obtained for different y^o_{O2}/ y^o_{EtOH} ratios at (a) 300^oC, (b) 375^oC and (c) 400^oC
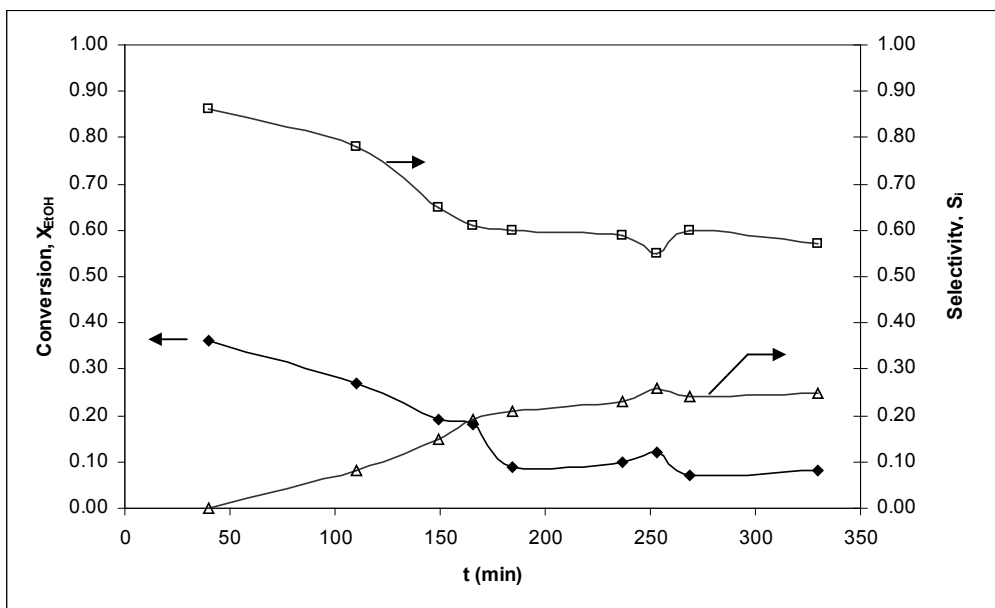
Fig. 4.44 Conversion and selectivity values obtained on the catalyst V_4 for the GHSV of 64.7 h^{-1} in the non-oxidative dehydrogenation reaction at 400°C. (♦) EtOH conversion, (□) acetaldehyde selectivity, (△) ethylene selectivity.
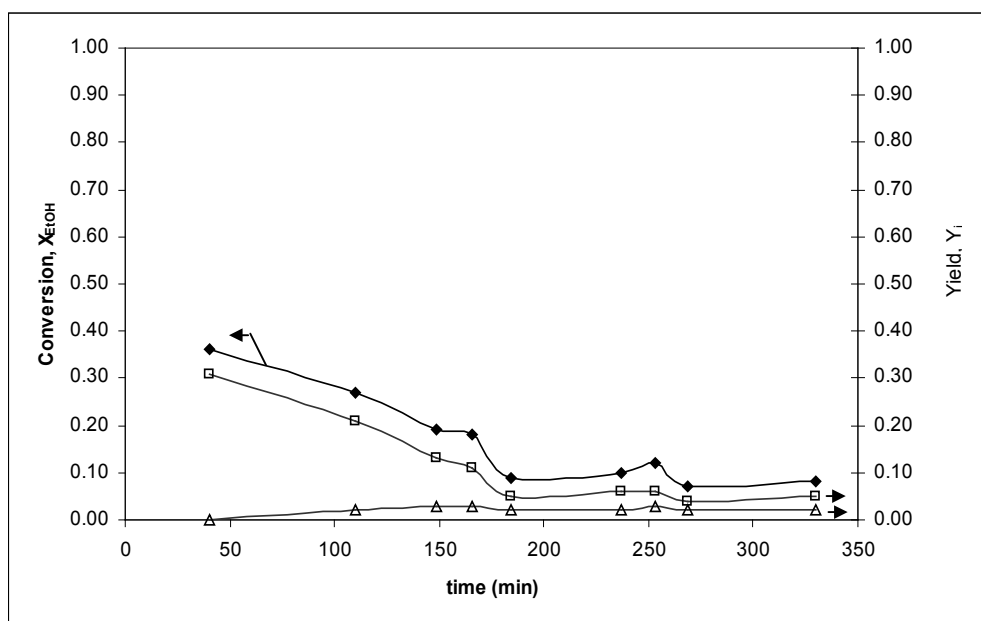
Fig. 4.45 Conversion and yield values obtained on the catalyst V_4 for the GHSV of 64.7 h^{-1} in the non-oxidative dehydrogenation reaction at 400°C. (♦) EtOH conversion, (□) acetaldehyde yield, (△) ethylene yield.

Before the non-oxidative dehydrogenation reaction of ethanol, the catalyst bed was swept with helium for about three hours at the reaction temperature so that no adsorbed oxygen is left on the catalyst. Keeping this in mind (i.e., no adsorbed oxygen is left on the catalytic sites), a detailed observation of Figure 4.44 brings about very important findings considering the possible mechanism of the selective oxidation of ethanol. It is seen in Figure 4.44 that, formation of some acetaldehyde is observed at 400°C, at the initial times. The total conversion of ethanol, on the other hand, shows a decreasing trend from 0.36 down to 0.08 within about 200 minutes in the absence of oxygen gas. Parallel to this decrease of total conversion, acetaldehyde yield values also decrease from 0.31 down to 0.05. At the initial times, no ethylene formation is observed in the absence of oxygen . Although some increase of ethylene selectivity is observed with time, ethylene yield values remain around 0.02 in these experiments. These results indicate that the lattice oxygen of the catalyst is involved in the formation of acetaldehyde during the selective oxidation of ethanol. Elimination of an hydrogen from the adsorbed ethoxy species, probably by a lattice oxygen of the catalyst is expected to be responsible for the formation of acetaldehyde on the catalyst surface. The reduction of the catalytic activity and the corresponding decrease in the acetaldehyde yield are essentially due to the consumption of the lattice oxygen and the reduction of the catalyst. In the presence of oxygen, the catalyst is reoxidized and a redox mechanism is expected to be responsible for the formation of acetaldehyde.

Formation of no or very small amounts of ethylene in the absence of oxygen gas is a clear indication of the involvement of the adsorbed oxygen in the formation of ethylene over this catalyst. Ethylene is expected to be formed on the catalyst surface majorly as a result of the oxidative dehydrogenation of the adsorbed ethoxy species. With an increase in temperature and oxygen concentration, a bridged structure involving an adsorbed oxygen may form on the catalyst surface which then may give ethylene. Small amounts of diethyl-

ether observed at low O_2/EtOH feed ratios and at lower temperatures are expected to be formed by the dehydration reaction of ethanol on the acid sites, as well. By increasing the temperature over 300 ^{o}C, decomposition of diethyl-ether to ethylene is expected. This may also contribute to the formation of ethylene at higher temperatures.

The findings of the above paragraphs lead to the proposal of the following reaction mechanism: Firstly, ethanol is expected to dissociatively adsorp on two different sites forming ethoxy species and adsorbed hydroxy species (or adsorbed hydrogen) as illustrated in Equation 4.2,

$$
\begin{array}{c}
CH_3 \\
| \\
CH_2 \\
| \\
O \qquad\quad H \\
\vdots \qquad\quad \vdots
\end{array}
$$

$$C_2H_5OH + S_1 + S_2 \rightarrow \quad -S_1 \!-\!\!-\!\!-\!\!-\!\!-\! S_2 - \qquad (4.2)$$
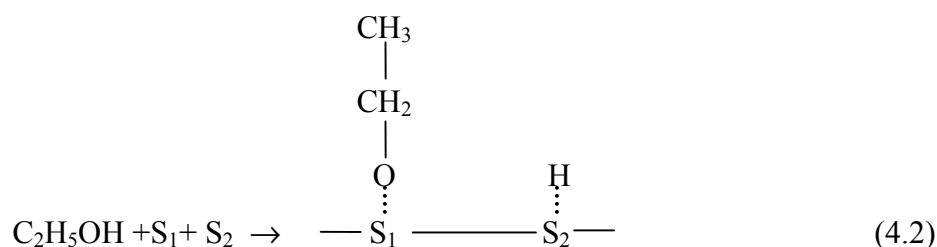
Secondly, by the elimination of a hydrogen of the ethoxy species by an adsorbed oxygen atom; first a bridged structure and then ethylene forms (Equation 4.3).

$$
\begin{array}{ccc}
CH_3 & & \\
| & & \\
CH_2 & & \\
| & & \\
O & O \quad H & O \\
\vdots & \vdots \quad \vdots & | \\
-S_1- & S_1 - S_2 & \rightarrow C_2H_4 + H_2O + \quad -S_1 - S_1 + S_2
\end{array}
\qquad (4.3)
$$
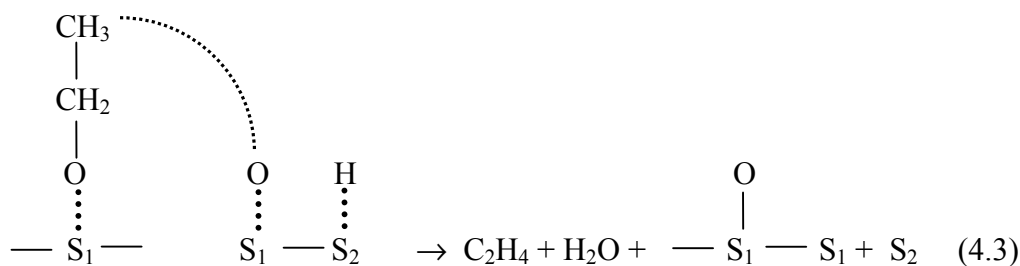
The formation of acetaldehyde, on the other hand, is expected to take place by the elimination of the hydrogen of an ethoxy species by a lattice oxygen following a redox mechanism (Equation 4.4),

$$\begin{array}{c} CH_3 \\ | \\ CH_2 \cdots \cdots \\ | \quad \cdots \\ O \qquad O \quad H \qquad\qquad\qquad O \\ \vdots \qquad \vdots \quad \vdots \qquad\qquad\qquad | \\ -S_1- \qquad S_2-S_2 \quad \rightarrow CH_3CHO + H_2O + S_1 + S_2 + S_2 \qquad (4.4) \end{array}$$

$$\begin{array}{c} O \quad\; O \\ \vdots \quad\;\; \vdots \\ O_2 + S_2 + S_2 \;\rightarrow\; S_2 + S_2 \qquad\qquad\qquad\qquad (4.5) \end{array}$$
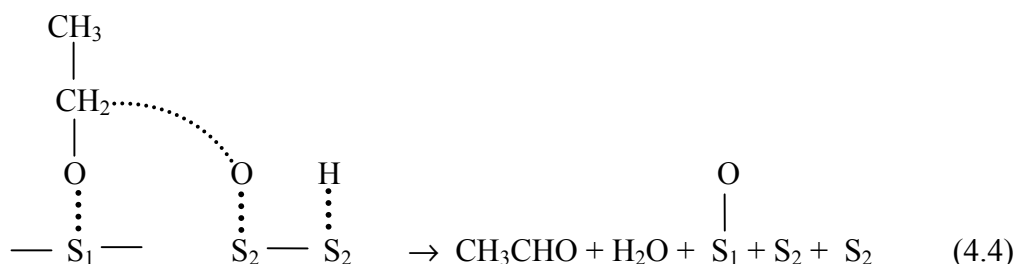
In the final set of experiments (Figure 4.46) with the catalyst V_4, CO_2 is used as the oxidant. In this set of experiments only acetaldehyde is formed and the conversion of the reaction did not fall below 0.3. The minimum yield obtained in this set of experiments (at $T = 375^oC$ and GHSV = 64.7 h^{-1}) is 0.28. If Figure 4.43.b is revised, it is seen that the maximum acetaldehyde yield obtained with oxygen at the same conditions (at $T = 375^oC$ and GHSV = 64.7 h^{-1}) is 0.29. Hence, the use of carbon dioxide seems to be very sucessful for the production of acetaldehyde through the selective oxidation of ethanol over a high surface area V-MCM-41 catalyst.

Carbon dioxide is a mild oxidant and it seems that it is sufficient to generate the redox reaction necessary for the production of acetaldehyde by using CO_2. In this case the formation of some carbon monoxide is also expected.

Interestingly, in the set of experiments performed with CO_2, no ethylene is formed. This result is another justification of the need for the gas phase oxygen for the production of ethylene. Most probably oxygen gas is adsorbed by dissociation and these adsorbed oxygen species are involved in the formation of ethylene. Further DRIFTS studies can eloborate these findings,
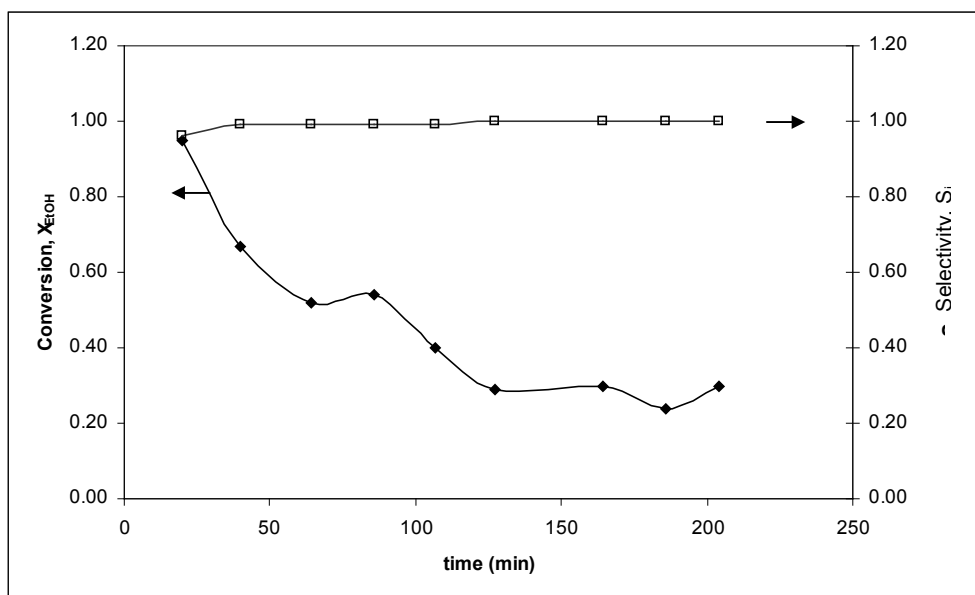
Fig. 4.46 Conversion and selectivity values obtained on the catalyst V_4 for the GHSV of 64.7 h^{-1} in the CO_2 experiments at 375°C for a CO_2/EtOH feed ratio of 1.86. (♦) EtOH conversion, (□) acetaldehyde selectivity.

however, using the thus far obtained experimental data, the following set of reactions may be proposed for the production of ethylene and acetaldehyde.

Ethylene is expected to be formed by the involvement of the gas phase oxygen,

$$\underline{S} + C_2H_5OH + \tfrac{1}{2}\,O_2 \rightarrow C_2H_4 + H_2O + \underline{SO} \qquad (4.6)$$
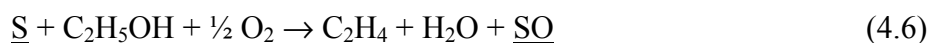
When one mole of ethylene forms, x moles of acetaldehyde is also expected to be formed in a parallel reaction following a redox mechanism involving the lattice oxygen,

$$x\,[C_2H_5OH + O\text{-}S^* \rightarrow CH_3CHO + H_2O + S^*\,] \qquad (4.7)$$

$$x\,[S^* + \tfrac{1}{2}\,O_2 \rightarrow O\text{-}S^*] \qquad (4.8)$$

108
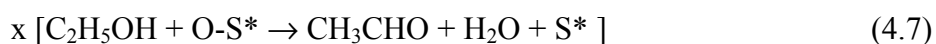
In Equations 4.7 and 4.8, the oxygen atom in O-S* corresponds to a lattice oxygen.

Oxygen is expected to adsorb on the catalyst surface by dissociation as given in Equation 4.9.

$$\frac{1}{2} O_2 + S \rightarrow O\text{-}S \qquad (4.9)$$

In the presence of excess oxygen, further oxidation of some of the formed acetaldehyde to carbon dioxide is expected to take place using the adsorbed oxygen,

$$\underline{SO} + 1/5\ CH_3CHO \rightarrow 2/5\ CO_2 + 2/5\ H_2O + \underline{S} \qquad (4.10)$$
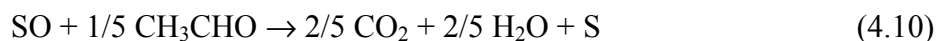
The following overall reaction can be written for the production of ethylene, acetaldehyde and carbon dioxide at excess oxygen conditions,

$$(1+x)C_2H_5OH + \frac{1}{2} O_2 \rightarrow C_2H_4 + [(6x\text{-}1)/5]CH_3CHO + 2[(1\text{-}x)/5]CO_2 + [(3x+7)/5]H_2O \qquad (4.11)$$
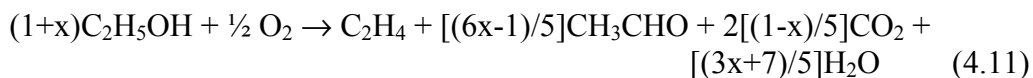
The extent of the reaction to acetaldehyde, i.e., x, can be determined by using experimental data at excess oxygen conditions. Once, x is found, it can be used to estimate the coefficients in Equation 4.11.

For instance, at $400^\circ C$, for an O_2/EtOH feed ratio of 2.0, x is calculated as 0.25. The insertion of this value into Equation 4.11 yielded the coefficient of CO_2 (i.e., the expected selectivity to CO_2) as 0.3. It is seen that; at this experimental run, a selectivity of 0.27 is obtained for CO_2. Hence, the proposed set of reactions seems correct, however, checks must be made at other experimental points, as well.

4.5.2 Experiments with the catalyst MCM-41

The catalyst MCM-41 (sample 1) is also tried in the selective oxidation of ethanol at the stoichiometric O_2/EtOH ratio of 0.5 in the

temperature range of $200^{\circ}C$ -$400^{\circ}C$ (Figure 4.47). Lower conversion values are obtained with respect to the catalyst V_4. However, due to the high surface area (1400 m^2/g), and the large pores which enhances diffusion; MCM-41 is also an active catalyst which yields conversions as high 0.56 at the temperatures of 375^0C and $400^{\circ}C$. In terms of selectivity, the use of MCM-41 as the oxidation catalyst favors the acetaldehyde production. Contrary to the results obtained with the catalyst V_4 for which the acetaldehyde selectivities were 0.28 and 0.26 at the temperatures of $375^{\circ}C$ and $400^{\circ}C$, respectively, the acetaldehyde selectivities are now 0.52 and 0.54. In other words, the use of MCM-41 catalyst instead of V-MCM-41 increases the selectivity to acetaldehyde production. Ethylene selectivity, on the other hand, is very low on the MCM-41 catalyst. Hence, it is proved that the introduction of the vanadium
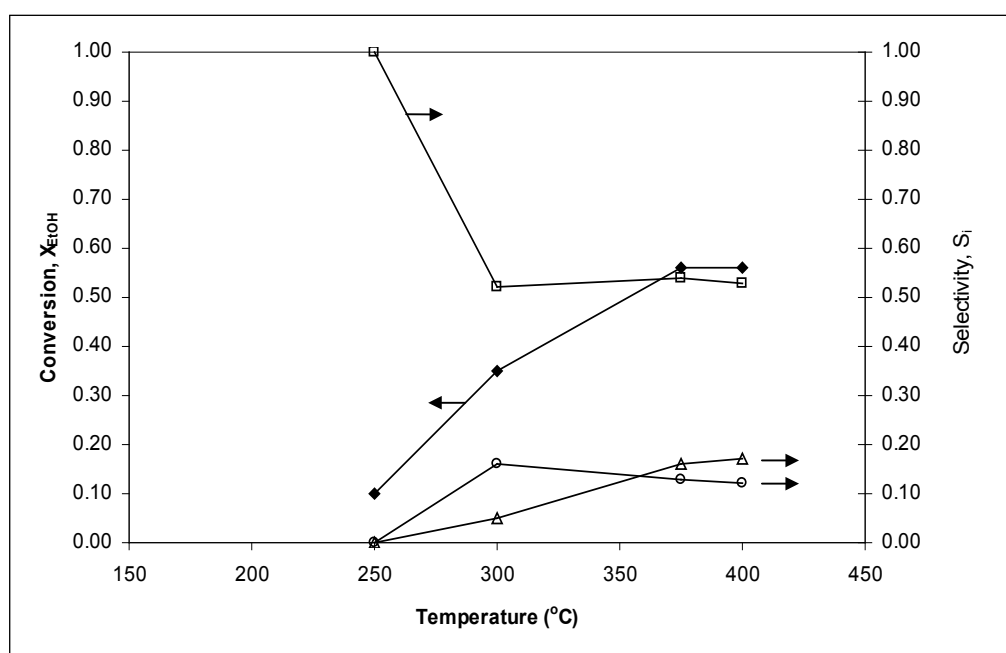
Fig. 4.47 Conversion and selectivity values obtained on the catalyst MCM-41 (sample1) for the GHSV of 64.7 hr^{-1} at the O_2/EtOH feed ratio of 0.5
($\bullet$) EtOH conversion, ($\square$) acetaldehyde selectivity, ($\triangle$) ethylene selectivity and ($\circ$) carbon dioxide selectivity.

110

into the MCM-41 structure increases both the catalytic activity and the selectivity of ethylene production.

In terms of yields, Fig 4.48 shows that the catalyst MCM-41 gives higher yields of acetaldehyde than the catalyst V_4. Ethylene yield, on the other hand, is much higher when the catalyst V_4 is used, especially at high temperatures.
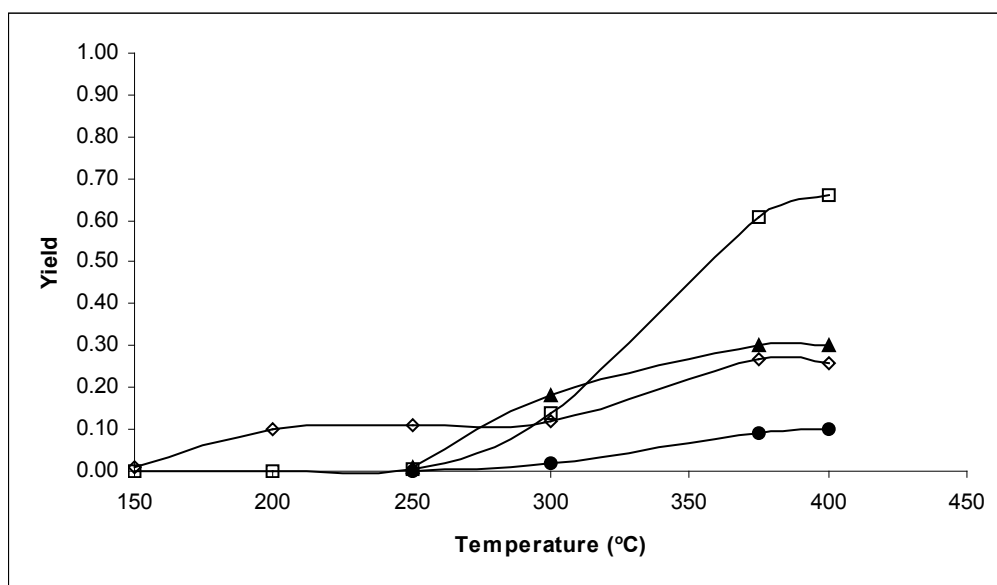
Fig 4.48 Yield values obtained on the catalyst MCM-41 (sample 1) and the catalyst V_4 for the GHSV of 64.7 hr^{-1} at the O_2/EtOH feed ratio of 0.5.
(□) ethylene yield on the catalyst V_4, (◇)acetaldehdye yield on the catalyst V_4,
(▲) acetaldehyde yield on the catalyst MCM-41 (sample 1) and
(●) ethylene yield on the catalyst MCM-41 (sample 1).

4.5.3 Effect of the V/Si ratio on the catalyst activity and selectivity

In order to see the effect of the V/Si ratio on the activity and selectivity of the used oxidation catalyst, another catalyst, namely, catalyst V_2 with the BET surface area of 1315 m^2/g and the V/Si ratio (in the solid) of 0.0063 is also used in the reaction experiments. The results obtained with catalyst V_2 are compared with the results obtained with the catalysts V_4 and MCM-41 in

Figures 4. 49 and 4.50 (note that the catalyst MCM-41 has a V/Si ratio of 0.0 since no vanadium is incorporated into its structure).

It is seen that the reaction conversion increases with increasing V/Si ratio which suggests that the catalytic activity increases as more vanadium is incorporated into the structure.

The ethylene selectivity and yield increase and the acetaldehyde selectivity and yield decrease with increasing V/Si ratio which means that it is the acidity introduced by the vanadium atoms that brings about the formation of ethylene in expense of the formation of acetaldehyde.

Our results proved that there is an optimum V/Si ratio of the V-MCM-41 type catalytic materials which maximizes the ethylene yield. Among the catalysts studied in this work, the catalyst V_4, which contained a V/Si molar ratio of 0.04 gave the highest ethylene and the lowest acetaldehyde yields. Ethanol conversion showed an increasing trend with an increase in V/Si molar ratio of the catalyst, until a value of 0.04. For instance, with an increase in this ratio from 0.006 to 0.040, the fractional conversion of ethanol increased from 0.81 to 0.99. By the incorporation of higher amounts of vanadium into the catalyst structure, significant reduction was observed in the surface area of the catalyst [23] and the MCM-41 structure was somewhat distorted. The increase of the V/Si molar ratio over 0.04 caused a significant increase in the acetaldehyde selectivity, with a corresponding decrease in the ethylene selectivity. For instance, for the catalyst having a V/Si molar ratio of 0.13, acetaldehyde selectivity reached a value of 0.70 at 400°C . The decrease in the fractional conversion of ethanol with an increase in the V/Si molar ratio of the catalyst (over 0.04) is partly due to the reduction of the surface area of the catalyst by the increase of the vanadium content. However, bulk V_2O_5 was also reported to be not highly active for ethanol oxidation [128]. Also for pure V_2O_5, the major product is acetaldehyde. Acidity of the V_2O_5 is expected to decrease by the incorporation of vanadium into the SiO_2 structure of MCM-41.
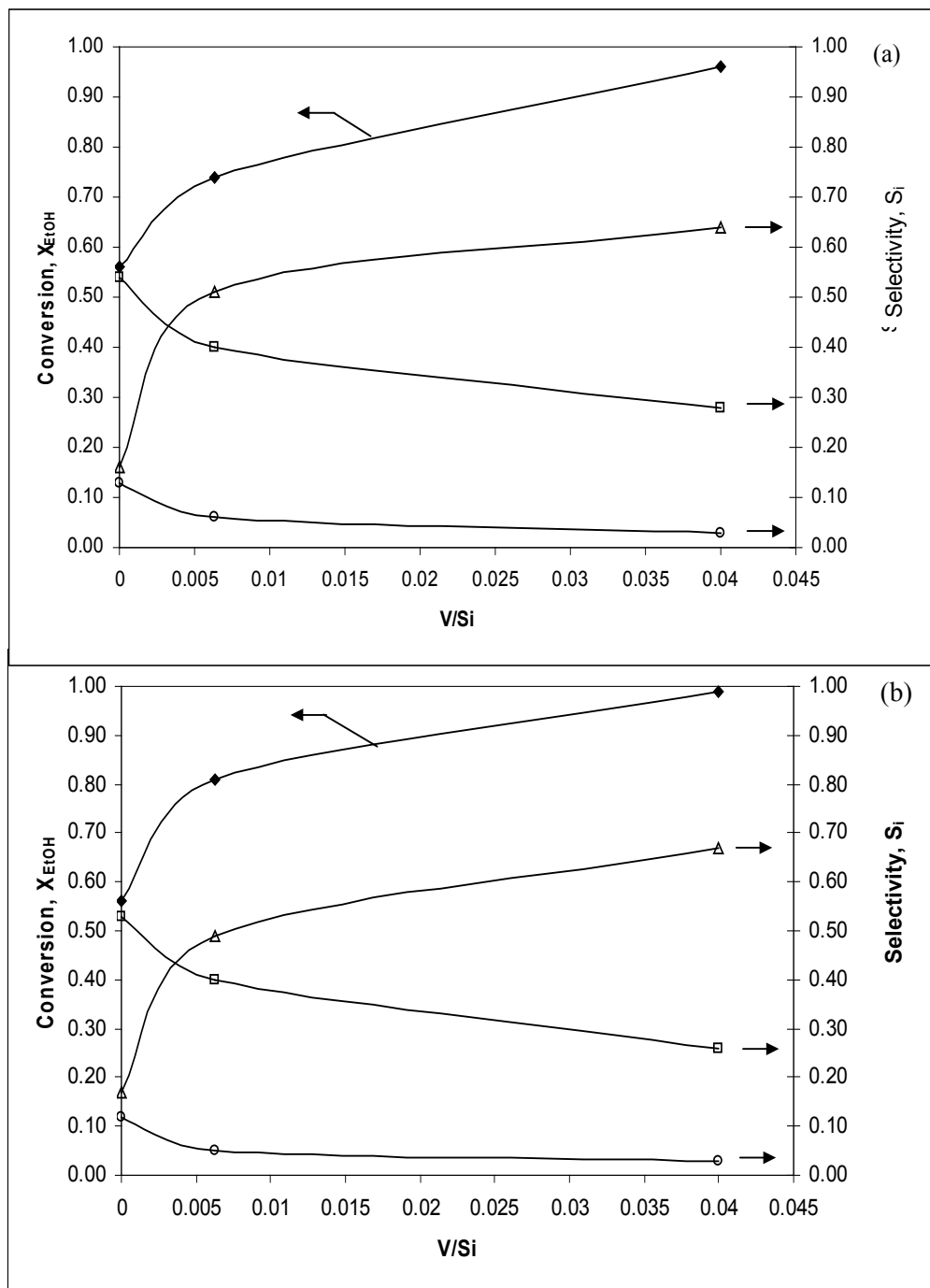
Fig 4.49 Conversion and seletivity values obtained for different V/Si ratios on sample 1, sample V_1 and sample V_4 for the GHSV of 64.7 hr^{-1} at the O_2/EtOH feed ratio of 0.5 at (a) 375°C and (b) 400°C.
($\blacklozenge$) EtoH conversion, ($\square$) acetaldehyde selectivity ($\triangle$) ethylene selectivity, and ($\circ$) carbon dioxide selectivity.

Fig 4.50 Conversion and yield values obtained for different V/Si ratios on sample 1, sample V_1 and sample V_4 for the GHSV of 64.7 hr^{-1} at the O_2/EtOH feed ratio of 0.5 at (a) 375°C and (b) 400°C.

(♦) EtoH conversion, (□) acetaldehyde yield and (△) ethylene yield.

With decreasing acidity, desorption of the C_2H_4 formed on the surface is expected to become faster, reducing further oxidation.

4.5.4 Side products

In addition to the main products ethylene and acetaldehyde, side products such as acetic acid, ethane, diethyl ether, diethyl acetal and ethyl acetate are also produced in many of the experimental runs performed. For instance, for the lean oxygen conditions (at an $O_2/EtOH$ ratio of 0.17) over the catalyst V_4, the selectivities given in Table 4.10 are obtained for the side products along with the main products.

Table 4.10 depicts that at low $O_2/EtOH$ ratios ethane is a more important side product than ethylene. In addition, low amounts of methane and diethyl ether are also produced.

Table 4.10 Conversions and selectivities obtained at the $O_2/EtOH$ feed ratio of 0.17 for the GHSV of 37.8 h^{-1}

$T(^oC)$	X_{EtOH}	S_{AA}	S_{ethy}	S_{ethane}	$S_{methane}$	S_{CO2}	S_{DIE}	S_{DIA}	S_{EtAc}	S_{AcAc}
300	0.09	0.82	0.04	0.11	0.02	0.00	0.01	0.00	0.00	0.00
320	0.14	0.64	0.09	0.19	0.00	0.00	0.05	0.00	0.00	0.00
350	0.23	0.55	0.12	0.27	0.01	0.00	0.05	0.00	0.00	0.00
375	0.23	0.56	0.15	0.27	0.01	0.0	0.08	0.00	0.00	0.00
400	0.25	0.49	0.20	0.24	0.02	0.00	0.05	0.00	0.00	0.00

If the $O_2/EtOH$ ratio is increased to the stoichiometric value of 0.5 (Table 4.11) over the same catalyst, the product distribution changes; ethylene is no longer a side product and in fact it becomes the major product at high temperatures. Ethane is no more formed and the other side products observed are methane, carbon dioxide, diethyl ether, diethyl acetal, ethyl acetate and acetic acid all with low selectivity values.

Table 4.11 Conversions and selectivities obtained at the O_2/EtOH feed ratio of 0.5 for the GHSV of 64.7 h^{-1}

T(^{o}C)	X_{EtOH}	S_{AA}	S_{ethy}	S_{ethane}	$S_{methane}$	S_{CO2}	S_{DIE}	S_{DIA}	S_{EtAc}	S_{AcAc}
250	0.13	0.82	0.06	0.00	0.00	0.01	0.06	0.03	0.02	0.00
300	0.24	0.49	0.28	0.00	0.00	0.01	0.09	0.07	0.05	0.01
375	0.96	0.28	0.64	0.00	0.01	0.03	0.02	0.01	0.00	0.00
400	0.99	0.26	0.67	0.00	0.01	0.03	0.02	0.01	0.00	0.00

Further increase of the O_2/EtOH ratio to 2.0 (i.e., excess oxygen conditions) over the same catalyst yields the results given in Table 4.12. It is seen that, in this case also ethylene is the major product at high temperatures. Combustion products such as methane and carbon dioxide now have selectivities around 0.1-0.3 due to the excess oxygen used. Some diethyl ether is also formed with very low selectivities.

Table 4.12 Conversions and selectivities obtained at the O_2/EtOH feed ratio of 2.0 for the GHSV of 64.7 h^{-1}

T(^{o}C)	X_{EtOH}	S_{AA}	S_{ethy}	S_{ethane}	$S_{methane}$	S_{CO2}	S_{DIE}	S_{DIA}	S_{EtAc}	S_{AcAc}
300	0.95	0.40	0.41	0.00	0.02	0.06	0.06	0.00	0.04	0.01
375	0.99	0.08	0.59	0.00	0.09	0.22	0.02	0.00	0.00	0.00
400	0.99	0.06	0.61	0.00	0.06	0.27	0.00	0.00	0.00	0.00

The presence of acetic acid, diethyl ether, carbon dioxide and diethyl acetal in the product distribution suggests that a set of reactions similar to those suggested by Tesser et al. [116] must be operative for the selective oxidation of ethanol over V-MCM-41 catalysts (see Section 2.5.2).

In Appendix G, detailed information is given in the form of tables for selected experimental runs in terms of the peak areas of the products obtained during the gas chromatography analyses.

4.5.5 Experiments with the catalyst Mo$_7$

In order to see the effect of using the Mo-MCM-41 catalysts as oxidation catalysts in the partial oxidation of ethanol, a set of experiments is designed where the sample Mo$_7$ (which has a BET surface area of 488 m^2/gram and a Mo/Si ratio (in the solid) of 0.03) is used as the oxidation catalyst at the stoichiometric O$_2$/EtOH ratio of 0.5.

In this set of experiments, the results given in Figure 4.51 are obtained. It is seen that the Mo-MCM-41 catalyst is less active than the V-MCM-41 catalyst (V$_4$) at the same space time and O$_2$/EtOH ratio.

In terms of the acetaldehyde selectivity, somewhat lower values are obtained with the catalyst Mo$_7$ compared to the catalyst V$_4$ but there is not a very significant difference.
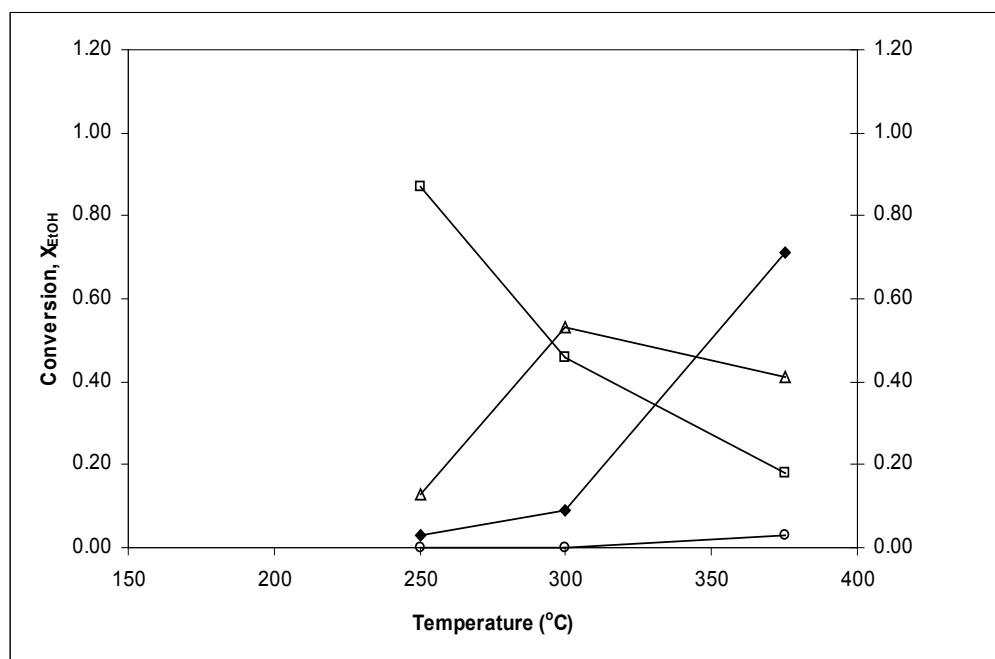
Fig. 4.51 Conversion and selectivity values obtained on the catalyst Mo$_7$ for the GHSV of 66.7 hr^{-1} at the O$_2$/EtOH feed ratio of 0.5 (♦) EtOH conversion, (□) acetaldehyde selectivity, (△) ethylene selectivity and (○) carbon dioxide selectivity.

In terms of ethylene selectivity, the catalyst Mo_7 gives higher selectivities at 250^0C (0.13 vs. 0.06) and (0.53 vs. 0.28) than the catalyst V_4. However, the selectivity falls to 0.41 when the temperature is raised to 375^oC whereas the selectivity of ethylene was 0.64 at the same temperature over the catalyst V_4.

Hence, in general, the molybdenum incorporated MCM-41 catalyst seems to be less active and selective than the vanadium incorporated MCM-41 catalyst. However, if the surface areas and the Mo/Si ratios of the Mo-MCM-41 catalysts synthesized by the acidic route can be increased, more active and selective oxidation catalysts can be produced for the partial oxidation of ethanol. Also, further analysis of molybdenum incorporated MCM-41 catalysts can elaborate these findings.

CHAPTER 5

CONCLUSIONS AND RECOMMENDATIONS

High surface area (400-1452 m^2/g) V-MCM-41, MCM-41 and Mo-MCM-41 catalysts are synthesized in this study by using the one-pot alkaline and acidic synthesis routes.

The as-synthesized catalysts, in addition to high surface areas, are also found to have high porosities, homogeneous pore size distributions, good crystalline structures and high amounts of metal loading levels.

The one-pot alkaline synthesis method is found to be very successful for the production of V-MCM-41 and MCM-41 type catalysts with high surface areas of 481-1452 m^2/g, high porosity values around 70% and good crystalline structures even at high metal loadings. The metal loadings could be increased, without the destruction of the structure, up to V/Si molar ratios of 0.16 in the synthesized product.

In the case of the Mo-MCM-41 catalysts, the one-pot alkaline synthesis method is found to be less successful, when compared to the V-MCM-41 catalysts, in terms of metal incorporation since the maximum Mo/Si ratio obtained in the catalysts is 0.01. However, a revision of literature shows that this value is also significant when molybdenum incorporated oxidation catalysts are considered.

The Mo-MCM-41 catalysts synthesized by the one-pot *acidic* synthesis route are found to have higher metal loading levels than those synthesized through the one-pot *alkaline* synthesis route. However their XRD patterns were less successful than the catalysts synthesized by the alkaline route. Hence, the

synthesis of Mo-MCM-41 catalysts can be enhanced by developing the acidic route further to obtain high quality XRD patterns.

The MCM-41 and Mo-MCM-41 catalysts synthesized in this work are found to have high activities in the *selective oxidation of ethanol* with conversion levels of 0.56 and 0.71, respectively, at $375^{o}C$ at the stoichiometric $O_2/EtOH$ ratio of 0.5. Both catalysts showed high selectivities to acetaldehyde at low temperatures. The MCM-41 catalyst did not favor the production of ethylene; however, over the Mo-MCM-41 catalyst tried, ethylene selectivities as high as 0.53 are obtained at $300^{o}C$.

The V-MCM-41 catalysts had very high activities in the slective oxidation of ethanol at almost all the $O_2/EtOH$ feed ratios studied. The conversion levels are found to exceed 95% around the relatively low temperature of $350^{o}C$ for the $O_2/EtOH$ feed ratios of 0.5 to 2.0. The acetaldehyde selectivity is found to be very high (0.82-1.00) at low temperatures and a maximum yield of 0.58 is obtained at $300^{o}C$.

Interestingly, the use of carbon dioxide instead of oxygen also gave significant acetaldehyde yields with the catalyst V_4 (this catalyst has a V/Si RATİO OF 0.04 in the product and a surface area of 1062 m^2/g). The steady state acetaldehyde yield obtained by using carbon dioxide, i.e., 0.3, is found to be higher than many of the selectivity values obtained with oxygen at similar experimental conditions.

The V-MCM-41 catalysts are found to be very active and selective in the production of **ethylene** through the selective oxidation of ethanol contrary to the literature findings where ethylene is always listed as a minor side product. The **maximum ethylene yield** obtained in this study over the catalyst V_4 is **0.66** at the stoichiometric $O_2/EtOH$ ratio of 0.5 at $400^{o}C$.

The **yield** value of **0.66** obtained for **ethylene** at $400^{o}C$ is a challenging result since it is significantly higher than the yield values obtained with the industrial production methods such as thermal cracking and oxidative dehydrogenation of ethane at higher temperatures.

Hence, the most important conclusion of this work is the production of ethylene with high yields from a **non-petroleum** feed-stock, namely ethanol, using a selective oxidation process over V-MCM-41 type catalytic materials.

Ethanol can economically be produced by fermentation of crop and/or sugar wastes. Thus, these results may open new avenues for the production of ethylene which is one of the chief feed-stocks of the petrochemical industry.

This study can be extended further by obtaining the TEM (Transmission Electron Microscopy) photographs and the TPD (temperature programmed desorption) studies of the synthesized catalysts. The TEM photographs depict the structure more clearly than SEM photographs due to the higher magnifications used. Hence, strengths or defects of the structures may be detected and new synthesis recipes may be developed to obtain the desired structures. The TPD results, on the other hand, can be used to determine the surface concentartion of the OH^{-1} groups found in the structure and give an idea about the surface acidity of the catalysts.

In addition, sensitive XPS (X-Ray Photoelectron Spectroscopy) can be employed to determine the surface concentrations and the oxidation states of the incorporated metals. The reaction mechanisms can also be determined by using detailed DRIFTS studies.

REFERENCES

1. IUPAC manual of symbols and terminology, *Pure Appl. Chem.*, **31**(1978) 578.

2. J.B. Nagy, P. Bodart, I. Hannus and I. Kiricsi, "Synthesis, Characterization and Use of Zeolitic Microporous Materials", DecaGen, Szeged, 1998.

3. R.A.Khan, "Metal Incorporation in MCM-41 for Hydrodesulfurization", MSc Thesis, King Fahd University of Petroleum and Minerals, January 2003.

4. G. Oye, J. Sjöblom and M. Stöcker, *Adv. in Coll. and Inter. Sci.*, **89-90**(2001) 439.

5. M.E. Davies, C.Saldarriaga, C.Montes, J.Garces and C.Crowder, *Nature*, **31** (1988) 698.

6. A. Merrouche, J. Patarin, H. Kessler, M. Soulard, L. Delmotze, J.L. Goth and J.F. Jolly, *Zeolites*, **12**(1992) 226.

7. J.R. Anderson, W.R. Jackson, D. Hay, Z.P. Yang and E.M. Campi, *Zeolites*, **16**(1996) 15.

8. S.T. Wilson and E.M. Flanigen, *ACS Symp. Ser.,* **398**(1989) 329.

9. C.C. Freyhardt, M. Tsapatsis, R.F. Lobo, K.J. Balkus and M.E. Davis, *Nature*, **381**(1996) 295.

10. M. Hewat, *Zeolite Catalysts and Sieves: Microscopic Architecture*, 2005, http://www.ill.fr/dif/3D-crystals/zeolites.html.

11. T. Shimizu, T. Yanagisawa, K. Kuroda, and C. Kato, *Annual Meeting of the Chemical Society of Japan*, Abstract No. 1XII D42,1988 I761.

12. T. Yanagisawa, T. Shimizu, K. Kuroda, and C. Kato, *Bull. Chem. Soc. Jpn.*, **63**(1990) 988.

13. T. Yanagisawa, T. Shimizu, K. Kuroda, and C. Kato, *Bull. Chem. Soc. Jpn.*, **63**(1990) 1535.

14. S. Iganaki, Y. Fukushima, and K. Kuroda, *J. Chem. Soc. Chem. Commun.*, **8**(1993) 680.

15. S. Iganaki, Y. Fukushima, and K. Kuroda, *Stud. Surf. Sci. Catal.*, **84**(1994) 125.

16. A. Taguchi and F. Schüth, *Microp. and Mesop. Mater.,* **77**(2005) 1.

17. C.T. Kresge, M.E. Leonowicz, W.J. Roth, J.C. Vartuli, and J.S. Beck, *Nature*, **359**(1992) 710.

18. J.S. Beck, J.C. Vartuli, W.J. Roth, M.E. Leonowicz, C.T. Kresge, K.D. Schmitt, T.T.-W. Chu, D.H. Olson, E.W. Sheppard, S.B. McCullen, J.B. Higgins, and J.L. Schlenker, *J. Am. Chem. Soc.*, **114**(1992) 10834.

19. K. Schumacher, P.I. Ravikovitch, A.D. Chesne, A.V. Neimark, and K.K. Unger, *Langmuir,* **16**(2000) 4648.

20. J.M. Thomas and R. Raja in: Studies in Surface Science and Catalysis, **Vol. 148**, (Ed: Terasaki), Elsevier Science, Amsterdam, 2004, p.169.

21. A.Corma, *Chem. Rev.*, **97**(1997) 2373.

22. A.S. Arajuo and M.Jaroniec, *Thermochimica Acta*, **363** (2000) 175.

23. Y. Gucbilmez, T. Dogu, and S. Balci, *Catal. Today*, **100**(2005) 473.

24. N. Lang, P. Delichere, and A.Tuel, Microp. and Mesop. Mater., **56**(2002) 203.

25. S.C. Laha and R.Kumar, *Microp. and Mesop. Mater.*, **53**(2002) 163.

26. F.A. Twaiq, A.R. Mohamed, and S. Bhatia, *Microp.and Mesop. Mater,.* **64**(2003) 95.

27. E. Byambajav and Y. Ohtuska, *Fuel*, **82**(2003) 1571.

28. Q.N. Le, R.T. Thomson, and G.H. Yokomizo, *U.S. Patent 5,134,241*, 1992.

29. B.P. Pelrine, K.D. Schmidt, and J.C. Vartuli, *U.S. Patent 5,105,051*, 1992.

30. E. Armengol, M.L. Cano, A. Corma, H. García, and M.T. Navarro, *J. Chem. Soc., Chem. Commun.*, (1995) 519.

31. M. Spagnol, L. Gilbert, and D. Alby in: The Roots of Organic Development, Editors: J.R. Desmurs and S. Ratton, Elsevier Science, New York, 1996, p. 29.

32. K.R. Kloetstra and H.Van Bekkum, *J. Chem. Soc., Chem. Commun.*, (1995) 1005.

33. A. Corma, S. Iborra, S. Miquel and J. Primo, *J. Catal.*, **173**(1998) 315.

34. E.F. Godefroi and J. Meers, *U.S. Patent 3,575,999*, 1971.

35. K. Bauer, D. Garbe, and H. Surburg, "Common Fragances and Flavors Materials", 2nd ed., VCH, Weinheim, 1990.

36. M. Pillinger, I.S. Gonçalves, A.D. Lopes, P. Ferreira, J. Rocha, G. Zhang, M. Schäfer, O. Nuyken, and F.E. Kühn, *Phys. Chem. Chem. Phys.*, **4**(2002) 696.

37. Suzuki, N.; Asami, H.; Nakamura, T.; Huhn, T.; Fukuoka, A.; Ichikawa, M.; Saburi, M.; and Wakatsuki, Y. *Chem. Lett.* **4**(1999) 341.

38. Maschmeyer, T.; Rey, F.; Sankar, G.; Thomas, J. M., *Nature*, **378**(1995) 159.

39. D. Zhao, P. Yang, N. Melosh, J. Feng, B.F. Chmelka, and G.D. Stucky, Adv. Mater., **10**(1998) 1380.

40. Ogawa, M.; Ishikawa, H.; Kikuchi, T., *J. Mater. Chem*., **8**(1998) 1783.

41. Corma, A.; Fornes, V.; Garcia, H.; Miranda, M. A.; Sabater, M. J., *J. Am. Chem. Soc.*, **116**(1994) 9767.

42. C.T.Kresge, J.C.Vartuli, W.J.Roth and M.E. Leonowicz in: Studies in Surface Science and Catalysis, Vol. 148, (Ed: Terasaki), Elsevier Science, Amsterdam, 2004, p.53.

43. M.E. Leonowicz, J.A. Lawton, S.L. Lawton, and M.K. Rubin, *Science*, **264**(1994) 1910.

44. C.T.Kresge, W.J. Roth, K.G. Simmons and J.C.Vartuli, *US Patent 5,229,341*, 1993.

45. W.J. Roth, C.T. Kresge, J.C. Vartuli, M.E. Leonowicz, A.S. Fung, S.B. McCullen in: Catalysis by Microporous Materials, Studies in: Surface Science and Catalysis, Vol. 94, (Eds: H.K. Beyer, H.G. Karge, I.Kiricsi and J.B. Nagy), Elsevier Science, 1995, p.301.

46. L. Wang, J. Shi, J. Gao, S. Tomura, and D.Yan, *J. Non-Crys.Soids.*, **278**(2000) 178.

47. Y. Toda, S. Ishimaru, R. Ikeda, T. Mitani, S. Kitao, and M. Seto, *J. Phy. and Chem. of Solids.*, **65**(2004) 471.

48. R.J. Hunter, "Introduction to Modern Colloid Science", Oxford University Press, New York; 1993.

49. J. Ying, C.P. Mehnert, and M.S. Wong, *Angew. Chem. Int. Ed.*, **38**(1999) 56.

50. S. Namba, A. Mochizuki, and M. Kito, *Stud. Surf. Sci. Catal.*, **117**(1998) 257.

51. H.P. Lin and C.Y. Mou, *J. Cluster Sci.*, **10**(1999) 271.

52. S. Namba and A. Mochizuki, *Res. Chem. Int.*, **24**(1998) 561.

53. A. Sayari and Y. Yang, *J. Phys. Chem. B*, **104**(2000) 4835.

54. M.Grün, K.K. Unger, A.Matsumoto and K.Tsutsumi, *Microp. and Mesop. Mater.*, **27**(1999) 207.

55. W. Lin, Q. Cai and W. Pang, *Microp. and Mesop. Mater.*,**33**(1999) 187.

56. C.Y. Chen, H.Y. Li, and M.E. Davis, *Microp. Mater.*, **2**(1993), 17.

57. Q. Huo, D.I. Margolese, U. Ciesla, D.G. Demuth, P. Feng, T.E. Gier, P. Sieger, A. Firouzi, B.F. Chmelka, F. Schuth, and G.D. Stucky., *Chem. Mater.*, **6**(1994) 1176.

58. D. Lensveld, "On the Preparation and Characterisation of MCM-41 supported heterogeneous nickel and molybdenum catalysts, Ph-D Thesis, Utrecht University, 2003. (http:www.library.uu.nl/digiarchief/dip/diss/2003-0325-14324/inhoud.htm)

59. J.C. Vartuli, K.D. Schmitt, C.T. Kresge, W.J. Roth, M.E. Leonowicz, S.B. Mc Cullen, S.D. Hellring, J.S. Beck, J.L. Schlenker, D.H. Olsen, E.W. Sheppard, Chem Mater., **6** (1994) 2317.

60. X.S. Zhao, G.Q. (Max) Lu and G.J. Millar, *Ind.Eng.Chem.Res.*, **35**(1996) 2075.

61. M.J. Lawrence, *Chem.Soc.Rev.*, **23**(1994) 417.

62. P. Fromherz, *Chem. Phys. Lett.* **77**(1981) 460.

63. D. Myers, Surfactant Science and Techonology; VCH: New York, 1992.

64. J.N. Israelachvili, D.J. Mitchell, and B.W. Ninham, *J. Chem. Soc. Faraday Trans. 2*, **72**(1976) 1525.

65. V. Alfredsson, M. Keung, A. Monnier, G.D. Stucky, K.K. Unger, and F. Schüth, *J. Chem. Soc. Chem. Commun.* **8**(1994) 921.

66. C.-Y. Chen, S. L. Burkett, H.-X. Li, M. E. Davis, *Microp. Mater.*, **2**(1993) 34.

67. A. Steel, S. W. Carr, M. W. Anderson, *J. Chem. Soc. Chem. Commun.*, (1994) 1571.

68. A. Monnier, F. Schüth, Q. Huo, D. Kumar, D. Margolese, R. S. Maxwell, G. D. Stucky, M. Krishnamurty, P. Petroff, A. Firouzi, M. Janicke, and B. F. Chmelka, *Science* **261**(1993), 1299.

69. G. D. Stucky, A. Monnier, F. Schüth,Q. Huo, D. Margolese, D. Kumar,K M. Krishamurty, P. Petroff, A. Firouzi, M. Janicke, B. F. Chmelka, *Mol. Cryst. Liq. Cryst.*, **240**(1994) 187.

70. T. Yanagisawa, T. Shimizu, K. Kuroda, and C. Kato, *Bull. Chem. Soc. Jpn.*, **63**(1990) 988.

71. S. Inagaki, Y. Fukushima, and K. Kuroda, *J.Chem. Soc. Chem. Commun,*.1993, 680.

72. Y. Fukushima, S.Inagaki, *Mater. Sci. Eng. A*, **217 − 218** (1996) 116.

73. J. C. Vartuli, C. T. Kresge, M. E. Leonowicz, A. S. Chu, S. B. McCullen, I. D. Johnson, and E. W. Sheppard, *Chem. Mater.*, **6**(1994) 2070.

74. O. Regev, *Langmuir*, **12**(1996) 4940.

75. R. Ryoo, and S.Jun, *J.Phys. Chem .B*, **101** (1997) 317.

76. H-H. Lee, J-W. Ahn and H. Kim, *Ceramics International* (2004).

77. G. S-Ekloff, J. Rathousky and A.Zukal, *Int. Jour. of Inor. Mat.*, **1**(1999) 97.

78. V.M. Mastikhin, O.B. Lapina in: D.M. Grant, R.K. Harris (Eds), Encylopedia of NMR, **Vol 8**, 1996, 4892.

79. M.Chatterjee, T. Iwasaki, H. Hayashi, Y. Onodera, T. Ebina and T. Nagase, *Chem. Mater.*, **11**(1999) 1368.

80. K.J. Chao, C. N.Wu, H. Chang, L.J. Lee, and S. Hu, *J.Phys. Chem.B*, **101**(1997) 6341.

81. S.T. Oyama, *Res. Chem. Intermediates*, **15**(1991) 165.

82. X. Gao, S.R. Bare, B.M. Weckhysen, I.E. Wachs, *J.Phys. Chem.,***102**(1998) 10842.

83. M. Banares, X. Cao, J.L.G. Fierro, and I.E. Wachs, *Stud. Surf. Sci. Catal.*, **110**(1997) 295.

84. J.Le Bars, J.C. Vedrine, A. Aurox, S. Trautman, M. Baerns, *Appl. Catal. A: Gen.,* **88**(1992) 179.

85. M. Puglisi, F. Arena, F. Frusteri, V. Sokolovskii, and A. Parmaliana, *Cat. Lett.,***41**(1996) 41.

86. L. Owens, H.H. Kung, *J.Catal.*, **144**(1993) 202.

87. J.M. Lopez Nieto, G. Kremenic, J.L.G. Fierro, *Appl. Cat.*, **61**(1990) 235

88. M.L. Pena, A. Dejoz, V. Fornes, F. Rey, M.I. Vazquez, and J.M. Lopez-Nieto, *Appl. Catal. A: Gen.,* **209**(2001) 155.

89. Q. Zhang, Y. Wang, Y. Ohishi, T. Shishido, and K. Takehira, *J. Cat.,* **202**(2001) 308.

90. B. Solsona, T. Blasco, J.M. Lopez Nieto, M.L. Pena, F. Rey and A. Vidal-Moya, *J. Cat.,***203**(2001) 443.

91. S.C. Laha and R. Kumar, *Microp. and Mesop. Mater.*, **53**(2002) 163.

92. N. Lang, P. Delichere and A. Tuel, *Microp. and Mesop. Mater.*, **56**(2002) 203.

93. G. Grubert, J. Rathousky, G. S-Ekloff, M. Wark and A. Zukal, *Microp. and Mesop. Mater.*, **22** (1998) 225.

94. G. Centi, F. Fazzani, L. Canesson and A. Tuel, *Stud. Surf. Sci. Catal.*, **110**(1997) 893.

95. Ayyappan and N. Ulagappan, *Proc. Indian Acad. Sci. (Chem. Sci.)*, **108** (1996) 505.

96. S.D. Djajanti and R.F. Howe, *Stud. Surf. Sci. Catal.*, **105**(1997) 2067

97. R.K. Rana, A.C. Pulikottil and B. Viswanathan, *Stud. Surf. Sci. Catal.*, **113**(1998) 211

98. R.K. Rana and B. Viswanathan, *Catal. Lett.*, **52**(1998) 25.

99. D-H. Cho, T-S. Chang, S-K. Ryu and Y.K. Lee, *Catal. Lett.*, **64** (2000) 227.

100. J-Y. Piquemal, E. Briot, M. Vennat, J-M. Brégeault, G. Chottard and J-M. Manoli, *Chem. Commun.*, 1999, 1195.

101. J-Y. Piquemal, J-M. Manoli, P. Beaunier, A. Ensuque, P. Tougne, A-P. Legrand and J-M. Brégeault, *Micropor. Mesopor. Mater.*, **29**(1999) 291.

102. W. Zhang, J. Wang, P.T. Tanev and T.J. Pinnavaia, *Chem. Commun.*, 1996, 979

103. R. Tsumara, S. Higashimoto, M. Matsuoka, H. Yamashita, M. Che and M. Anpo, *Catal. Lett.*, **68**(2000) 101.

104. S. Higashimoto, R. Tsumara, S.G. Zhang, M. Matsuoka, H. Yamashita, C. Louis, M.Che and M. Anpo, *Chem. Lett.*, **29**(2000) 408.

105. Z.Li, L. Gao, and S. Zheng, *App. Cat. A: General*, **236**(2002) 163.

106. S-Tin Wong, H-Ping Lin, and C-Yuan Mou, *App. Cat. A: Gen*., **198**(2000) 103.

107. J. Ramirez, R. Contreras, P. Castillo, T. Klimova, R. Zarate and R. Luna, *App. Cat. A: Gen*., **197**(2000) 69.

108. R. K. Rana and B. Viswanathan, *Cat. Letters*, **52**(1998) 25.

109. C. Song, and K.M. Reddy, *App. Cat. A: Gen*., **176**(1999) 1.

110. B. M. Zied, and A.M. El-Awad, *J. Molec. Cat. A: Chem.*, **176**(2001) 227.

111. M. Qian, M.A. Liauw and G. Emig, *App. Cat. A: Gen*., **38**(2003), 211.

112. West Virginia University, Department of Chemical Engineering, 2005, http://www2.cemr.wvu.edu/~wwwche/publications/projects/large_proj/Acetaldehyde.PDF

113. F.S. Wagner, Kirk-Othmer Encyclopedia of Chemical Technology, Acetic Acid, 2005. http://www.mrw.interscience.wiley.com/kirk/articles/acetwagn.a01/sect5-fs.html

114. Wang et al., Cat. Letters, **50**(1998) 107.

115. Z. Wang, W. Wang and G. Lu, **28**(2003) 151.

116. R. Tesser, V. Maradel, M. Di Serio and E. Santacesaria, Ind. Eng. Chem. Res., **43**(2004) 1623.

117. Delft Solid Solutions, 2005, http://www.solids-solutions.com/porosity.html

118. Photometrics Inc., 2005, http://www.photometrics.net/eds.html

119. Evans Analytical Group, 2005, http://www.cea.com/tech.htm#eds1

120. Charles Evans and Associates, 2005, http://www.cea.com/whatis.htm

121. J.C. Russ, "Fundamentals of Energy Dispersive X-ray Analysis", 1984, Butterworths and Co., London.

122. George Mason University, The Shared Research Instrumentation Facility, Atomic Absorption Spectroscopy, 1998, http://www.gmu.edu/departments/SRIF/tutorial/aas/aas.htm

123. University of Nebraska Lincoln, Electron Microscopy, 2005, http://www.unl.edu/CMRAcfem/em.htm

124. PhotoMetrics Inc., Atomic Force Microscope/Scanning Probe Microscopy, 2005, http://www.photometrics.net/AFM.html

125. JCPDS-International Centre for Diffraction Data, 2002, 49-1712.

126. A. Corma, Q. Kan, M.T. Navarro, J.Perez-Pariente, and F. Rey, *Chem. Mater.,* **9**(1997) 2123.

127. K.M. Reddy, I. Moudrakovski, and A. Sayari, *J. Phys. Chem*., **100**(1996) 19595.

128. T. Feng,and J.M. Vohs, J. Phys. Chem.. **B**, 109(2005) 2120.

129. U. Ciesla, and F. Schüth, *Microp. and Mesop. Mater.*, **27**(1999) 131.

130. S. Brunauer, "The Adsorption of Gases and Vapors. Vol. 1, Physical Adsorption", Princeton University Press, Princeton, N.J., 1943.

127

APPENDIX A

CALCULATION OF THE GAS HOURLY SPACE VELOCITIES (GHSV) FOR THE EXPERIMENTAL RUNS

In this study, the flow rates are reported as GHSV values in the text and in the figure and table captions. GHSV has the dimensions of h^{-1} and its definition is given in Equation A.1,

GHSV = hourly gaseous flow rate / volume of reactor ....(A.1)

where the volume of the tubular flow reactor, V_r, is calculated as,

$V_r = l_r * S_r$ ....(A.2)

where l_r = length of the reactor = 45 cm

and S_r = cross sectional area of the reactor = $\pi*0.91^2 / 4 = 0.650$ cm^2

Hence,

$V_r = 0.650 * 45 = 29.3$ cm^3

Then, using the value of V_r calculated above the GHSV values can be calculated by employing Equation A.1,

For instance, if the gaseous flow rate of reactants to the reactor is 31.6 ml/min (1896 ml/hr) , the corresponding GHSV can be found as,

$$GHSV = 1896 \ (ml \ / \ hr) \ / \ 29.3 \ ml$$
$$= 64.7 \ h^{-1}$$

APPENDIX B

GAS CHROMATOGRAPHY CALIBRATION FACTORS

Calibration experiments are carried out using calibration mixtures in order to determine the retention times and the calibration factors of the products obtained. The experimentally determined calibration factors are given in Table B.1 below and they are also used, as shown in Appendix F, while calculating the selectivity, conversion and yield values of the obtained products.

Table B.1 Gas Chromatography Calibration Factors of the Products Obtained in the Selective Oxidation of Ethanol

Product ID	Calibration Factor
Ethanol, (EtOH)	1.00 (*)
Ethylene, (Ethy.)	1.75
Acetaldehyde, (AA)	1.33
Carbon dioxide, (CO_2)	1.87
Ethane (Ethan.)	1.80
Methane (Meth.)	3.00
Water, (H_2O)	2.61
Diethyl ether, (DIE)	0.64
Diethyl acetal, (DIA)	0.90
Acetic acid, (AcAc)	1.18
Ethyl acetate, (EtAc)	0.68

* Ethylene is arbitrarily assigned a calibration factor of 1.00.

APPENDIX C

NOMENCLATURE OF THE SYNTHESIZED CATALYSTS

The catalysts synthesized in this study are named according to their synthesis methods and their Metal/Si molar ratios in the solution. The corresponding nomenclatures are given in Tables C.1 and C.2.

Table C.1. Nomenclature of the Synthesized MCM-41 and V-MCM-41Catalysts

Sample ID	Metal Source	Metal/Si (in solution)	Synthesis Method	Comments
Sample 1	-	0.00	One-pot alkaline	-
Sample 2	-	0.00	One-pot alkaline	-
V_1	Vanadyl sulfate hydrate	0.01	One-pot alkaline	-
V_2	Vanadyl sulfate hydrate	0.03	One-pot alkaline	-
V_3	Vanadyl sulfate hydrate	0.09	One-pot alkaline	-
V_4	Vanadyl sulfate hydrate	0.09	One-pot alkaline	Calcined in excess air (> 1 l/min)
V_5	Ammonium vanadate	0.09	One-pot alkaline	A suspension formed during the synthesis
V_6	Ammonium vanadate	0.09	One-pot alkaline	A non-homogeneous gel formed during the synthesis

Table C.2. Nomenclature of the Synthesized Mo-MCM-41Catalysts

Sample ID	Metal Source	Metal/Si (in solution)	Synthesis Method	Comments
Mo_1	Ammonium molybdate tetrahydrate	0.03	One-pot alkaline	-
Mo_2	Ammonium molybdate tetrahydrate	0.06	One-pot alkaline	-
Mo_3	Ammonium molybdate tetrahydrate	0.09	One-pot alkaline	-
Mo_4	Ammonium molybdate tetrahydrate	0.03	One-pot acidic	Synthesized without the aging step
Mo_5	Ammonium molybdate tetrahydrate	0.09	One-pot acidic	Synthesized without the aging step
Mo_6	Ammonium molybdate tetrahydrate	0.03	One-pot acidic	Synthesized with the aging step
Mo_7	Ammonium molybdate tetrahydrate	0.09	One-pot acidic	Synthesized with the aging step

APPENDIX D

SAMPLE CALCULATION FOR THE ESTIMATION OF THE APPARENT DENSITIES AND THE PORE WALL THICKNESS VALUES

In order to determine the pore wall thickness values, δ, for the synthesized catalysts, the average pore diameters, d_p, and the lattice parameters, "a", can be employed by using the following equation [77]:

$$\delta = a - 0.95d_p \quad \text{.. (D.1)}$$

where the lattice parameter "a" is the repeating distance between two pore centers and can be found from [77, 129]:

$$a = 2d_{(100)}/\sqrt{3} \quad \text{..(D.2)}$$

and d_{100} is the d-spacing value given by Equation 4.1.

For instance, for sample 1, the lattice parameter "a" was evaluated as 3.49 nm (see Table 4.1). Hence; using the pore diameter, d_p, for sample 1 (from Table 4.1) and the value of a , the wall thickness, δ, can be calculated as

$$\delta = 3.49 - 0.95*2.7 = 0.94 \text{ nm}$$

133

The solid density values given in Table 4.1 are obtained on a helium pycnometer. Then, by using the solid density values and the pore volume values (given in Table 4.1), the apparent (bulk) density values are calculated from Equation D.4,

$$1/\rho_{app} = V_{pore} + 1/\rho_s ....(D.4)$$

Finally, the porosity is found by using Equation D.5;

$$\varepsilon = 1-\rho_{app}/\rho_s ....(D.5)$$

For instance, for sample ρ_s was determined as 1.9 g/cm^3 (see Table 4.1),

Thus,

$$1/\rho_{app} = 1.00 + 1/1.9$$

and

$$\rho_{app} = 0.66 \text{ g/cm}^3$$

Hence,

$$\varepsilon = 1 - 0.66/1.9$$

$$= 0.66$$

APPENDIX E

NITROGEN ADSORPTION ISOTHERMS FOR MCM-41 TYPE MATERIALS

Adsorption isotherms follow one of the six common types, five of which were assessed numbers by Brunauer [130]. MCM-41 fits the type IV adsorption isotherm (see Fig. E.1) according to this classification.

The adsorption isotherm of MCM-41 can be divided into five regions. In region I, monolayer adsorption of nitrogen on the surface of MCM-41 (both on the external surface and inside the mesopores) takes place. Since the surface area is high, the monolayer adsorption requires a large amount of nitrogen to be used. Upon monolayer adsorption, multilayers of nitrogen start to develop at higher relative pressures (region II). Also in this case both the external surface area and the mesopores contribute to the physisorption process. Therefore, the data collected in this part are used for the determination of the surface area by the Brunauer, Emmett and Teller (BET-method).

At a relative nitrogen pressure of about 0.35, a sudden steep increase in the amount of adsorbed nitrogen is observed (region III). This steep increase is caused by the capillary condensation of nitrogen inside the mesopores. The Kelvin equation can be used in this region to determine the pore diameter of the material. Because the filling of the mesopores takes place over a relatively small range of relative pressures ($P/P_o \cong 0.35\text{-}0.40$) the pores associated with this process are nearly equal in size and the MCM-41 material has a very narrow pore size distribution [58].

When the mesopores become completely filled with the nitrogen gas; only the external surface of MCM-41 remains accessible for adsorption in region III. The very shallow slope of this region indicates that the surface area corresponding to the external surface of MCM-41 material is very small compared to the mesopore surface area [58]. In region IV, the nitrogen uptake by the sample increases again and a small hysteresis loop forms as the desorption of nitrogen starts [58].
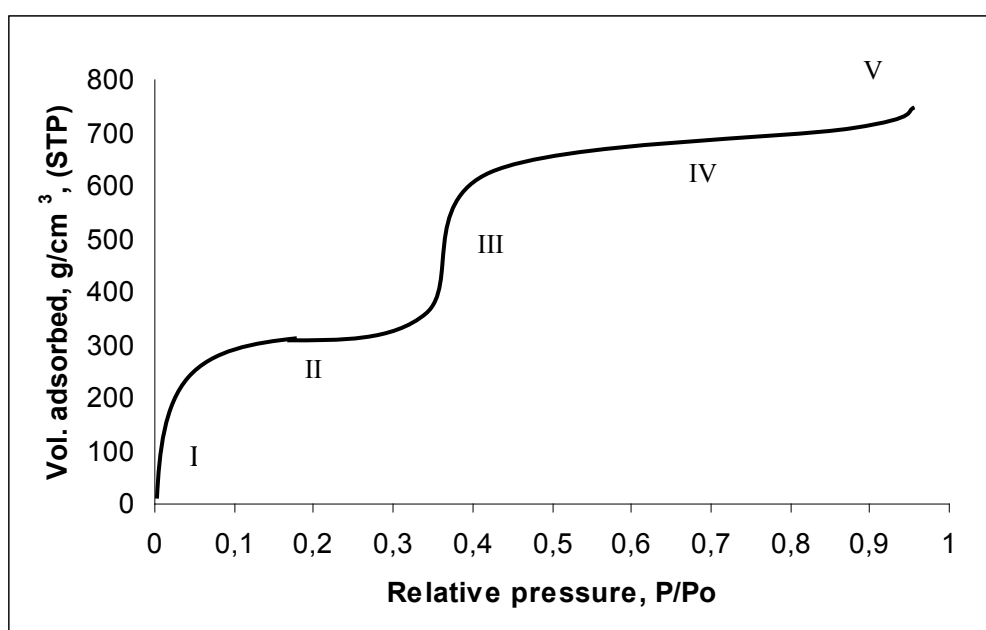
Fig. E.1 Type IV adsorption isotherm of MCM-41

APPENDIX F

ESTIMATION OF THE CONVERSION AND SELECTIVITY VALUES BY USING THE GAS CHROMATOGRAPHY DATA

The selectivity, conversion and yield values given in all the figures and tables in this work are calculated from the individual peak areas of each product by multiplying the peak area with the calibration factor of the product. The peak areas are obtained from the gas chromotograms corresponding to each experimental run. The calibration factors (also given in Appendix B) are experimentally determined by using the same separation program described in Section 3.11.

Table F.1 lists the peak areas and the number of moles of the main and side products for a sample run at $375^{o}C$ at the stoichiometric O_2/EtOH ratio of 0.5. The number of moles corresponding to each product is found by multiplying the peak area of that product with its calibration factor.

Once the number of moles of each product is determined, the initial number of moles of ethanol, n_o, can be found by using the formula given in Equation F.1.

$$n_o = n_{EtOH} + n_{AA} + n_{Ethy.} + n_{Ethan.} + \tfrac{1}{2}\, n_{Methan.} + \tfrac{1}{2}\, n_{CO2} + 2n_{DIE} + 3n_{DIA} + n_{AcAc} + 2n_{EtAc} \ ....(F.1)$$

Hence, for the experimental run given in Table F.1, n_o can be found as:

$$n_o = 46 + 270 + 354 + 0 + \tfrac{1}{2}*0 + \tfrac{1}{2}*56 + 2*9 + 3*1.4 + 4.1 + 2*1.5$$
$$= 1008 \text{ moles}$$

Table F.1 The Number of Moles of Products Estimated from Peak Areas

Product ID	Peak Area	Calibration Factor	Number of Moles
Ethanol, (EtOH)	46	1.00 ([*])	46
Ethylene, (Ethy.)	354	1.75	620
Acetaldehyde, (AA)	203	1.33	270
Carbon dioxide, (CO_2)	30	1.87	56
Ethane (Ethan.)	0	1.80	0
Methane (Meth.)	0	3.00	0
Water, (H_2O)	220	2.61	574
Diethyl ether, (DIE)	14	0.64	9
Diethyl acetal, (DIA)	1.5	0.90	1.4
Acetic acid, (AcAc)	3.5	1.18	4.1
Ethyl acetate, (EtAc)	2.2	0.68	1.5

[*] Ethylene is arbitrarily assigned a calibration factor of 1.00.

Equation F.1 is indeed the carbon balance for the reaction system. Hence, each product has a coefficent C_i related to the number of carbon atoms in its molecular formula. For instance, a product which has only one carbon atom in its molecular formula (such as CO_2) is multipled by 1/2, a product which has two carbon atoms in its molecular formula (such as ethylene) is multiplied by 1.0 and so on. In other words the coefficient of each product in Equation F.1 is calculated as:

$$C_i = 1/2* (\text{\# of carbon atoms in the molecular formula}) \dots\dots\dots\dots(F.2)$$

After finding n_o, the conversion of ethanol to products can be found by using the definition

$$X_{EtOH} = (n_o - n_{EtOH})/n_o \dots\dots\dots\dots\dots\dots\dots\dots\dots\dots\dots\dots\dots\dots\dots\dots(F.3)$$

Hence,

X_{EtOH} = (1008-46)/1008

     = 0.95

Then, the selectivity of each product can be estimated by using Equation F.4,

$$S_i = C_i * n_i / (n_o - n_{EtOH}) \dots\dots (F.4)$$

For instance, for ethylene the selectivity corresponding to this experimental run is,

$S_{ethy.}$ = 1.0*620 / (108-46)

    = 0.64

Finally, the yield of each product can be found by multiplying its selectivity with the conversion of ethanol:

$$Y_i = S_i * X_{EtOH} \dots\dots (F.5)$$

Hence,

$Y_{ethy.}$ = 0.64 * 0.95

    = 0.61

EXPERIMENTAL DATA

In the following pages, selected experimental data over the catalyst V_4 is given in terms of the peak areas of the obtained products to indicate the reproducibility of the performed experiments.

Table G.1 Experiments with the Catalyst V_4 where GHSV = 64.7 h^{-1} and O_2/EtOH feed ratio = 0.5

T (ºC)	A_{EtOH}	A_{AA}	A_{H2O}	A_{O2}	A_{C2H4}	A_{CH4}	A_{CO2}	A_{DIE}	A_{DIA}	A_{EtAc}	A_{AcAc}
150	1491	13	17	112	5	-	-	-	-	-	-
150	1456	11		128	4	-	-	-	-	-	-
200	458	38		545	-	-	-	-	-	-	-
250	975	97	63	209	-	-	3	7	2	3	-
250	1037	75	52	218	-	-	2	5	2	2	-
300	852	98	66	182	40	-	4	17	7	12	-
300	856	99	50	188	46	-	3	18	8	11	2
375	46	203	220	49	354	10	30	14	2	2	4
375	26	184	251	32	360	5	29	15	2	2	4
375	56	246	227	41	375	9	29	17	3	3	3
400	8	137	275	92	273	7	36	20	2	-	1
400	9	154	229	56	301	5	23	15	3	-	1
400	10	163	195	69	326	5	28	16	4	-	1
400	9	143	253	60	272	4	24	15	3	-	1

Table G.2 Experiments with the Catalyst V_4 where GHSV = 64.7 h^{-1} and O_2/EtOH feed ratio = 1.2

T (^{o}C)	A_{EtOH}	A_{AA}	A_{H2O}	A_{O2}	A_{C2H4}	A_{CH4}	A_{CO2}	A_{DIE}	A_{DIA}	A_{EtAc}	A_{AcAc}
200	815	72	37	312	-	-	-	-	-	-	-
200	804	86	27	309	-	-	-	-	-	-	-
250	791	103	58	311	-	-	-	-	-	-	-
300	13	139	263	134	107	-	51	20	9	3	10
300	8	144	314	138	92	9	49	20	7	1	10
300	7	145	313	140	106	8	48	20	7	1	6
375	4	91	307	162	121	10	58	-	-	-	-
375	4	77	375	115	101	7	39	23	-	-	-
400	3	31	322	176	95	5	111	15	-	-	-
400	3	70	322	150	130	7	52	21	-	-	-

VITA

Name: Yesim Gucbilmez
Date of Birth: 17.12.1973
Place of Birth: Ankara

EDUCATION

1999 - 2005   Ph-D in Chemical Engineering, Middle East Technical University (METU)

1996 - 1999   MSc in Chemical Engineering, Middle East Technical University (METU)

1992 – 1996   BS   in Chemical Engineering, Middle East Technical University (METU)

1985 – 1992   Ted Ankara Koleji

WORK EXPERIENCE

Company Name: ASELSAN, Macunköy, Ankara.

Duration: 07.1995 – 09.1995

Position: Intern

Responsibilities: Intern at the Electroplating and Waste Water Treatment Departments

TEACHING EXPERIENCE

Place: Middle East Technical University, Department of Chemical Engineering

Duration: 07.1996 – 09. 2004

Responsibilities: Teaching Assistant of various graduate and undergraduate lessons.

INTEREST AREAS

- Materials Synthesis and Characterization.
- Reaction Engineering.

PUBLICATIONS

- Y. Gucbilmez, "Vanadium and Molybdenum Incorporated MCM-41 Catalysts for Selective Oxidation of Ethanol", Ph-D thesis, Middle East Technical University, June 2005.
- Y. Gucbilmez, T. Dogu and S.Balci, "A Novel Approach for Ethylene Production by Selective Oxidation of Ethanol Using Mesoporous V-MCM-41 Catalysts", manual submitted to the Science Journal.
- Y. Gucbilmez, T. Dogu and S.Balci, "Vanadium Incorporated High Surface Area MCM-41 Catalysts", *Catal. Today,* **100**(2005) 473.
- Y. Gucbilmez, I. Tosun and L. Yılmaz, "Optimization of the Locations of Side Streams in a Filter Cake Washing Process", *Chem. Eng. Commun.*, **182**(2000) 49.
- Y. Gucbilmez, "Analysis and Prediction of Filter Cake Washing", MSc thesis, Middle East Technical University, July 1999.

SCIENTIFIC EVENTS

- Mesoporous and Related nano-Structured Crystals' Symposium, Stockholm, Sweden, 2004.
- 11th Nordic Symposium on Catalysis, Oulu, Finland, 2004.
- 8th World Filtration Congress, Brighton, England, 2000.

COMPUTER SKILLS

- Microsoft Office Applications (Very Good)
- Fortran 77 (Good)
- Experience in several software (Mathcad, Aspen Plus)

LANGUAGES

Turkish: Mother tongue

English: Advanced level

INTERESTS AND HOBBIES

Reading: English Literature

Sports: Archery, Basketball

Arts: Music and playing the piano

Other: Travelling and sightseeing